DEVELOPMENT AND APPLICATION OF A METHOD FOR COMPUTING CUMULUS TRANSPORTS

by

ROBERT ALVIN HOUZE, JR.

B. S., Texas A & M University
(1967)

S. M., Massachusetts Institute of Technology
(1969)

SUBMITTED IN
PARTIAL FULFILLMENT
OF THE REQUIREMENTS FOR THE
DEGREE OF DOCTOR OF PHILOSOPHY
at the
MASSACHUSETTS INSTITUTE OF
TECHNOLOGY
February, 1972

Signature of Author . . . . . .
Department of Meteorology, February 2 , 1972

Certified by . . . . . .
Thesis Supervisor

Accepted by . . . . . .
Chairman, Departmental Committee
on Graduate Students

Lindgren

MASS. INST. TECH.
MAR 29 1972
LIBRARIES

DEVELOPMENT AND APPLICATION OF A METHOD
FOR COMPUTING CUMULUS TRANSPORTS
by
ROBERT ALVIN HOUZE, JR.

Submitted to the Department of Meteorology on 2 February 1972
in Partial Fulfillment of the Requirements for
the Degree of Doctor of Philosophy.

ABSTRACT

This study is concerned primarily with the role of cumulus convection as a vertical transport process. The characteristics of the convection are determined from precipitation patterns and, consequently, non-precipitating cumulus elements are excluded. The three principle components of the investigation are: (1) a synthesis of rain gauge and radar data to establish the nature and relative importance of precipitation associated with cumulus convection; (2) the development of a model for computing vertical transports by cumulus updrafts, with rainfall data as the basic input; and (3) the application of the model in a climatological study of the vertical transports of sensible heat and angular momentum.

Precipitation patterns (referred to as storms) were studied for 6 cyclonic and 2 thunderstorm situations in New England. Cumulus-scale showers (cells) in each storm were located within small mesoscale precipitation areas (SMSA's), 100 to 400 km^2; on the average four cells were in a SMSA at any one time. Altogether, life histories of 25 SMSA's and 125 cells were examined. In an air mass thunderstorm situation SMSA's were isolated; however, in all the other cases SMSA's occurred in groups of three to six within large mesoscale areas (LMSA's), 2000 to 5000 km^2. A supplementary study showed that LMSA's in seventeen cyclones formed banded structures aligned within $\pm$ 30 deg of the surface isobars. In cyclonic storms, LMSA's were grouped within synoptic-scale rainfall areas with a density of 1 to 6 per 10^5 km^2. Depth of cells ranged from 1 to 14 km and the cellular rain ranged from 2% to 25% of the total in a LMSA.

Equations for computing model quantities express the conservation of properties in cumulus-scale updrafts. The effects of entrainment and detrainment are specified. The mass of air transported upward $M_c(z)$, where z is height, in cellular updrafts is computed from the conservation of water, given the amounts of cellular and mesoscale precipitation. Important factors which must be considered are the efficiency with which condensate is converted to precipitation in cells and the amount of mesoscale precipitation which should be attributed to cellular lifting. That some mesoscale rain comes from cumulus cells is suggested observationally since each SMSA studied for its lifetime contained at least one cell. The temperature difference, $T_c(z) - T'(z)$, between cumulus-scale updrafts and their environment is calculated from conservation relations for vertical momentum and water. Temperature $T_c(z)$

in cells is approximated by a moist adiabat representing atmospheric conditions and T'(z) is a computed quantity, the second variable being the hydrometeor mixing ratio. The environment is assumed saturated since the modelled cells are embedded in mesoscale rainfall areas. For the temperature calculations, the vertical velocity is specified from a knowledge of cell depth, available measurements of cumulus updraft speeds being referred to for making realistic estimates. The vertical velocity used in the calculation of temperature differences is estimated independently of the calculation of $M_c(z)$. The latter, which is not a rate of transport, is later converted to a vertical velocity only to provide a guide for selecting realistic modelling parameters. The westerly wind speed difference between model cells and their environment is calculated from the conservation of horizontal momentum in the updrafts. The form drag exerted by the relative wind on the updrafts is included but contains a large uncertainty. The vertical transports of sensible heat and angular momentum by cumulus-scale updrafts are proportional to $M_c(z)\,[T_c(z) - T'(z)]$ and $M_c(z)\,[u_c(z) - u'(z)]$ respectively. The uncertainty in each of these transports is estimated to be plus or minus a factor of four, by considering extreme assumptions.

The model equations are tested on 1900 hr of detailed rainfall data representing four seasons at Boston, Mass.; New Orleans, La.; San Juan, P.R.; and Tatoosh, Wash. The computed cumulus-scale vertical transports for different months are plausible, and during certain seasons at each station, the cumulus-scale fluxes are the same order of magnitude as larger-scale fluxes. The cumulus-scale sensible heat flux at Boston in July at the 6 km level is 70% as large as the average annual synoptic-scale heat flux, for Tatoosh in October a similar comparison gives 60% at the 4 km level, for New Orleans above 6 km the cumulus-scale flux exceeds the synoptic-scale heat flux by a factor of five in April and July, while at San Juan in October the cumulus-scale sensible heat transport at 7.5 km is 100% as large as the total required flux. Similar results are obtained by comparing cumulus-scale fluxes of angular momentum with the transport accomplished by the mean meridional circulation. Cumulus-scale transports become negligible in such locations as Tatoosh in summer and small in regions represented by Boston in winter and San Juan in winter and spring.

Analysis of the uncertainties in the calculations indicates that more accurate cumulus-scale transports may be obtained from a better understanding of the condensation and precipitation processes in cells and mesoscale areas. The model would be made more general by incorporating downdrafts, but too little appears to be known about them for their present quantitative inclusion. The plausibility of the results of this study indicates that the modelling technique could be applied to a more extensive climatological study of global transports.

Thesis Supervisor: James M. Austin
Title: Professor of Meteorology

ACKNOWLEDGEMENTS

The author most gratefully acknowledges his principal advisors, Professor James M. Austin and Dr. Pauline M. Austin for their guidance and encouragement during the development of this thesis. The critical comments and advice of Professor Frederick Sanders were also most helpful.

Appreciation is extended to Mrs. Mary Wolf for typing the final manuscript and to Mr. Steven Ricci for drafting the figures. The author's wife, Mrs. Yolonda Houze, was most helpful in typing initial drafts and proofreading the manuscript. The careful and accurate technical assistance of Mr. Christopher Schmandt in the data processing for Chapter IV was invaluable and especially marked by his interest.

The Massachusetts Institute of Technology and the National Science Foundation provided the author and his family with financial support and comfortable living conditions during their stay at M.I.T.

The author thanks his wife Yolonda for four and a half years of patience and his daughter Rebecca for the joy she has provided.

TABLE OF CONTENTS

TITLE	1
ABSTRACT	2
ACKNOWLEDGEMENTS	4
TABLE OF CONTENTS	5
LIST OF TABLES	8
LIST OF FIGURES	9
CHAPTER I. INTRODUCTION	13
CHAPTER II. TYPICAL PRECIPITATION PATTERNS	17
A. Occurrence of precipitation areas of various scales	18
1. New England	18
2. Other geographical areas	21
B. Characteristics of areas of various scales	24
1. Cells	24
2. Small mesoscale areas	25
3. Large mesoscale areas	27
4. Intensity of precipitation	27
C. Origin of mesoscale precipitation	29
D. Outcome of descriptive studies; empirical basis for modelling	35
CHAPTER III. MODEL STORM	37
A. General description of model	37
B. Role of entrainment in model	46
C. Mass of air transported upward	48
1. Basic equation for cellular mass transport	48
2. Specification of entrainment and vertical variation of $M_c(z)$	49
3. Expression for total cellular condensation	54
4. Mesoscale and synoptic mass transport	56
D. Temperature difference between cells and environment	57
E. Horizontal wind speed difference between cells and environment	64
F. Consistency between water budget and kinematics	65
1. Cells	66
2. Water budget and kinematics of whole storm	67
3. Limits and best estimates for cellular condensation	71

CHAPTER III cont'd

G. Uncertainties 72
H. Determination of input quantities 73
1. Cellular precipitation 74
2. Mesoscale and synoptic precipitation 74
3. Vertical structure of storm 75
4. Temperature in cells 76
5. Humidities 77
6. Synoptic-scale wind field 77
I. Computational scheme 77
J. Examples of calculations 80

CHAPTER IV. CLIMATOLOGICAL STUDY OF CUMULUS TRANSPORTS 85
A. Data sample 85
1. Selection of stations 85
2. Description of data 87
B. Data processing 90
1. Rain-gauge records 91
2. Radar data 93
3. Soundings 93
C. Monthly transports for each station 94
1. Computation of monthly curves 94
2. Standards of comparison 96
3. Results for Boston 98
4. Tatoosh 101
5. San Juan 102
6. New Orleans 105
D. Climatology of cumulus transports 107
E. Comment on temporal concentration of cumulus transports 113

CHAPTER V. CONCLUSIONS AND SUGGESTIONS FOR FURTHER RESEARCH 114

FIGURES 117

APPENDIX A. DATA AND METHODS OF ANALYSIS USED IN DESCRIPTIVE STUDIES OF NEW ENGLAND PRECIPITATION PATTERNS 151

APPENDIX B. SPECTRAL ANALYSIS OF RAIN-GAUGE RECORDS 157

APPENDIX C. CHARACTERISTICS OF LARGE MESOSCALE AREAS 164

APPENDIX D. INVESTIGATION OF SURFACE VORTICITY AND DIVERGENCE IN THE VICINITY OF MESOSCALE PRECIPITATION AREAS 169

APPENDIX E. FLOWCHART OF MODEL COMPUTATIONS FOR A STORM 173

BIOGRAPHICAL NOTE 179

REFERENCES 181

LIST OF TABLES

Table		Page
1	The average number and density of small mesoscale areas in each large mesoscale area at any one time.	20
2	Durations of small mesoscale areas.	26
3	Average areas and durations of large mesoscale precipitation areas.	26
4	Rainfall rates in areas of various scales for different storms.	28
5	Rate at which water is deposited by various parts of large mesoscale areas.	28
6	Vertical velocities considered realistic for model cells at heights of maximum updraft.	62
7	Peak updraft velocities measured in cumulus clouds.	62
8	Comparison of storm-averaged vertical velocities computed from model storm and from wind data.	69
9	Precipitation parameters for storm of 24-25 March 1969.	82
10	Total number of storms and total number of hours with at least 0.01 in of precipitation in data sample.	88
11	Total rainfall and the amounts considered cellular for 12 mo at Tatoosh.	103
12	Summary of comparisons of monthly cumulus-scale transports with transports by circulations of other scales.	108
A-1	Characteristics of Weather Radars at MIT.	151

LIST OF FIGURES

Figure		Page
1	Precipitation pattern showing large mesoscale areas, small mesoscale areas, and cells.	117
2	Distribution of number of large mesoscale areas appearing simultaneously in area observed by the radar, a circle with 200-km radius.	118
3	Distributions for average number at one time and density of cells within small mesoscale areas.	118
4	Plan position display of a hurricane as viewed with an airborne radar.	119
5	Average vertical extent of cells and of surrounding precipitation during different storms.	120
6	Examples of distributions of the durations of cells for individual storms.	121
7	Relations between depth, duration, and rainfall intensity for cells.	122
8	Distributions of areas of small mesoscale precipitation areas.	122
9	Relative humidity pattern shown by hourly soundings at Bedford, Mass.	123
10	Schematic diagram of model storm.	124
11	Sketch illustrating entrainment, detrainment, and vertical transport of an arbitrary quantity in cumulus cells.	125
12	Computed vertical mass transports for various assumptions about entrainment and detrainment.	126
13	Model cell radius and entrainment rate as functions of cell depth.	127
14	Model profiles of mass transport, entrainment rate, entrainment, detrainment, and net entrainment.	128

Figure		Page
15	Calculations of cellular temperature excess and hydrometeor content for different sets of assumptions.	129
16	Computed values of difference in westerly wind speed inside and outside of cells for two extreme values of drag coefficient.	130
17	(a) Curves of cellular temperature excess as computed from physical principles and approximated in model-storm program. (b) Temperature excesses for two different values of θ_e which characterizes the lapse rate in the cells.	131
18	Thirty-second average rainfall rates printed out by computer for the hours 1000 to 1200 EST, 25 March 1969, West Concord, Mass.	132
19	Photograph of MIT WR-66 radar RHI for 25 March 1969, 1140 EST.	133
20	Temperature soundings for Nantucket, Mass., 24-25 March 1969.	134
21	Westerly winds and least-square fits for Nantucket, Portland, and Albany, 24-25 March 1969.	135
22	Model cumulus-scale vertical mass transport, sensible heat transport, angular momentum transport and associated model temperature and westerly wind speed differences between cells and their immediate environment for the hour 1100 to 1200 EST, 24-25 March 1969, at West Concord, Mass.	136
23	Model cumulus-scale vertical mass transport, sensible heat transport, angular momentum transport and associated model temperature and westerly wind speed differences between cells and their immediate environment for the hour 1200-1300 EST, 9 July 1962, at West Concord, Mass.	137
24	Monthly upward transport of sensible heat by cumulus-scale cells at Boston.	138
25	Monthly downward transport of angular momentum by cumulus-scale cells at Boston.	140

Figure		Page
26	Monthly upward transport of sensible heat by cumulus-scale cells at Tatoosh.	142
27	Monthly downward transport of angular momentum by cumulus-scale cells at Tatoosh.	143
28	Monthly upward transports of sensible heat by cumulus-scale cells at San Juan.	144
29	Monthly downward transport of angular momentum by cumulus-scale cells at San Juan.	145
30	Monthly upward transport of sensible heat by cumulus-scale cells at New Orleans.	146
31	Monthly downward transport of angular momentum by cumulus-scale cells at New Orleans.	147
32	Latitude-height distribution of upward transport of heat by large-scale eddies in a model of the atmospheric general circulation, after Manabe et al (1970).	148
33	Latitude-height distribution of vertical transport of angular momentum by the large-scale eddies in an atmospheric general circulation model, after Smagorinsky et al (1965).	148
34	Winter heat budget for the belts 5^{o} N to 32^{o} N and 32^{o} N to 90^{o} N, and the vertical heat fluxes through the 500-mb surface and from the earth's surface. After Palmen and Newton (1969).	149
35	The winter total mass circulations and angular momentum budget north and south of latitude 30^{o} in the northern hemisphere. After Palmen and Newton (1969).	149
36	Vertical absolute angular momentum flow due to standing and transient eddies plus friction, on a meridional cross section through the atmosphere. After Starr et al (1970).	150

Figure		Page
A-1	Example of data from high-resolution tipping-bucket rain gauge.	155
B-1	Spectra of rainfall rate for seven periods of precipitation at Boston.	158
B-2	Spectrum obtained by converting individual spectra to a scale of wavelength and averaging the spectra for seven storms.	161
C-1	Precipitation pattern, as depicted by WR-66 radar, and surface winds and isobars for 5 November 1969, 1300 EST.	166
C-2	Distribution of elongation of banded structures formed by large mesoscale areas.	167
C-3	Orientation of elongated rain areas relative to surface isobars and surface wind direction.	167
D-1	Vorticity and divergence computed by the triangulation method from surface winds at three stations enclosing an area of 605 km^2 during a period when mesoscale precipitation areas were passing over the triangle.	170

CHAPTER I

INTRODUCTION

Meteorologists have studied cumulus convection from a variety of viewpoints such as its relationship to synoptic map parameters, its climatology, the dynamics and thermodynamics of cumulus development, and its accompanying condensation or precipitation processes. For the last two considerations, models of cumulus clouds have been postulated and explored (e.g. Weinstein, 1970; Simpson and Wiggert, 1969, 1971). Much of this modelling effort has been concerned with the question of what determines the vertical growth of a cumulus cloud. The investigation reported in this thesis has a different objective, namely, to study the role of cumulus convection as a transport mechanism in the atmosphere. The present concern, therefore, is the effect of cumulus rather than its mode of development.

Although it is recognized that cumulus convection transports such quantities as sensible heat and horizontal momentum vertically, quantitative estimates of the relative role of cumulus-scale processes in the total spectrum of atmospheric motions are difficult to obtain. The small horizontal dimensions and the turbulent nature of the cumulus phenomenon make it practically impossible to obtain useful measurements of such dynamically significant quantities as wind, temperature, pressure, and humidity. If cumulus transports are to be computed, a modelling technique is required. The inability to obtain satisfactory measurements of the conventional variables in and around cumulus clouds also has led the various investigators of growth aspects of cumuli to adopt a modelling approach.

From a climatological viewpoint, cumulus activity can be classified according to the occurrence or non-occurrence of precipitation. When cumulus cells are accompanied by precipitation, an important product of the convection, namely the rainfall, can be measured. The question arises whether cumulus transports can be deduced or modelled from a knowledge of the detailed nature of the precipitation associated with the convection. This study has been concerned, therefore, with the development of a consistent model which satisfies such readily observed aspects of the cumulus elements as cloud depth and surface rainfall amounts while remaining consistent with only the grosser features of the larger-scale environmental fields of temperature, humidity, and horizontal wind. The approach was suggested by Austin (1968). The applicability of the transport model which is developed here is tested, or at least indicated, by comparing the cumulus-scale transports of sensible heat and angular momentum, computed for a climatological sample of rainfall data, with fluxes which have been calculated by other investigators for larger-scale atmospheric modes of overturning. The comparison also provides some insight into the relative importance of cumulus-scale motion as a vertical transport mechanism in the atmosphere.

Chapter II of this thesis deals with the question of whether cumulus convection is organized within atmospheric precipitation systems in such a way that the rainfall associated with convective activity may be readily identified, measured, and represented in a parameterized manner. Further, an assessment of the cumulus-scale component of the total precipitation indicates the climatological significance of the process. Extensive analyses of precipitation observed with radars and

high-resolution rain gauges show that storms in all types of situations are in fact composed of certain basic structures.* The smallest are cumulus-scale elements or cells which have the largest rainfall rates and are 1 to 10 km^2 in area. Cells are always found within small mesoscale areas which are of the order of 100 km^2 and are less intense. Small mesoscale areas are usually found grouped together in large mesoscale areas of the order of 1000 km^2. Synoptic areas are larger than 10^4 km^2 and are usually associated with cyclones. Synoptic areas contain a number of large mesoscale areas which in turn contain small mesoscale areas and cells. Although a particular storm may not contain all of these scales, whenever one occurs, all of the smaller more intense ones are found within it. The origin of the mesoscale precipitation does not appear to be known and several possible explanations for its occurrence may be offered. One hypothesis is that part of the mesoscale precipitation is produced within the cumulus cells. This possibility is an important consideration for the modelling of cumulus-scale transports which are related to the amount of condensation that occurs in cells.

A model storm for which cumulus-scale transports of sensible heat and angular momentum are computed is developed in Chapter III. The model is composed of cells, mesoscale areas, and synoptic areas within which net transports of air upward are deduced from given or observed precipitation amounts. Temperature and horizontal momentum differences between cellular updrafts and their environments are computed from observed parameters of the vertical depth of the cells and broader

---

* The term storm in this study refers either to a horizontal area covered by precipitation or to a continuous period of precipitation at a point.

characteristics of the environment. Important aspects of the physical modelling involve specifying the entrainment process and relating condensation which occurs in cumulus updrafts to measurements of precipitation. Equations are developed from present theoretical and empirical knowledge of cumulus convection and uncertainties in the calculations are analyzed.

The model storm is applied in a climatological study of the vertical transports of sensible heat and angular momentum by cumulus updrafts. This investigation is discussed in Chapter IV. Input data for the model are obtained from a climatological sample of storms at Boston, Mass.; New Orleans, La.; San Juan, P.R.; and Tatoosh, Wash. These stations represent climates which on the basis of air mass properties would be expected to have different amounts of cumulus activity. From the calculations for these representative stations, a climatology of cumulus transports is constructed. This application of the model gives an indication of the relative importance of transports on the cumulus scale as compared with those arising from larger-scale motions in the atmosphere.

CHAPTER II

TYPICAL PRECIPITATION PATTERNS

In this chapter, several descriptive studies of precipitation patterns are discussed. These show that patterns in storms of different seasonal and synoptic types, and in different geographical locations, are composed of certain basic structures which may be described or modelled in a parameterized manner. In Chapter III, a model is described which has been designed to calculate the vertical transports of sensible heat and angular momentum by cumulus updrafts from certain observed parameters of a storm. As noted in Chapter I, a crucial aspect of this modelling involves estimating the amount of water condensed in cumulus cells from measurements of rainfall. Thus, an important observed parameter of the storm is the amount of rain which falls within intense cumulus showers. The descriptive studies discussed in this chapter, however, show that cumulus cells are typically organized within mesoscale precipitation areas of a few hundred to a few thousand square kilometers in dimension and that part of the mesoscale precipitation also may have been condensed within cumulus cells. It is therefore necessary to measure both cumulus and mesoscale rainfall to properly assess the amount of condensation which occurs within cumulus updrafts. Much of the present chapter is devoted to the description of the characteristics of basic features of precipitation patterns. It is this knowledge of typical patterns which makes it possible to identify and measure the observed input parameters for the model storm described and applied in the following chapters.

A. Occurrence of precipitation areas of various scales

1. New England

Quantitative radar observations made at MIT over a number of years have shown that precipitation patterns in both cyclonic storms and thunderstorm situations are characterized by the consistent occurrence of precipitation areas on the order of one hundred to several thousand square kilometers. As noted in Chapter I, these have been generally referred to as mesoscale precipitation areas since they are intermediate between showers produced by cumulus convection and the broad regions of precipitation usually associated with warm frontal lifting in extratropical cyclones. A particularly notable feature of mesoscale areas is that they are regions where cumulus activity is likely to be found.

Austin and Houze (1972) investigated quantitatively the structure of precipitation areas in New England with particular emphasis on the characteristics of mesoscale areas and their observed relationships to larger- and smaller-scale phenomena. The basic data used were quantitative radar PPI (Plan Position Indicator) and RHI (Range Height Indicator) displays and tipping-bucket rain-gauge records. The data and methods of analysis are described in more detail in Appendix A. Altogether, Austin and Houze examined precipitation patterns in 25 storms representing a variety of synoptic and seasonal situations.

They define the following horizontal scales for precipitation areas.

(1) Synoptic areas are 10^4 km^2 or more in area.

(2) Large mesoscale areas (LMSA's) are 10^3 to 10^4 km^2 in area.

(3) Small mesoscale areas (SMSA's) are 50 to 10^3 km^2 in area.

(4) Cells are 1 to 10 km^2 in area; they are assumed to be associated with cumulus convection.

The observed characteristics of cells, SMSA's, and LMSA's are described in some detail in section B of this chapter and in Appendix C. An example of a precipitation pattern containing all of the above scales is shown in Figure 1. An area of any of these scales is identified as a region with higher rainfall rates than its surroundings.

Synoptic areas were observed in each cyclonic storm analyzed, but not with a cold frontal passage or air mass thunderstorms.

Within every synoptic precipitation area there was at least one LMSA, usually several. The number of LMSA's present within a circle 200 km in radius surrounding MIT, ranged from one to six; the observed distribution is shown in Figure 2.

Within every large mesoscale area, both those in the synoptic precipitation areas and the frontal band which was per se a LMSA, several small mesoscale areas were found. Also, with the exception of the air mass thunderstorms, which in themselves were separate small mesoscale areas, SMSA's rarely, if ever, were observed outside of LMSA's. The number and concentration of small mesoscale areas within each large mesoscale area were recorded at several times during the lifetime of each large mesoscale area, and the average values of these quantities for any one time are listed in Table I.

Cells were almost always located either within a clearly identifiable SMSA or in a cluster forming an area of similar size. At least one cell was found within each SMSA. The number and concentration of cells within individual SMSA's

Table 1. The average number of small mesoscale areas in each large mesoscale area at any one time, N_{SM}, and the average density of SMSA's within each LMSA, D_{SM}.

	N_{SM}	D_{SM} (SMSA's per 2500 km^2)
18 May 1963	3	2
	4	4
8 July 1963 a	3	2
	4	3
8 July 1963 b	5	5
29 August 1962	5	3
17 September 1963	5	4
	6	3

were recorded at several times during their lifetimes and an average for each SMSA was obtained, the results being summarized in Figure 3.

The basic pattern which was observed is that a precipitation area of any of the three sizes, synoptic, LMSA or SMSA, contains one or several of the next smaller-sized areas. It should be pointed out, however, that the structures are not rigid. The lifetimes of the smaller areas are considerably shorter than those of the larger ones. A synoptic area may last several days moving along with the cyclone: LMSA's typically have lifetimes of several hours; SMSA's last about an hour; and the duration of cells ranges from a few minutes to about half an hour. Therefore the basic precipitation pattern continually changes texture as LMSA's build and dissipate within the synoptic areas, SMSA's build and dissipate within the LMSA's, and the individual cells are relatively short-lived components of the SMSA's.

An attempt was made to analyze the scales present in rainstorms more objectively and for a larger sample of data by performing a spectral analysis on tipping-bucket rain-gauge records. After several storms were analyzed, it became apparent that large mesoscale areas, small mesoscale areas, and cells which are notable by their rainfall intensities, horizontal and vertical dimensions, durations, and motions are not clearly characterized by local periodicities which are detectable by spectral analysis. The spectral computations are discussed in Appendix B.

2. Other geographical areas

Similar behavior in precipitation patterns is observed in other geographical areas. Browning and Harrold (1969) studied the detailed precipitation

pattern within a wave depression which passed over Great Britain. Within this disturbance, they found generally band-shaped areas with widths of 50 - 100 km and lengths of 300 - 900 km; within the bands there were more intense "small areas" of the order of 1500 km^2; clusters of cells were located within the "small areas."

Matsumoto, Ninomiya, and Akiyama (1967) described a family of mesoscale disturbances which passed over a dense rawinsonde network in Japan. They detected areas of upward motion of the same horizontal dimensions as Austin's and Houze's large mesoscale areas. Heavy snowfalls were associated with the passage of these areas, and cumulus-scale cells within these disturbances were observed by radar.

Mesoscale phenomena associated with frontal rainstorms in California are described by Elliott and Hovind (1964, 1965). They found that these storms were characterized by alternating warm-moist and cold-dry regions of the order of 10^4 km^2 in area, oriented roughly parallel to the frontal zone. Superposed on the first warm-moist area preceding the frontal passage they found bands of relatively more intense precipitation. These bands apparently also corresponded in dimension to Austin's and Houze's large mesoscale areas, and they contained cumulus showers of a few square kilometers in area.

Patterns of large mesoscale areas containing smaller ones which in turn contain cumulus-scale elements are also observed in the tropics. Figure 4 contains a quantitative plan position display obtained in a hurricane with an airborne radar. The rainbands which form a spiral pattern around the eye of the storm have the general dimensions of large mesoscale areas. Numerous small mesoscale areas

are aligned along each band; some of these appear as regions outlined by a particular contour of intensity while others are denoted as clusters of cells. In several instances, cells denoted by a contour of one level appear within a small mesoscale area which is outlined by a lower valued contour. In the northeast quadrant of the radar display, breaks along azimuthal lines in the precipitation pattern are caused by banking of the aircraft.

Mason (1970) notes that pictures from geostationary satellites reveal that, over the tropical oceans, cumulus and cumulonimbus clouds, individually 1 - 10 km across tend to group into mesoscale units up to 100 km in diameter and that these, in turn, form "cloud clusters" of 100 - 1000 km in diameter. These large mesoscale to synoptic-scale clusters are generally associated with the troughs of lower-tropospheric wave disturbances of characteristic wavelength 2,000 - 10,000 km or with the "intertropical convergence zone."

All of the above findings suggest that precipitation patterns at different latitudes and longitudes have some similar features in their horizontal structure. However, in view of the differences in the stability of air masses influencing the climates of different geographical areas, the cumulus-scale phenomena may be more extensively observed in some regions than others.

The occurrence of certain basic structures which may be identified in all types of storms allows the construction of model storms which may be used for a variety of purposes, such as to study precipitation mechanisms or, as described in the next chapter of this thesis, to evaluate cumulus convective transports.

B. Characteristics of areas of various scales

This section, with Appendix C, summarizes the detailed characteristics of precipitation areas of the different scales defined and studied by Austin and Houze (1972). More detail may be found in their paper and in Houze's (1969) thesis. Knowledge of these characteristics is used to set criteria for identifying and measuring basic parameters of the model storm described in the next chapter.

1. Cells

Horizontal dimensions of the cells could not be determined because they often appeared to be at least as small as the dimensions of the radar beam, but vertical extents were observed on the RHI by viewing cells at close ranges. In any single storm, the cells tended to be roughly the same height at their maximum development, but the depths of the cells and the position of the layer containing them varied considerably from storm to storm. Vertical extent of cells and height of the surrounding precipitation for each of the storms studied are shown in Figure 5. In the summer showers and thunderstorms the cells appeared to extend throughout the depth of the surrounding precipitation and protruded above, while in the cyclonic storms they seemed to be completely embedded in the more widespread rain.

Figure 6 shows distributions of the durations of cells measured in several storms. The distribution for 2 December 1962 is typical of the three winter storms in which most of the cells lasted only a few minutes. In cyclonic storms in other seasons there are also very many cells with only a few minutes' duration, but the distribution is broader as on 17 September 1963. In summer showers and thunderstorms cell lifetimes are usually between 15 and 25 minutes with very few shorter

than 10 minutes and very few longer than 30 minutes, the distribution for 9 June 1965 being typical.

The durations, depths and intensities of cells are more or less linearly related, as indicated in Figure 7. Each of the points in the figure represents one storm, showing the average values for the cells observed in that storm. The lines of least-square fit indicate that the cells tend to last about 5 minutes for every 2 km of height and for each 12 mm hr^{-1} of intensity.

The motions of cells observed from the radar were compared with the winds at the level midway between the top and bottom of the cells. Because of their short duration, cell motions were sometimes difficult to determine and in some of the storms appeared quite variable. On the average, however, velocities in each storm were roughly in agreement with the wind flow at the mid-cell level (within $\pm$ 25 degrees in direction and $\pm$ 50% in speed in all cases, and generally much closer.)

2. Small mesoscale areas

For each of the small mesoscale areas examined, the average area was computed from a number of individual observations during its lifetime, the values being given in Figure 8. The majority of the SMSA's were between 100 and 400 km^2, with occasional larger ones up to 800 km^2. Durations could be observed for only 15 of the SMSA's: for the other nine, either the data were interrupted or the areas moved out of range. The durations varied from 20 to 150 minutes as shown in Table 2, the median value being 50 minutes.

With the exception of the one isolated thunderstorm complex that was studied, the motion of the SMSA's appeared to be approximately the same as that of

Table 2. Duration of small mesoscale areas.

Time Interval (Minutes)	Number of SMSA's
<20	0
20-39	4
40-59	5
60-79	2
80-99	2
100-119	
120-139	
140-159	2

Table 3. Average areas and durations of large mesoscale precipitation areas.

Date	Area (km^2)	Duration* (min.)
18 May 1963	3000	200
	2200	240
8 July 1963 a	3000	80
	3300	> 80
8 July 1963 b	2500	720
29 August 1962	4000	240
17 September 1963	3300	> 210
	4500	> 210

*Durations preceded by > could not be determined more precisely because the data were interrupted.

the cells within it (again within $\pm$ 25 degrees in direction and $\pm$ 50% in speed).

3. Large mesoscale areas

Large mesoscale precipitation areas were recognizable in all of the storms except the air mass thunderstorm complex; however, the characteristics of LMSA's have not been determined as conclusively as the typical features of cells and SMSA's. The average areas, durations, and motions for those LMSA's which could be identified and followed for most of their lifetimes are listed in Table 3. The detailed characteristics of LMSA's, as observed by Austin and Houze (1972), are discussed in Appendix C.

4. Intensity of precipitation

Of the characteristics of precipitation areas, probably the most important for the model which is described in Chapter III are the relative precipitation rates in areas of various scales. In the modelling, cells and mesoscale areas are detected from rain-gauge records. Relative rates together with a knowledge of typical durations over the gauge are used to determine whether precipitation is cellular, mesoscale, or synoptic in the storms from which input data for the model are obtained.

Precipitation rates within the various areas, as determined from the radar and rain-gauge data, are summarized in Table 4. Although the rainfall rates within the mesoscale areas varied considerably from day to day, on any given day the variations were generally slight, except in the thunderstorm situations on 9 June 65 and 8 July 63 b. The ratios were about the same in all of the storms with the large mesoscale rate being 2 to 4 times as great as the small mesoscale rate, and

Table 4. Rainfall rates in mm hr^{-1} for synoptic-scale precipitation areas (r_S), large mesoscale areas (r_{LM}), small mesoscale areas (r_{SM}), and cells (r_C) in each storm.

Date	r_S	r_{LM}	r_{SM}	r_C
12 Jan 63	0.5	*	1-2	3-4
2 Feb 63	0.5-1	*	2-3	5-10
18 May 63	0.2-0.5	2-3	5	10-15
9 Jun 65	0	0	5-20	45-90
8 Jul 63 (a)	0.5-1	2	5	10-40
8 Jul 63 (b)	0	0.5-5	5-25	20-100
29 Aug 62	0.5-2	5	10	15-20
17 Sep 63	Trace	0.5-1	2	4-15
6 Dec 62	0.5-1	*	3-6	10-50

*Not possible to determine.

Table 5. Water deposited by various parts of the larger mesoscale areas. LM denotes region in LMSA's but outside of SMSA's; SM is in SMSA's but outside of cells, and C denotes within cells.

Date	Total for LMSA (10^7 m^3 hr^{-1})	Percent in each area		
		LM	SM	C
18 May 63	10.4	52	42	6
	7.1	33	65	2
8 Jul 63 a	10.4	51	44	5
	15.7	27	48	25
8 Jul 63 b	31.2	11	54	35
29 Aug 62	32.7	22	69	9
17 Sep 63	2.8	37	42	21
	3.4	29	55	16

the small mesoscale rate about twice the size of the large mesoscale rate. The rates in the cells varied more widely, ranging from 2 to 10 times as large as the small mesoscale rate.

The rate at which water was deposited by areas of each scale was computed from their observed rainfall rates and their average areas during the lifetime of each large mesoscale area. In these computations an area of 8 km^2 was assigned to each cell. The rates of deposit which were calculated are in Table 5; it is evident that of the total water deposited by the large mesoscale areas, significant fractions came from each of the small and large mesoscale regions, while the cellular contribution ranged from 2 to 35 percent.

C. Origin of mesoscale precipitation

In this section, the term mesoscale precipitation refers both to the enhancement over the synoptic rate in regions surrounding cumulus cells in cyclonic storms and to the lighter precipitation observed in the vicinity of the intense cells in bands or complexes of thunderstorms. While there is little doubt that the rain which falls from the cells is condensed within cumulus updrafts, the origin of the mesoscale precipitation does not appear to be known. Several explanations which may be offered for the occurrence of mesoscale precipitation areas are discussed in this section. It is important to understand the origin of the rain which falls from areas of different scales since in the modelling described in Chapter III, the amount of water condensed in cells is estimated from measurements of precipitation.

An hypothesis is advanced by Austin and Houze (1972) that part of the mesoscale precipitation is actually formed in cumulus updrafts and is spread by

divergence aloft or simply left as cloud when the updraft dies. In particular, this hypothesis is directed toward explaining the origin of the precipitation in SMSA's which appear to have a close relationship with the cells, shown by the facts that every SMSA contained at least one cell and that their motions were very similar to those of the cells within them. As pointed out by Houghton (1968) cumulus updrafts are generally of such short duration that they have a low precipitation efficiency. During the time that the updraft is active, water is condensed out rather rapidly in a region of limited horizontal extent. When the updraft dies part of the condensate falls out quickly forming the sharp showers we call cells, but considerable amounts of condensate remain aloft as cloud or small precipitation particles which fall slowly and may be spread by divergence over a larger area. If several updrafts or cells form close to each other either simultaneously or in a sequence, the condensate which they leave aloft would accumulate to create a small mesoscale precipitation area which would last as long as cells continue to develop within it but would rain out and disappear shortly after the cessation of convective activity. This hypothesis is supported by the results of Melvin (1968) who, using quantitative radar displays, examined six thunderstorm complexes for their entire lifetimes and also a developing squall line. He found that the precipitation areas appeared to develop around the cells and lasted only as long as cells continued to form. He also computed the updraft velocities which would be required to produce the condensate for the observed precipitation and for various assumed values of the efficiency of precipitation; the resulting values appeared quite reasonable.

Qualitatively, this hypothesis appears plausible for small mesoscale areas in cyclonic storms also. If cells are embedded in more widespread precipitation, any condensate which is not deposited in the resulting shower would be added to the general rain forming a small mesoscale area around a group of showers. At least one cell was observed in every SMSA; but in some of them, the percentage of rain in the cells is extremely small compared with that in the small mesoscale areas, and some other mechanism may be involved.

Enhanced precipitation in mesoscale areas could reflect variations on the mesoscale of any one of several other quantities such as vertical velocity, humidity, temperature, or condensation nuclei.

There does not appear to be much basis to expect that mesoscale precipitation areas are associated with systems of lifting on the same scale. The presence of cumulus activity in mesoscale precipitation areas indicates that these regions are probably characterized to some extent by conditional instability. Bjerknes (1938) showed that conditional instability is more likely to be released in cumulus convection than any larger-scale mode of overturning. Moreoever, spectral analyses of wind data such as those of Van der Hoven (1957) and Oort and Taylor (1969) suggest a dearth of atmospheric motion systems between cumulus and synoptic scales. Their data, however, are probably more representative of average atmospheric conditions than of unstable flow in particular.

Another factor which might influence the mesoscale distribution of precipitation is the natural inhomogeneity in the humidity field. Austin's and Houze's (1972) observations indicate that the precipitation rate in a small or large mesoscale

area is about twice that in the region outside the mesoscale area. If a 2 - 3 km layer of air in an otherwise saturated air mass is too dry to become saturated except in certain mesoscale areas, it is possible that the rainfall rate resulting from a given amount of vertical motion in a broad area will be twice as great in the mesoscale moist regions than in the rest of the area outside the mesoscale regions. To investigate this possibility, 168 soundings taken at hourly intervals at Bedford, Mass., were used to construct a time cross section of the relative humidity field. (These data are published by Court and Salmela, 1961.) The period of observation included four rainy and cloudy spells alternating with relatively dry periods. One moist and one dry period are shown in Figure 9. During all of the wet periods, the depth of the moist layer varied by 1 to 3 km in a regular pattern with maximum depths appearing at intervals of approximately 3 hr. This suggests that some areas of mesoscale dimension were becoming saturated more quickly than others during the rainy periods. Whether this is due to moisture inhomogeneity is not clear; however, one reason to suspect that it is not is that during the dry periods similar regular fluctuations in humidity were not observed.

The horizontal variation of temperature is not important in determining mesoscale precipitation patterns. It can easily be verified that doubling the rainfall rate in an atmosphere with a moist adiabatic lapse rate and a parabolic vertical velocity profile between 0 and 10 km requires an increase in the 1000 mb temperature of about 10^{o} C. Thus, to account for the factor of two differences between the precipitation rate within a mesoscale area and that outside the area would

require horizontal temperature variations of 10^{o} C on this scale. Synoptic experience clearly denies the existence of variations of this sort.

It might be suggested that horizontal variations in the concentration of natural ice nuclei lead to variations in the areal distribution of precipitation intensity. However, some computations by Houghton (1968) suggest that this is highly unlikely. He indicates that while spatial variations in nuclei concentration may affect the time of onset of precipitation, they are not likely to affect the instantaneous rainfall rate within an established stratiform rain situation. The concentration of ice nuclei which are activated tends to increase exponentially with decreasing temperature; as a result, the effect of variations in the nucleus concentration at a particular height is to raise or lower, by not more than about $\pm$ 1 km, the level at which sufficient precipitation particles are formed in order to initiate the precipitation process. The concentration of ice crystals formed is usually sufficient to remove all the condensate in the form of liquid water; therefore, within a well-established storm system the horizontal distribution of natural ice nuclei should not be reflected in the instantaneous precipitation patterns. Since many mesoscale precipitation areas are observed well within the interior of established synoptic-scale precipitation areas, it seems that the horizontal variation of ice nuclei concentration is probably not the factor determining their existence.

Of the considerations concerning the origin of mesoscale precipitation, the one offered by Austin and Houze (1972) is the only one which requires the presence of cumulus cells within mesoscale areas. All of the others suggest a means for enhancing the rainfall rate in a mesoscale region that would work just as well without

cells present. Yet mesoscale areas always contain some degree of cumulus activity, and it is hard to believe that this is a coincidence. Therefore, the postulate of a cellular origin for at least part of the mesoscale precipitation, namely that in the small mesoscale areas, seems most attractive. The plausibility of this hypothesis makes it an important consideration in the calculations of cumulus transports as described in the following chapters of this thesis. In these calculations, the total amount of water condensed within cumulus updrafts is estimated from measured precipitation amounts. According to the hypothesis of Austin and Houze, a fraction of the total mesoscale precipitation should be considered part of the cellular condensation. As a consequence, it becomes necessary to measure both the cellular and mesoscale components of the total precipitation deposited by a storm if the processes within it are to be modelled realistically. However, since Austin's and Houze's hypothesis has not been proved conclusively, and since it probably does not apply to the large mesoscale areas, an uncertainty concerning the amount of total mesoscale precipitation which can be considered of cellular origin is taken into account in the calculation of cumulus transports of physical quantities in the following chapters.

A better understanding of the origin of mesoscale precipitation might be obtained if the dynamics of atmospheric disturbances associated with the mesoscale precipitation areas were understood. The possible role of "conditional instability of the second kind (CISK)" (Charney and Eliassen, 1964) in the development of mesoscale areas was investigated. This study was inconclusive; however, it is described in Appendix D.

D. Outcome of descriptive studies; empirical basis for modelling

From the extensive study of precipitation patterns, it has been determined that certain characteristics occur consistently in all types of storms while others vary considerably from storm to storm. In the horizontal, it has been found that four distinct scales of precipitation areas occur; synoptic areas which are larger than 10^4 km^2 and have a lifetime of one or several days; large mesoscale areas which range from 10^3 to 10^4 km^2 and last several hours; small mesoscale areas which cover 100 - 400 km^2 and last about an hour; and cells which are roughly 10 km^2 and often last only a few minutes, rarely as long as half an hour. In the cases which were analyzed not every storm contained areas of all of these scales; however, when an area of any particular scale occurred, it contained areas of each of the smaller scales, one within the other. The vertical location and depth of the layer containing cumulus cells varied greatly from one storm to another, but remained about the same within any particular storm.

The consistent occurrence of precipitation patterns with similar characteristics and behavior in a variety of storms makes it possible to describe any storm in a parameterized manner which retains the storm's basic features while eliminating much cumbersome detail. Moreover, as discussed in the next chapter, the parameters used to describe the storm may be chosen so that other physical properties of the storm may be computed from them. In this way small-scale phenomena within a storm may be investigated without having to observe temperature, pressure, humidity, and wind at subsynoptic-scale grid points.

The model storm described in the next chapter is designed specifically to calculate vertical transports of physical quantities by cumulus updrafts given certain observed parameters of the storm. A crucial aspect of this particular modelling is that an estimate of the total condensation within cumulus updrafts can be obtained from measurements of surface precipitation. With an approximate knowledge of the storm's vertical structure and the general synoptic-scale distribution of other variables, an estimate can be made of the mass of air that had to rise through various levels in cells to produce the total cellular condensation. The important observed parameter would appear to be the cellular precipitation. However, the consistent occurrence of cells within mesoscale areas and the plausibility that part of the mesoscale precipitation is of cellular origin make it necessary to consider both the cellular and mesoscale precipitation in estimating cellular condensation.

A realistic storm model could also be useful for studying the precipitation mechanisms in areas of the various scales. A model for this purpose, however, would be more complex and detailed than the one developed in the next chapter for computing cumulus transports. It is hoped that experience with the present model will be useful in designing one for studying precipitation processes.

CHAPTER III

MODEL STORM

A model storm designed to calculate the vertical transports of physical quantities by cumulus cells is described in this chapter. The model is based both on the observational experience related in Chapter II and on current dynamical and empirical knowledge of cumulus convection. For input it requires detailed measurements of precipitation but only the general synoptic-scale distributions of other variables. The application of this model in a climatological study of the vertical transports of sensible heat and angular momentum by cumulus convection is discussed in Chapter IV.

A. General description of model

The model storm is conceived of as a region of precipitation composed of cumulus cells, mesoscale areas, and synoptic areas, one within the other. Descriptive studies show that precipitation patterns are typically composed of areas of these various scales regardless of the season, synoptic situation, or geographical area. The vertical distribution of properties and processes within each of the basic areas are also represented in an idealized manner for the model storm. In particular, transport processes associated with cumulus-scale convection within a storm are simulated. It is noted that the condensation which precedes the fallout of a certain amount of precipitation in a storm necessarily is accompanied by the transport of air upward through various levels of the atmosphere. Any part of the rising air that is contained within cumulus updrafts has temperatures and horizontal velocities

which are systematically different from those in the larger-scale environment at each level. Depending on the signs of these differences, then, either more or less sensible heat and angular momentum is transported upward by the ascending air at each level in the storm than if there were no cells and all of the air rose with the temperature and horizontal momentum of the larger-scale atmosphere.

Equations for computing the excess transports of sensible heat and angular momentum due to air rising in cumulus updrafts within the model storm are developed in subsequent sections of this chapter. Quantities assumed to be given in these equations are obtained by observing certain properties of the atmosphere during an actual rainfall situation. The primary measured quantity is precipitation. Measurement of rainfall in an actual storm could be made either with areal detail at given instants, as with a radar, or for a period of time at a point with a high-resolution rain gauge. The latter method is used in this investigation and the term storm as used throughout this chapter refers to a continuous period of rainfall at a station. The model can be envisioned in terms of a time-vertical cross section as shown in Figure 10. The quantities in the figure that are inferred from atmospheric observations as input for more detailed model calculations are:

R_c = amount of cellular precipitation

R_m = amount of mesoscale precipitation

R_s = amount of synoptic precipitation

T_c = temperature in cells

q_c = water vapor mixing ratio in cells

q_o = water vapor mixing ratio outside storm

u' = westerly wind speed outside cells

z_T = height of cell tops

z_B = height of cell base

z_P = depth of layer of lighter rain in mesoscale and synoptic areas surrounding cells.

The exact methods by which the above quantities are derived from the data are discussed more precisely in section H of this chapter, however, some general comments about each are made here.

Of the measured quantities, only the precipitation amounts, R_c, R_m, and R_s, are derived from observations which must be available continuously during the passage of the actual storm being modelled. The rain gauge must also have sufficient resolution to detect showers associated with cumulus-scale cells. Criteria to determine when cells, mesoscale areas, and synoptic areas are over the gauge are based on typical relative magnitudes of rainfall rates in the areas of different scales and their typical durations over the gauge. The criteria used are consistent with the observational experience described in Chapter II. No distinction is made in the present model between large and small mesoscale areas. Experience in analyzing precipitation patterns has shown that this differentiation can be made in a particular storm only by detailed study of a sequence of two-dimensional horizontal precipitation patterns, such as given by a radar PPI. However, such detailed analysis would preclude treatment of a sufficient number of storms for a climatological study,

Also recorded with the precipitation amounts are the total times Δt_c, Δt_m, and Δt_s that cells, mesoscale areas, and synoptic areas are over the rain gauge. These time periods do not play a major role in the computations of transports; they are involved only in minor and indirect roles. The basic precipitation parameters for the model calculations are amounts, not rates.

Of particular interest for the modelling is how much of the total precipitation is condensed within cumulus updrafts. Austin and Houze (1972) point out that part of the mesoscale precipitation may in fact originate within the cumulus-scale cells. This possibility is taken into account in the model by introducing the parameter α which is shown in Figure 10 and is the fraction of mesoscale precipitation assumed to have been condensed in cells. In the model computations, α is assigned values ranging from zero to one since the question of how much mesoscale rain comes from the cells is not yet resolved. Although all the possible values of α are considered, values close to unity are probably unrealistically large in most cases since the hypothesis of a cellular origin for mesoscale rainfall refers only to the small mesoscale areas, while the precipitation to which α is applied is the total, small plus large, mesoscale amount.

The quantities T_c, q_c, q_o, and u' which are functions of height are inferred from rawinsonde observations made at standard 12 hr intervals in and around the actual storm being modelled. The temperature T_c in the cells is assumed to follow a moist adiabat which approximates the vertical distribution of temperature shown by soundings of the real storm. The measured temperatures of the large-scale environment may be used to indicate in an idealized manner the temperatures in the

cells since cells and environment never differ by more than about 2^{o} C and the quantity which is sought for the calculation of transports is an estimate of the difference between the temperature of the cells and that of their immediate environment. The temperature of the latter is represented by the symbol T' in Figure 10 and is computed as a deviation from T_c by means of equations expressing the dynamics, condensation processes, and entrainment in the cumulus updrafts. Since the quantity needed for the heat transport calculations is the difference T_c - T', it is immaterial which of T_c and T' is considered given and which computed in the model calculations. The equations were found to be slightly easier to program with T_c being given; hence T' is the computed quantity in this investigation..

In any region of the model where precipitation occurs, the air is assumed to be saturated. Thus in the cells, q_c is the saturation mixing ratio corresponding to the moist-adiabatic temperature distribution T_c. In the mesoscale areas and synoptic areas q' is the saturation mixing ratio corresponding to the temperature distribution T'. The mixing ratio q_o of water vapor outside the storm, is approximated by multiplying the relative humidity function indicated in Figure 10 times the saturation mixing ratio q'. The two-layer relative humidity distribution shown in the figure is an approximation to the distribution of humidity shown by the soundings taken immediately outside the real storm. The symbol H_1 represents the mean relative humidity in lower layers while H_2 is the mean relative humidity aloft. The level separating the regions to which H_1 and H_2 refer is allowed to vary from storm to storm as are the magnitudes of H_1 and H_2. In Figure 10, the mixing ratio in the synoptic area is indicated as either q_o or q' implying that in any storm a synoptic

precipitation area may or may not be present; the saturation value q' is used if synoptic rainfall is observed, if not, the unsaturated value q_o is used.

The temperatures and humidities shown by the soundings in and around storms do not vary enough during the course of most storms to justify having T_c, q_c, and q_o vary with time in the model; therefore, they are assumed constant in a particular storm.

Only the westerly component of the wind is considered since in the transport computations the quantity of interest is the angular momentum about the earth's axis. The westerly wind speed in the storm, outside the cells, is approximated as a linear fit to winds observed between 850 and 400 mb at standard sounding times. Since the wind shear often varies considerably from one sounding to the next, values of the linear shear are interpolated according to the time when cumulus cells occur between soundings. The westerly wind u_c in the cells is computed as a deviation from u^* from principles of cumulus dynamics and entrainment.

The height parameters, z_T, z_B, and z_p are determined from records of a radar RHI which shows the vertical structure of the precipitation in a storm at representative times during its passage over the station. The quantities z_B and z_T are assumed constant in a modelled storm since the descriptive studies show that the layer containing cells is typically uniform within individual storms, although it varies greatly from storm to storm. The height z_p is assumed constant for simplicity. It is not a particularly important quantity in the calculations of transports and it is difficult to measure very precisely.

The model-storm quantities shown in Figure 10 which are computed from the various observed storm parameters are:

T' = temperature in air immediately outside cells

u_c = westerly wind speed in cells

M_c = mass of air transported upward per unit area through different levels within cumulus cells

M_m = mass of air transported upward per unit area in mesoscale areas

M_s = mass of air transported upward per unit area in synoptic areas

C = total amount of water condensed in cumulus cells

The quantities M_m and M_s are not directly involved in computing the heat and angular momentum transports by cumulus convection; however, they are involved in an analysis of the overall water budget and kinematic consistency of the model storm. From the first three computed quantities listed above, the transports of sensible heat and angular momentum due to air rising in the model storm within cumulus updrafts are formulated as

$$\mathcal{T}_{SH}(z) = M_c(z)\, C_p\, [T_c(z) - T'(Z)] \tag{1}$$

and

$$\mathcal{T}_{AM}(z) = M_c(z)\ a\ \cos\phi\ [u_c(z) - u'(z)] \tag{2}$$

where z is height, C_p is the specific heat of air at constant pressure, a is the earth's mean radius and ϕ is the latitude where the storm occurs. These are the quantities computed and analyzed for a climatological sample of storms in the next chapter.

The heat and angular momentum transports expressed in (1) and (2) are only a part of the total transports accomplished by cumulus convection in a rainstorm. The upward transport of air which is computed for the cells is the net result of upward plus downward motion in the convective elements which is required to produce the total cellular condensation C. What is computed then is a lower limit for the amount of air which rose in the upward branch of the convection, where the downdrafts are viewed as updrafts in reverse for the calculation of mass transports. The effects of the downdrafts upon transports of heat and horizontal momentum are not calculated because too little appears to be known about the mechanisms involved to handle them in a quantitative manner. It is noted qualitatively, however, that the effect of downdrafts would be to add to the cumulus-scale transports of heat and angular momentum. The compensating upward transport should be included in $M_c(z)$ and, it is noted, the downdraft air would have a temperature deficit rather than excess relative to the environment and also the difference in the horizontal momentum would probably be of the opposite sign to that of the rising air.

It is emphasized that the transports of air upward, M_c, M_m, and M_s, are not rates of transport, but are simply the net amounts of air transported upward per unit area to produce the condensation which occurs in the areas of different scales. Since the gross effect of transports in numerous storms over climatological time periods is being investigated, it is not necessary to know the instantaneous rates of transport and questions concerning the time scales of lifting in the various areas can be avoided for the most part.

The quantities M_c, M_m, and M_s are related to the condensation which occurs in cells, mesoscale areas, and synoptic areas, respectively. The measured quantity is precipitation and the condensation is deduced from observations of rainfall. The synoptic rainfall, R_s, and the portion of the mesoscale rainfall which does not originate in cells, $(1-\alpha) R_m$, are assumed to be equal to the condensation in the synoptic and mesoscale areas respectively. The fraction α of mesoscale rainfall R_m which is assumed to have originated in the cells must be properly attributed to the cellular condensation C. Another problem in relating C to measurements of precipitation involves modelling the inefficient nature of the precipitation processes in cumulus convection. It is shown observationally by Braham (1952) and from microphysical considerations by Houghton (1968) that cumulus updrafts leave considerable amounts of condensate aloft as cloud when they die. The question arises whether this condensate left behind by the cumulus cell is ultimately rained out somewhere else in the total storm, as within the mesoscale areas, or whether when the large-scale storm complex dies out some of this condensate is left behind. Another parameter β is therefore introduced in the computations to represent the inefficiency of the cells in producing rainfall from condensate. β is the ratio of the total mass of condensate C formed in cells to the amount of that condensate which is deposited as precipitation anywhere within the storm. A final, but not too important, consideration in estimating cellular condensation from precipitation involves correcting the rainfall R_c observed at the ground directly beneath cells for the amounts of rain produced above and below the cells.

Following sections of this chapter give more detailed descriptions of the principles and methods involved in calculating $M_c(z)$, $T_c(z) - T'(z)$, $u_c(z) - u'(z)$, $M_m(z)$ and $M_s(z)$ from the observed model parameters.

B. Role of entrainment in the model

The calculations of $M_c(z)$, $T_c(z)$, and $u_c(z) - u'(z)$ each involve the concept of horizontal entrainment of air into cumulus updrafts. This concept may be considered in terms of the conservation of an arbitrary quantity ξ in the region of a cell bounded by z and z + dz as shown in Figure 11. This conservation is expressed by the differential equation

$$M_c \xi_c - [M_c \xi_c + (dM_c)_i \xi_c - (dM_c)_o \xi_c + M_c d\xi_c] + \xi'(dM_c)_i - \xi_c (dM_c)_o = S dz \qquad (3)$$

where the subscript c refers to quantities evaluated in the cell, the prime refers to quantities evaluated in the environment, $(dM_c)_i$ and $(dM_c)_o$ are positive quantities representing the masses of air entering and leaving the cell in the layer dz, and S is the change in $M_c \xi_c$ per unit depth that results from various sources of ξ_c acting on the cell between z and z + dz. The term cell in this discussion and those to follow is used in reference to the region of updraft in which the water appearing as a cumiliform shower is condensed. The showers themselves are usually also called cells in discussions of precipitation patterns. The quantities on the left-hand side of (3) represent the amounts of ξ carried into and out of the cell by air entering and leaving vertically and horizontally. It is noted that in (3) the terms involving $(dM_c)_o$ disappear by cancellation. From physical considerations, this happens because

the exiting air in no way influences the dilution of property ξ in the cell. Only the air entering laterally from the environment characterized by a value of ξ different from that in the cell can do this. On entering a cell, air from the environment is assumed to mix completely and instantaneously with the air in the cell to preserve homogeneity in the cell. After making cancellations, rearranging terms, and dividing through by $M_c dz$, equation (3) may be rewritten as

$$\frac{d\xi_c}{dz} = \frac{1}{M_c}\left(\frac{dM_c}{dz}\right)_i (\xi' - \xi_c) + \frac{S}{M_c} \quad . \tag{4}$$

In the model calculations described below, the cell properties, $M_c(z)$, $T_c(z) - T'(z)$, and $u_c(z) - u'(z)$, all are obtained from equations of this form.

The term $M_c^{-1} (dM_c/dz)_i$ in (4) is called the "entrainment rate" and has been studied considerably in laboratory experiments with buoyant convective elements in the forms of steady state jets (e.g., Morton, Taylor and Turner, 1956) and bubbles (e.g., Scorer, 1957). These experiments show that the entrainment rate may be parameterized in terms of the radius r of the convective elements in the form

$$\frac{1}{M_c}\left(\frac{dM_c}{dz}\right)_i = \frac{\epsilon}{r} \tag{5}$$

where ϵ is an empirically determined constant. Turner (1962, 1963) finds appropriate values of ϵ to be 0.2 for jets and 0.6 for bubbles. Levine (1959, 1965) gives a theoretical basis for expressing the entrainment rate inversely proportional to the radius. Following these developments, Malkus (1960), Simpson and co-workers (1965, 1969, 1971) and Weinstein (1970) have applied equations of the form (4) in

which $M_c^{-1} (dM_c/dz)_i$ is expressed as ϵ/r with $\epsilon = 0.2$ with some success to the prediction of cumulus cloud development. Warner (1970) cautions, however, that applying these equations is of a somewhat empirical nature and parameters such as ϵ may be "calibrated" to particular atmospheric situations. From the laboratory experiments and from Simpson's work it is nevertheless evident that the entrainment rate can be adequately expressed by (5) with ϵ on the order of .1, but with some disagreement on its exact value.

Assumptions which are made concerning entrainment in the present model are kept in as close a correspondence to laboratory and field experience as possible, and cloud or cell properties obtained from model calculations are simply interpreted as the best estimates possible given the current knowledge of cumulus dynamics. Since this knowledge is incomplete, the quantities estimated have associated with them uncertainties which must be considered as carefully as possible.

C. Mass of air transported upward

1. Basic equation for cellular mass transport

If ξ represents the water vapor mixing ratio in equation (4), the source term S is given by dm/dz which is the mass of water condensed per unit depth and horizontal area in cumulus cells during a particular storm. Substituting these quantities into (4) we obtain

$$-\frac{dq_c}{dz} = -\frac{1}{M_c}\left(\frac{dM_c}{dz}\right)_i (q'-q_c) + \frac{1}{M_c}\frac{dm}{dz} \quad . \qquad (6)$$

Integration of (6) from cell base z_B to cell top z_T gives

$$C \equiv \int_{z_B}^{z_T} dm = \int_{z_B}^{z_T} M_c \left[\frac{1}{M_c} \left(\frac{dM_c}{dz} \right)_i (q' - q_c) - \frac{dq_c}{dz} \right] dz. \quad (7)$$

The aim is to solve (7) for $M_c(z)$ given a value of the cellular condensation C which is estimated from measurements of precipitation. Other observed quantities which are provided are the cell base z_B, cell top z_T, and the water vapor mixing ratio q_c in the cells. The mixing ratio q' is the saturation mixing ratio for the computed temperature T'(z) outside the cells. Since M_c is a function of z and is inside the integral it is necessary to make some specifications regarding its form in order to solve for the magnitude of M_c. The entrainment rate $M_c^{-1} (dM_c/dz)_i$ is also prescribed.

2. Specification of entrainment rate and vertical variation of $M_c(z)$

The entrainment rate and the z-dependence of $M_c(z)$ in equation (7) should be specified together in a kinematically consistent way. The derivative of $M_c(z)$ is expressed as the difference between the masses of air entering and leaving the cell laterally per unit depth of cell. This is written

$$\frac{dM_c}{dz} = \left(\frac{dM_c}{dz} \right)_i - \left(\frac{dM_c}{dz} \right)_o \quad (8)$$

where $(dM_c/dz)_i$ is called the "entrainment," which is to be distinguished from the "entrainment rate" $M_c^{-1} (dM_c/dz)_i$, and $(dM_c/dz)_o$ is called the "detrainment." According to (8), the choices of the entrainment rate and the z-dependence of $M_c(z)$ automatically determine a pattern of detrainment. It seems reasonable to require

from the outset that $M_c(z)$ increase monotonically from a minimum at z_B to a maximum at some level ζ between z_B and z_T and then decrease monotonically to another minimum at z_T. With dM_c/dz positive below ζ, it is evident from (8) that the detrainment is smaller than the entrainment below ζ, and by similar reasoning, detrainment outweighs entrainment above ζ. Although very little appears to be known about the vertical distribution of detrainment, at least the above limitations seem rather definite.

Throughout the calculations of $M_c(z)$, $T_c(z) - T'(z)$, $u_c(z) - u'(z)$, the entrainment rate is expressed as ϵ/r as in equation (5) with $\epsilon = 0.2$ and with r determined appropriately but considered constant for each individual storm. This is consistent with the current knowledge of cumulus dynamics and is identical to the formulation used by Simpson and Wiggert (1969, 1971) and Weinstein (1970) in their most recent work.

The z-dependence of $M_c(z)$ below level ζ is expressed by the function $f_c(z)$ in the relation

$$M_c(z) = M_c(\zeta)\, f_c(z) \qquad (z \leq \zeta). \quad (9)$$

The quantity $f_c(z)$ is non-dimensional, positive, and monotonically increasing from a value which is less than or equal to 1 at z_B to a maximum of 1 at ζ. The various forms which $f_c(z)$ may take when the entrainment rate is expressed as a constant (ϵ/r, r = constant for a storm) are investigated by considering limiting cases. As mentioned above, these are determined, below ζ, by detrainment equal to entrainment

at one extreme, and by no detrainment at the other. It is readily determined from (8), upon substituting from (9) for $M_c(z)$ and from (5) for the entrainment rate, that $f_c(z) = 1$ in the case of detrainment equal to entrainment and $f_c(z) = \exp\left[\left(-\frac{\epsilon}{n}\right)(\zeta - z)\right]$ in the case of no detrainment.

Several curves of $M_c(z)$, shown in Figure 12, are obtained from equation (7) for an amount of cellular condensation which is arbitrary but the same for all the curves. The mixing ratios q' and q_c are expressed as simple analytic functions which are also the same for all cases shown. A curve is obtained for the extreme cases of no detrainment and detrainment equal to entrainment for different values of ζ for cells 6 km in depth with bases at 1 km. A cell radius of 0.2 km which is considered to be smaller than realistic is chosen because it exaggerates the difference between the curves for the two extreme f_c's. Above ζ, $M_c(z)$ is simply allowed to decrease linearly to a value of zero at the top of the cells. The shaded area is the region within which similarly computed curves for other ζ's would be located. This area may be interpreted as the uncertainty in the choice of a particular profile for $M_c(z)$ and the best estimates of the correct curve would be expected to lie near the middle of this region.

The solid curve in Figure 12 which lies near the middle of the shaded area is also obtained from equation (7) and is the one which is chosen for the calculations described in the next chapter. From Figure 12 it appears that the upper and lower limits indicated by the extremities of the shaded area are within a factor of two of the curve selected for computations except for a shallow layer at the top. Therefore, it is concluded that the uncertainty introduced by assumptions regarding

the entrainment rate and the shape of the mass transport curve is approximately plus or minus a factor of two at any level. It is noted, however, that this is mainly an uncertainty in the distribution of $M_c(z)$ in the vertical and does not have much effect on the vertical average of $M_c(z)$. The uncertainty in the overall magnitude of $M_c(z)$ is mainly that associated with specifying the cellular condensation on the left-hand side of (7) from measured rainfall amounts.

The particular z-dependence illustrated by the solid curve in Figure 12 and used in computations was obtained by trial and error; its analytic expression is given by (9) with

$$f_c(z) = \frac{2}{2-\frac{\epsilon}{r}} \exp\left[\left(\frac{\epsilon}{r}\right)(z-\zeta)\right] - \frac{\frac{\epsilon}{r}}{2-\frac{\epsilon}{r}} \exp\left[2(z-\zeta)\right] \qquad (10)$$

below ζ . The units of r, z, and ζ in (10) are kilometers.

Above ζ , $M_c(z)$ is simply obtained by interpolating parabolically between $M_c(\zeta)$ and $M_c(z_T)$. The latter quantity is the mass transport at the cell top, and in the example illustrated in Figure 12, $M_c(z_T)$ is zero. However, in actual calculations this quantity is set equal to the mesoscale mass transport $M_m(z_T)$ pro-rated by the ratio $\Delta t_c / \Delta t_m$ where Δt_c is the time during the storm when cells are over the rain gauge and Δt_m is the time when mesoscale areas are over the gauge, i.e., $M_c(z_T) = M_m(z_T)\,(\Delta t_c / \Delta t_m)$. $M_m(z)$ is determined from equation (16) which is given in a later section.

The height at which M_c is a maximum is set at

$$\zeta = z_B + \frac{3}{4}(z_T - z_B) \qquad (11)$$

and the cell radius is expressed as

$$r = 0.133\,(z_T - z_B - 1.0) \tag{12}$$

in all cases. The units of ζ, z_B, z_T and r in (11) and (12) are kilometers. It was determined, also by trial and error, that specifying ζ and r according to (11) and (12) assures that $f_c(z_B)$ given by (10) will be approximately 0.33 for any cell depth, so that the mass transport M_c at the cell base will also be one-third of the maximum M_c at level ζ in all storms. The value of about one-third was suggested from inspection of a number of calculations of cloud properties obtained from a steady-state jet model similar to the one described by Squires and Turner (1962)*. With the mass transport at the cell base always one-third of its maximum value and the level of maximum M_c always 3/4 of the way up from ceil base to cell top, the shapes of the curves of $M_c(z)$ are similar for different cell depths.

The physical realism of ζ and r expressed according to (11) and (12) can be assessed only on a very limited basis. Cumulus clouds modelled as steady-state jets have a maximum of vertical mass flux at their tops. On the other hand, the vertical mass flux profile inferred from Braham's (1952) data for Ohio thunderstorms shows a maximum nearer the middle of cells. The cell radius r and corresponding entrainment rate ϵ /r are plotted as functions of cell depth in Figure 13. The slope of the curve for the radius gives a ratio of depth to radius of about 7.5.

---

*The exact model referred to was developed by Professor N.A. Phillips of M.I.T. and has been programmed and used by several students in the Department of Meteorology at M.I.T.

For cumulus clouds over Florida, Plank (1969) found typical ratios of two to one for depth to radius of clouds; however, the ratio of updraft depth to radius for these same clouds are probably less since portions of the visible cloud may be occupied by non-vertically moving air, or possibly downdrafts. The thunderstorms described by Byers and Braham (1949) appear in their mature stage to have an average updraft depth to radius ratio of about five to one. Inspection of many radar and rain-gauge records indicates that the showers which are called cells rarely exceed one or two kilometers in diameter but often have vertical extents of three to ten kilometers or more. The updraft depth to radius ratio of 7.5 may not, therefore, be unrealistic.

The vertical distributions of entrainment, detrainment, and net entrainment dM_c/dz, associated with the entrainment rate and mass transport curve described above and used in actual calculations are shown in Figure 14.

3. Expression for total cellular condensation

The total cellular condensation C on the left-hand side of (7) is obtained indirectly from measurements of the rainfall in the storm being modelled. From an analysis of the variations in rainfall rate as the storm moves over the rain gauge the cellular, mesoscale, and synoptic components of the total precipitation deposited by the storm are estimated. These amounts are R_c, R_m, and R_s respectively. The total amount of condensate produced in cells is expressed in the modelling as

$$C = \beta \left[R_c + \alpha R_m - R_A - R_B \right] \qquad (13)$$

where β is the ratio of the condensate formed in cells to the total precipitation of

cellular origin, the latter being the quantity in brackets. The parameter α is the fraction of the mesoscale precipitation R_m that originated in cells and R_A and R_B are the components of R_C condensed above and below the layer containing the cells, respectively.

Reasonable choices of the parameters α and β in (13) generally depend on the characteristics of individual storms, therefore computations are made for each storm for a number of combinations with α ranging from 0 to 1 and β ranging from 1 to 3. Selection of the combinations which give best estimates and lower and upper limits for C are made a posteriori from considerations of kinematic and water-budget constraints described in section F of this chapter.

The quantities R_A and R_B in equation (13) are usually rather small, but are estimated by assuming that the lifting and condensation processes above and below the cell are similar to those in the mesoscale areas surrounding the cells laterally. Formally, R_A and R_B are expressed as

$$R_A = \begin{cases} \int_{z_T}^{z_P} \frac{\Delta t_c}{\Delta t_m} M_m(z) \left(-\frac{dq_c}{dz}\right) dz, & z_T < z_P \\ 0, & z_T \geq z_P \end{cases} \tag{14}$$

and

$$R_B = \int_{0}^{z_B} \frac{\Delta t_c}{\Delta t_m} M_m(z) \left(-\frac{dq_c}{dz}\right) dz \tag{15}$$

where $M_m(z)$ is the mesoscale mass transport determined from (16) given below.

The ratio $\Delta t_c / \Delta t_m$ pro-rates the mesoscale mass transport appropriately for the time that cells were over the rain gauge. No entrainment term appears in these equations because there is assumed to be no temperature or relative humidity difference between the regions directly above or below the cells and the surrounding mesoscale areas.

4. Mesoscale and synoptic mass transports

Although $M_m(z)$ and $M_s(z)$ do not affect the computation of cellular transports, except in the determination of the value of M_c at the cell top and in the estimation of R_A and R_B, they are used in the analysis of the storm's water budget and overall kinematics.

The masses of air transported upward per unit area in mesoscale and synoptic areas, respectively, are computed from equations similar to (7). $M_m(z)$ and $M_s(z)$ are allowed to increase parabolically between the ground and level ζ where they are largest and to decrease parabolically to zero at $z = 10$ km or $z = z_T$ whichever is higher. It is assumed that the synoptic and mesoscale areas are not characterized by entrainment of a turbulent nature as are the cells. There is thus no detrainment from synoptic or mesoscale areas below level ζ, nor is there any entrainment into these regions above ζ. It is further assumed that precipitation is formed from condensate with perfect efficiency and that the precipitation falls directly from these regions. The equations for $M_m(z)$ and $M_s(z)$ then are

$$(1-a)R_m = \int_0^{z_p} \left[(q_s - q_m)\left(\frac{dM_m}{dz} + \frac{dM_c}{dz}\right)^* - M_m \frac{dq_m}{dz} + (q_c - q_m)\left[\left(\frac{dM_c}{dz}\right)_i - \frac{dM_c}{dz}\right]\right] dz \qquad (16)$$

and

$$R_s = \int_0^{z_p} \left[(q_o - q_s)\left(\frac{dM_s}{dz} + \frac{dM_m}{dz} + \frac{dM_c}{dz} \right)^* - \frac{dq_s}{dz} M_s \right] dz \qquad (17)$$

where z_p is the top of the layer of lighter precipitation outside the cells, q_o is the mixing ratio outside of the storm, and q_s and q_m are the water vapor mixing ratios in the synoptic and mesoscale areas respectively. When a synoptic area is present both q_s and q_m are taken to be the saturation value q', discussed in section A. When no synoptic area is present, however, q_s and q_m have the values q_o and q', respectively. The terms with asterisks express the assumptions of no detrainment below level ζ and no entrainment above ζ ; the symbol ( )* has the value ( ) when $z \leq \zeta$ but is set equal to zero when $z > \zeta$. The quantities M_m, M_s, z_p, q_o, and q' are illustrated in Figure 10.

D. Temperature difference between cells and environment

The difference between the temperature of the cells and that of their environment may be computed from two equations of the form (4). In the first, ξ in (4) represents the vertical velocity w, and the source term S is, therefore, the change in momentum per unit depth of a rising mass of air in the cellular updraft. Equation (4) in this case may be written

$$w_c \frac{dw_c}{dz} = -w_c^2 \frac{1}{M_c}\left(\frac{dM_c}{dz}\right)_i + b - f \qquad (18)$$

where b is the buoyancy per unit mass of rising air while f is the frictional deceleration

of this mass. In obtaining (18), (4) is multiplied through by w_c to express (18) in terms of accelerations and w' the vertical velocity in the environment of the cell is neglected in comparison with the magnitude of w_c. The forms used here for the buoyancy b and frictional deceleration f are those derived by Levine (1965) and used by Simpson and Wiggert (1969, 1971). The buoyancy is expressed as

$$b = \frac{g}{1+\gamma}\left[\frac{T_c^*(1+\mu)^{-1} - T'^*}{T_c^*(1+\mu)^{-1}}\right] \tag{19}$$

where g is the acceleration due to gravity, γ is the apparent or virtual mass coefficient due to acceleration of the fluid surrounding the actively rising cloud element, μ is the mixing ratio of water in the form of hydrometeors, and T_c^* and T'^* are the virtual temperatures in the cell and its environment respectively, virtual temperature being defined as

$$T^* = [(1 + 1.609q)/(1 + q)]\, T. \tag{20}$$

The frictional deceleration f is expressed as

$$f = K_D w_c^2 \tag{21}$$

where K_D is a constant of proportionality between aerodymanic drag and w_c^2. The numerical value of K_D may range from zero to 1.125, the experimental value for a solid sphere at high Reynolds number. Simpson and Wiggert (1969, 1971) have obtained their most satisfactory results in field experiments using $\gamma = .5$ and $K_D = 0$ in (19) and (21) respectively. Simpson and co-workers have generally chosen values for such parameters as γ, K_D, and ϵ prior to their field experiments on the basis of theoretical considerations and laboratory results rather than by adjustment

after the fact to agree with cloud observations. Simpson et al (1965, 1969) point out that the values of γ and K_D which they use are consistent with: (a) Levine's (1965) postulate that when the element radius stays nearly constant, there is no drag at all ($K_D = 0$) and all resistance to cloud growth enters the momentum equation as a virtual mass effect ($\gamma \neq 0$); and (b) laboratory experiments which indicate the numerical value of γ should be approximately 0.5. Neither Levine nor Simpson have included in (18) the frictional drag exerted on hydrometeors.

In the present context, we are interested in obtaining from (18) an estimate of the temperature difference $T_c(z) - T'(z)$ between cells and environment. For this purpose, a vertical velocity distribution for cells of a given depth is specified with the same z-dependence as used for $M_c(z)$ in the previous section of this chapter. At cell top z_T the vertical velocity is set equal to zero. The level ζ where w_c is a maximum and the radius r of the cells are again specified according to (11) and (12), respectively. The entrainment rate is again expressed as ϵ /r with $\epsilon = 0.2$, a formulation which as noted previously is identical with that used by Simpson. Thus, the vertical velocity profiles and entrainment rates are kinematically consistent by reasoning analagous to that given in section C-2 of this chapter. As before, the temperature $T_c(z)$ in the cells is assumed to follow a moist-adiabatic distribution representative of the storm being modelled. Both the environment and the cells are assumed to be saturated since cells almost always appear to be surrounded by mesoscale precipitation areas. There remain two unspecified quantities in equation (18), $T'(z)$ and μ (z). This necessitates the introduction of a second equation involving these two unknowns.

Another equation of the form (4) expressing the conservation of water in the cellular updrafts may be written as

$$\frac{d\mu}{dz} = A\left[-\frac{dq_c}{dz} + \frac{1}{M_c}\left(\frac{dM_c}{dz}\right)_i (q' - \mu - q_c)\right] \qquad (22)$$

where the quantity in brackets is the total mass of water per unit mass of air which is condensed per unit height and A is the fraction of this condensate retained by the rising mass of air, the remainder being assumed to fall out as precipitation. Equation (22) is obtained by letting ξ in equation (4) represent the mixing ratio of water in all forms, i.e. $\xi = q + \mu$, and the source term S/M_c be expressed as the fraction, 1-A, of condensate per unit height which falls out of the rising air as precipitation. A more sophisticated modelling of the precipitation process such as used in recent work by Simpson and Wiggert (1969) was considered far beyond the scope of this thesis. The cruder representation used here, however, is essentially that with which Simpson obtained reasonably satisfactory results in earlier studies where A was arbitrarily assigned the numerical value of 0.5 (Simpson et al, 1965).

With appropriate substitutions from (19) and (21), equations (18) and (22) can be solved simultaneously by numerical methods for μ (z) and T'(z) when z_B, z_T, and $T_c(z)$ are provided from the particular storm being modelled and when the other required inputs are specified in the ways described above. The numerical integration of (18) and (22) is started with an initial value of $\mu = 0$ at $z = z_B$.

The crucial quantity which is specified in solving (18) and (22) appears to be the vertical velocity in the cells. In Figure 15 are some calculated values of

$T_c(z)$ - $T'(z)$ and μ (z) for cells with bases at z_B = 1 km and tops at z_T = 7 km. The temperature $T_c(z)$ was distributed moist-adiabatically between z_B and z_T with an equivalent potential temperature of θ_e = 321 K. Although comparison of Figures 15 a-c shows that while the temperature difference is not extremely sensitive to the magnitude of $w_c(z)$, $T_c(z)$ - $T'(z)$ does increase by a little more than a factor of 3 at most levels as the vertical velocity is increased by an order of magnitude. The values of the temperature difference are more uncertain near the cell top where the sign of $T_c(z)$ - $T'(z)$ is a bit ambiguous.

Since the vertical velocity is the important quantity which must be prescribed in order to calculate $T_c(z)$ - $T'(z)$, available empirical measurements of vertical velocity in cells were referred to for determining what appear to be realistic updraft speeds in cumulus clouds of different sizes. A simple linear function shown in Table 6 relates the cell vertical velocity at height ζ where it is a maximum to cell depth. This function was designed as a guideline for specifying vertical velocities where needed in model calculations. The consistency of the linear distribution with empirical data is indicated by comparing Table 6 with Table 7. The latter contains the results of various observational studies of updraft speeds which are listed for cells of different depths. The quantities in Table 7 show ranges and averages of peak upward vertical velocities encountered in cumulus clouds by various investigators.

When equations (18) and (22) are applied in model calculations for actual rainstorms, the vertical velocities are specified according to Table 6 since it appears to give estimates which are consistent with empirical data. According to

Table 6. Vertical velocities considered realistic for model cells at height of maximum updraft.

Cell Depth km	Vertical Velocity m sec^{-1}
1-3	3
3-5	4
5-7	5
7-9	6
9-11	7
11-13	8
13-15	9

Table 7. Peak updraft velocities measured in cumulus clouds.

Cloud depth km	Vertical velocity m sec^{-1}	Investigators	Method of observation
.7-4.0 (range)	3.5-6.5 (range)	Warner (1970)	Aircraft penetration
1.5-5.0 (range)	0-7 (range)	Cunningham et al (1964)	Cloud photography and aircraft penetration
12 (average)	5-7 (average)	Byers and Braham (1949)	Aircraft penetration
15 (single observation)	23 (single observation)	Barnes (1970)	Balloon ascent

Table 6, the appropriate choice for w_c at height ζ for cells 6 km in depth, is 5 m sec^{-1}, the value which was used in the computations shown in Figure 15b. The uncertainty in $T_c(z) - T'(z)$ associated with specifying the vertical velocity is shown by the ratio of the temperature difference curve in Figure 15b to those in Figures 15a and 15c. The intermediate estimate of the temperature difference in 15b is within plus or minus a factor of 1.5 of the extreme values in 15a and 15c except near the top of the cell where the sign of $T_c(z) - T'(z)$ appears to be somewhat uncertain.

From Figure 15b it is also apparent that when the maximum w_c is 5 m sec^{-1} the temperature difference is as much as 30% larger when there is no precipitation ($A = 0$) than when half of the condensate is precipitated in each vertical step ($A = 0.5$). The assumption that precipitation occurs with $A = 0.5$ is used in making computations since this most closely resembles the formulation used with some success by Simpson et al (1965) and since the updrafts modelled in this study are ones that produce precipitation.

Figure 15d illustrates that setting the parameter $\gamma = 0$ or 0.5 makes little difference in the calculation of $T_c(z) - T'(z)$.

Cells are modelled as having a saturated environment since they are surrounded by mesoscale precipitation areas. It is noted, however, that occasionally cumulus cells extend vertically above the layer of precipitation surrounding them (Figure 5). Figure 15e shows that reducing the relative humidity in the environment from 100% to 30% above the 4 km level has no significant effect on the computed

temperature differences. In the climatological study in Chapter IV, the only situations in which cells were frequently not accompanied by mesoscale precipitation at all occurred at San Juan, P.R., in winter and spring. The cells in these cases were weak and shallow and constituted a minor contribution to the transports over climatological time periods. The modelling technique, therefore, was not altered for these cells and they were treated as though they had a saturated environment.

E. Horizontal wind speed difference between cells and environment

The westerly component of the horizontal wind speed u also obeys a conservation equation of the form (4). In this case, ξ in (4) is equated to u and the only source term considered is the "form" drag associated with the pressure difference across the boundaries of the updraft which results when the updraft presents itself as an obstacle to the flow in its environment. As discussed by Malkus (1952), Hitschfeld (1960), and Bates and Newton (1965), this source term may be estimated by

$$S = \pm M_c \frac{C_D}{\pi r w_c} (u' - u_c)^2 \qquad (23)$$

where C_D is a dimensionless drag coefficient which would be zero if environmental air were not deflected at all by the updraft and would have the value 1.0 if the updraft acted as a solid cylinder embedded in the flow. The plus sign in (23) is used when $u' \geq u_c$; otherwise the minus sign is used. The westerly wind speed u'(z) in the environment is determined for modelled storms from rawinsonde data obtained in the vicinity of each storm. Then with the radius r of the updraft given again by equation (12) and the vertical velocity specified as in the temperature calculations, equation (4)

may be written in the form

$$\frac{du_c}{dz} = (u'-u_c)\frac{1}{M_c}\left(\frac{dM_c}{dz}\right)_i \pm \frac{C_D}{\pi r \omega_c}(u'-u_c)^2 \qquad (24)$$

and solved numerically for $u_c(z)$ if it is assumed that $u_c = u'$ at $z = z_B$.

The extreme values of $u_c(z) - u'(z)$ which result from assuming $C_D = 0$ and $C_D = 1$ are illustrated in Figure 16. The difference between the two curves shown there probably comprises much of the uncertainty in the estimate of the horizontal momentum deficit in the cells. This uncertainty, expressed in terms of the ratio of an intermediate value of $u_c(z) - u'(z)$ to its lower and upper limits, is less than plus or minus a factor of two at any level. In actual computations, a value of $C_D = 1$, rather than an intermediate value is used to give best estimates of $u_c(z) - u'(z)$ because there seems to be some observational evidence that cells do behave as an obstacle to the relative environmental flow (Shmeter, 1966; Fujita and Grandosa, 1968). It should be noted that this choice tends to result in an underestimate rather than an overestimate of the angular momentum transports.

F. Consistency between water budget and kinematics

The parameters α and β are introduced in equation (13) for the total cellular condensation to represent the relationship between mesoscale and cellular precipitation and the inefficiency of the cumulus precipitation mechanism. However, the arbitrariness of these parameters creates the possibility of prescribing an unrealistic amount of condensation in the model storm unless some constraints are placed upon the values which α and β are permitted to assume. Any increase

in condensation is accompanied by an increased upward mass transport for the storm as a whole and for the cells in particular. Some crude checks of model lifting against observations of upward motion both within cells and averaged over the whole storm are made. These checks guide the choices of appropriate combinations of α and β on which to base estimates of the cellular mass transport $M_c(z)$. The consistency of the kinematics and water budgets of both individual cells and the storm as a whole are considered below.

1. Cells

Although there is no necessity that the period of time during which precipitation falls from a cell be equal to the duration of the updraft, the observations of Byers and Braham (1949) suggest that they are comparable. Thus, the mass $M_c(z)$ of air transported upward per unit area in cells during a storm may be interpreted with some meaning in terms of an average cellular vertical velocity if it is divided by the total time during which cells were over the rain gauge and by the appropriate density of air.

The vertical velocity W^* computed in this way is used to indicate the validity of different combinations of α and β. As either α or β is allowed to increase, larger values of $M_c(z)$, and hence larger W^*'s, are computed since an increase of either parameter specifies an increase in the total cellular condensation according to (13).

The vertical velocities in Table 6 which are considered realistic by comparison with the various observational findings listed in Table 7 are used as

guidance in determining when W^* exceeds a realistic magnitude. When W^* is larger than the value in the table for cells of the depth observed in the model storm, it is deemed unrealistically large and the combination of α and β used to calculate W^* is discounted as an appropriate choice in determining $M_c(z)$. In this way, an upper limiting value of cellular condensation, determined by a certain combination of α and β and rainfall measurements, is arrived at for each storm. Occasionally combinations of α and β which produced values of W_c only slightly in excess of those in Table 6, no more than 2 m sec^{-1}, are allowed to remain as upper limits to the realistic possibilities.

2. Water budget and kinematics of whole storm

The consistency between the water budget and kinematics is considered for the storm as a whole, as well as for individual cells. Storm-averaged vertical velocities were computed for a number of cases and compared with vertical velocities inferred from the divergence pattern indicated by the triangulation method (Bellamy, 1949) using observed winds in the vicinity of the modelled storms. It was hoped that from these comparisons it might be evident whether any combinations of α and β, which determine the cellular condensation in the model storm, produced unrealistic amounts of larger-scale upward motion.

The storm-averaged vertical velocity at level ζ is calculated for the model as

$$\overline{W} = \frac{M_c(\zeta) + M_m(\zeta) + M_s(\zeta)}{\rho(\zeta)\,\Delta t} \qquad (25)$$

where $\rho(\zeta)$ is the density of air at ζ and Δt is the duration of the storm. $\overline{W}$ was computed for a number of storms modelled after rainfall situations at Boston, Mass. Vertical velocities were also computed from the divergence of the horizontal wind observed at 12 hr intervals during these same storms for stations at Albany, N.Y., Portland, Me., and Nantucket, Mass., which form a triangle surrounding Boston. The "model" and "triangle" vertical velocities which are compared are listed in Table 8. The values for the triangle which are given in the table are the maximum values in the vertical distribution of vertical velocity obtained at each observational time.

The following facts are noted from Table 8. The negative vertical velocities obtained from the triangle in storms #6 and #7 occur when the fraction of the triangle covered by precipitation is small. These vertical velocities are evidently not representative of their respective storms and are therefore ignored. The model appears to overestimate consistently the vertical velocity. Part of this overestimate may result from an adjustment which was made so that the vertical velocities computed from the triangle were zero at the highest level for which winds were observed. The triangle vertical velocities were consistently reduced by this adjustment. In the cases for which $\beta = 1$, however, agreement between model and triangle values can be argued to be within a factor of two, for at least one value of α and at least one sounding time in each storm except #13. The cases for which $\beta = 3$ and $\alpha = .67$ or 1.00 appear to be the only ones for which the model values are consistently much larger than the values for the triangle, at least a factor of two larger in all but one case and a factor of four or more larger in half of the storms. It is noted that all of

Table 8. Comparison of storm-averaged vertical velocity $\overline{W}$ computed from model storm and from wind data by the triangulation method. Numbers in parentheses show percentage of wind triangle covered by precipitation at observation time. Δ t is the storm duration and R_c is the cellular precipitation.

				Model				Triangle			
				α				Observation time			
Storm #	Δt (hr)	R_c (in)	β	0	.33	.67	1.00	1	2	3	4
				$\overline{W}$ (cm sec^{-1})				$\overline{W}$ (cm sec^{-1})			
1	30	2.75	1	34	38	41	45	15	18	15	13
			3	73	92	111	130	(50%)	(100%)	(100%)	(75%)
2	26	.92	1	14	17	19	22	5	10	3	
			3	31	42	53	64	(100%)	(100%)	(75%)	
3	21	.86	1	13	14	16	18	6	22		
			3	31	38	45	52	(5%)	(100%)		
4	14	.52	1	13	14	14	16	13			
			3	31	34	38	41	(30%)			
5	27	.40	1	17	18	20	22	13	8		
			3	27	36	47	57	(100%)	(50%)		
6	11	.36	1	14	15	16	17	-4			
			3	30	36	43	50	(25%)			
7	26	.32	1	7	8	9	10	-16	-14		
			3	12	17	21	26	(20%)	(30%)		
8	7	.32	1	12	13	13	14	7			
			3	31	34	37	40	(85%)			
9	30	.21	1	8	9	9	10	13	23		
			3	11	15	19	24	(75%)	(100%)		
10	6	.21	1	21	21	21	21	14			
			3	40	40	40	40	(100%)			
11	36	.16	1	14	15	16	16	11	14	12	5
			3	16	23	31	39	(50%)	(100%)	(100%)	(30%)
12	29	.12	1	4	6	9	11	1	5		
			3	7	15	23	31	(25%)	(not determined)		
13	7	.12	1	13	16	18	20	3			
			3	21	33	45	56	(75%)			
14	18	.11	1	5	5	6	6	6	5		
			3	9	10	11	12	(100%)	(100%)		
15	24	.11	1	12	18	23	28	7	7	14	
			3	16	35	55	75	(50%)	(50%)	(75%)	
16	9	.10	1	5	5	5	6	8			
			3	7	9	11	13	(50%)			

the storms for which these comparisons are made were 6 hr or more in duration and can, therefore, be considered synoptic-scale storms. Meaningful comparisons probably cannot be made for shorter storms since they are usually also characterized by less horizontal extent than the synoptic-scale storms so that the wind-observational triangle is not sufficiently covered by precipitation to give vertical velocities representative of the storm.

The significant finding of the above analysis is that the model tends to overestimate highly the storm-averaged vertical velocity for the combinations of large α with large β in storms of synoptic-scale duration. This result is consistent with qualitative reasoning which suggests that when cumulus cells are embedded in a synoptic-scale precipitation area, the condensate which they leave aloft in their naturally inefficient mode of precipitation production is rained out at some time and place within the larger-scale storm. As Austin and Houze (1972) point out, this fallout probably occurs in the mesoscale areas surrounding the cells and is represented in the expression for the total cellular condensation by the quantity αR_m on the right-hand side of equation (13). For a synoptic-scale storm, therefore, it would be inconsistent to allow simultaneously for α to be greater than 0 while β, the ratio of condensate to precipitation formed in cells, is greater than 1 since all of the condensate formed in cellular updrafts probably does, in fact, reach the ground as either cellular or mesoscale precipitation.

In storms of smaller horizontal extent and shorter total duration, such as mesoscale complexes of thunderstorms, it may be possible for a significant amount

of condensate to be left behind as cloud by the storm. In these cases β might well be greater than unity.

3. Limits and best estimates for cellular condensation

To remain consistent with the above findings, the policy adopted in dealing with the storms analyzed and discussed in the next chapter was to consider $\beta = 1$ to be the only realistic possibility in any storm which took more than 4 hr to pass over the rain gauge. That is, synoptic-scale storms are assumed in the modelling to convert all of their condensate to precipitation somewhere within the region occupied by the storm. Storms of shorter duration are allowed to have $\beta = 1$ to 3 as realistic possibilities.

In either case, the upper limit for the cellular condensation was determined from the α which in combination with one of the allowed β's gave the largest cellular vertical velocities not exceeding the values given in Table 6. The best estimate of $M_c(z)$ for a storm was determined by any combination of α and β which according to equation (13) gave a total cellular condensation of approximately three times the cellular precipitation R_c. This represents the inherent inefficiency of the cumulus precipitation process which is discussed by Houghton (1968) and most closely corresponds to Braham's (1952) water budget for cumulus cells. This system for making a best estimate was modified when the combination of α and β so chosen gave an unrealistically high cellular vertical velocity according to Table 6. In this case, the best estimate was simply determined from the α and allowed β which gave the largest cellular vertical velocities considered reasonable according

to the table. The lower limit of the cellular condensation was always considered to be the case for which $\beta = 1$ and $\alpha = 0$. Although this combination gives an absolute lower limit, it is physically unrealistic since it does not allow for any inefficiency in the cumulus precipitation process.

In each set of model-storm calculations, $M_c(z)$ is computed for the lower and upper limits as well as for the best estimate of the cellular condensation as defined above. In this way, the uncertainty in $M_c(z)$ associated with estimating the cellular condensation from measurements of precipitation is evaluated a posteriori. Computations show that upper and lower limits generally differ by less than a factor of ten and an intermediate value selected as best fit lies within a factor of three of either limit.

G. Uncertainties

In the foregoing sections, important physical assumptions which are made in estimating the model quantities M_c, $T_c - T'$, and $u_c - u'$ are pointed out, and the uncertainties involved in making these assumptions are evaluated quantitatively by considering limiting cases and computing ranges of values for the model quantities. The uncertainties which have been found to be associated with principal assumptions in the calculations are summarized as follows:

Specification of the vertical variation of $M_c(z)$ and entrainment	$\pm$ a factor of 2 at any level in $M_c(z)$
Estimation of cellular condensation C from precipitation measurements	$\pm$ a factor of 3 in $M_c(z)$
Specification of vertical velocity in temperature calculations	$\pm$ a factor of 1.5 in $T_c(z) - T'(z)$
Modelling of horizontal drag on cells	$\pm$ less than a factor of 2 in $u_c(z) - u'(z)$

Combining these uncertainties, which are discussed individually in more detail in sections C, D, E and F above, as if each were independent yields roughly plus or minus a factor of four for the cumulus-scale transports of sensible heat and angular momentum computed by equations (1) and (2). Every possible source of uncertainty has not been evaluated quantitatively, however the assumptions listed above appear to contain most of the theoretical uncertainties associated with the modelling technique. Uncertainties associated with measured quantities are not treated in this investigation.

For the computations which are discussed in the next chapter, best estimates of model quantities within their ranges of uncertainty are made from what seem to this author to be the most appropriate assumptions based on physical reasoning or observational experience. However, it should be evident from the discussions in the preceding sections of this chapter how any changes in the assumptions would affect the final calculations of heat and angular momentum transports.

H. Determination of input quantities

The quantities discussed below include those regarded as given or observed in the solutions of (7), (18), (22) and (24) for M_c, $T_c - T'$, and $u_c - u'$ which determine the cumulus transports τ_{SH} and τ_{AM}. Also described are the quantities needed to solve (16) and (17) for M_m and M_s which were used in the analysis of the consistency of the water budget and kinematics of the model storm. In that same analysis, time factors were used to convert mass transports to vertical velocities.

These time periods are also considered input quantities, although they do not have a direct effect on the calculation of cumulus transports.

1. Cellular precipitation

The input quantity R_c is the mass of water deposited per unit area by cells passing over the rain gauge. The total time Δt_c that cells are over the gauge is also recorded as input. The following criterion is used to determine when a cell is over the rain gauge. A peak in the rainfall trace is considered cellular if either:

(1) The rainfall rate at the peak is at least 5 mm hr^{-1} and at least twice as large as the minimum rainfall rate within $\pm$ 5 min of this peak;

or

(2) The rainfall rate at the peak is at least 20 mm hr^{-1}.

The total duration of a cell associated with a particular cellular peak is not allowed to be longer than 3 min, unless the rainfall rates at either end of the 3 min period exceeded 20 mm hr^{-1}. In this latter case the boundary of the cell is designated as the point at which the rainfall rate dropped below 20 mm hr^{-1}. The symbol R_c, then, refers to the total precipitation obtained by integrating the rainfall records over the durations of all the cells in a storm.

2. Mesoscale and synoptic precipitation

These quantities, represented by the symbols R_m and R_s, are the masses of water deposited per unit area by mesoscale and synoptic areas passing over the rain gauge. Whereas R_c is determined objectively for each storm, R_m and R_s are acquired somewhat more subjectively. When the precipitation rate increases

by about a factor of two or more for periods of roughly 15 min to 4 hr, it is assumed that mesoscale areas are passing over the rain rauge. Any time the rainfall rate exceeds 4 mm hr^{-1} for a period of a few minutes or more it is assumed that a mesoscale area is over the gauge. Precipitation accumulated when neither a mesoscale area nor a cell is over the gauge is called R_s. The total precipitation not included in either R_c or R_s is called R_m. The times Δt_m and Δt_s during which mesoscale and synoptic areas are over the gauge is also recorded.

The choices of criteria used to determine cellular, mesoscale and synoptic rainfall are guided by the typical characteristics of the various areas as described in Chapter II.

3. Vertical structure of storm

The cell base z_B is seldom apparent from RHI displays since rain falls more or less vertically through the cell base. The height z_B is estimated from radiosonde data if the synoptic situation suggests that cells are bounded below by the top of a stable layer such as a warm frontal inversion. Otherwise z_B is assumed to be 1.0 km at mid- to high-latitude stations and 0.5 km at tropical stations.

The height z_T of cell tops is obtained directly from radar Range Height Indicator (RHI) presentations which have been recorded photographically or verbally. What is obtained is the height of the cellular precipitation echo; it is assumed that this height is the same as the height of the top of the cumulus updraft which produced the precipitation.

The depth z_p of the layer of lighter precipitation surrounding the cells is difficult to measure. The detectability of rain with a radar decreases rapidly with

range. Consequently, the layer of lighter precipitation surrounding the cells can be estimated from RHI displays only for patterns observed within about 20 km of the radar site, and it is practically impossible to distinguish differences in the depths of precipitation in mesoscale and synoptic areas. Thus, z_p is always taken to be the same in both regions, and in the absence of radar data z_p is assumed to be equal to z_T, which is usually more or less the case when observations are available. It would appear to be possible to estimate z_p from radiosonde measurements obtained within the area of the storm since it is unlikely that an ascent would have been made within a cell. However, it was found in this study to be difficult to estimate from radiosonde data a value of z_p large enough to agree satisfactorily with the value obtained from radar observations in the same storm. This difficulty may be related to the generally recognized fact that humidity elements used in radiosondes underestimate the relative humidity.

4. Temperature in cells

The distribution of temperature in cells is approximated by a particular moist-adiabatic distribution which is determined to represent most closely the real distribution. The appropriate moist adiabat is designated by its equivalent potential temperature θ_e and is expressed in heights of the U.S. Standard Atmosphere rather than pressures. Data used to indicate the real distribution are from soundings made at the National Weather Service stations closest to the rain-gauge site at the standard times nearest to a storm's occurrence.

5. Humidities

The water vapor mixing ratios in the various regions of precipitation within the model storm are assumed to have their saturation values and are therefore not actually measured. The mixingratios $q_c(z)$ and $q'(z)$ are assumed to have their saturation values corresponding to temperatures $T_c(z)$ and $T'(z)$, respectively.

Outside the storm, the relative humidity is represented by a step function:

$$H = \begin{cases} H_1, & z \leq z_0 \\ H_2, & z_0 < z \leq z_p \end{cases} \tag{26}$$

where H_1, H_2, and z_0 are determined from soundings taken nearby, but not within the storm. Two layers with mean humidities H_1 and H_2 separated by level z_0 were used instead of a single layer represented by a single vertically averaged humidity because of the tendency for the lowest few kilometers of the atmosphere to be considerably more humid than the layer above.

6. Synoptic-scale wind field

For soundings made within and nearby the storm, least-square fits to the observed westerly winds are calculated. From these, an average shear B is obtained and used to represent the westerly wind in the vicinity of cells as

$$u' = u'(z_B) + B(z - z_B). \tag{27}$$

I. Computational Scheme

A computer program, hereafter to be called the "model-storm program," was written to calculate M_c, M_m, M_s, W^*, $\overline{W}$, $T_c - T'$, $u_c - u'$, τ_{SH}

and τ_{AM} for any storm for which the input quantities described in the preceding section are provided. For computational purposes, the model storm is subdivided into one-hour segments for which the rainfall parameters R_c, R_m, R_s, Δt_c, Δt_m, and Δt_s are provided individually. The westerly wind shear B is given for each standard sounding time during the storm and usually for the ones preceding and following its passage as well. From the shears at these times, hourly values of B are obtained by interpolation. The rest of the inputs, however, are provided as single values appropriate for the whole storm since they do not vary detectably during the storm. These are: the heights z_B, z_p, and z_T; the equivalent potential temperature θ_e which designates the particular moist adiabat to be used for T_c; and the relative humidities H_1, H_2, and H_3 which determine q' and q_o. The methods by which the various output quantities are produced by the model-storm program are discussed in the following paragraphs. A flowchart of the calculations is in Appendix E.

M_c, M_m, and M_s. Within the model-storm program, these quantities are obtained from equations (7), (16), and (17), respectively, just as described in section C of this chapter, except that the integrations indicated on the right-hand sides of these equations are done numerically by the trapezoidal rule with a height increment of 0.125 km. M_c is computed for α = 0, .33, .67, 1.00 and β = 1, 3 in each storm. The combinations of α and β giving lower limits, best estimates and upper limits are not determined within the program but rather in the analysis of the results of the computations, a posteriori. Since the cellular precipitation R_c which goes into determining M_c is usually apportioned quite unevenly during the time the storm passes over the gauge, and since the wind shear which determines $u_c - u'$

also varies considerably during this time, each storm was subdivided hourly so that τ_{AM} could be determined as the sum of the amounts of angular momentum transported upward during each hour of the storm. However, M_c is not determined from the data for each individual hour because representative proportions of cellular and mesoscale precipitation may not have been accumulated in a single hour. Therefore, M_c is always computed from the data for the whole storm, i.e. R_c and R_m in (13), the expression for the total cellular condensation, are the total amounts for the storm. Then M_c is apportioned in time according to the fraction of the total cellular precipitation which fell during each hour.

W^* and $\overline{W}$. These quantities are determined within the model-storm program exactly in the manner described in section F of this chapter.

$T_c - T'$. The observed values of z_B, z_T, and θ_e do not vary detectably during most storms; therefore, only one computation of the temperature differences needs to be made per storm. The simultaneous solution of (18) and (22) is not actually performed within the model-storm program itself but rather in a separate program where $T_c(z) - T'(z)$ is calculated for a range of θ_e and z_T with $z_B = 1$ km. A simple stepwise integration which starts with $\mu(z_B) = 0$ is used with a height increment of 0.25 km. Some of the results are shown by the solid curve in Figure 17. The curves obtained for different θ_e's and z_T's were then approximated by simple analytic functions, which are the dashed curves in Figure 17 and stored within the model-storm program. Then for each storm an appropriate value of $T_c(z) - T'(z)$ is obtained by interpolation between these stored solutions. Although the solutions to (18) and (22) were obtained with $z_B = 1$ km, they are applied to cells

with bases at other levels by simply shifting the stored curves along the z-axis by z_B - 1 km. The cell bases put into the storm model seldom deviated more than 0.5 km from z_B = 1 km.

$u_c - u'$. As has been noted, a value of the westerly wind shear B is obtained for each hour of the storm by interpolating between the shears obtained at regular sounding times which are separated by 12 hr. The westerly wind in the environment of the cells is then expressed with the interpolated shear B in a linear fashion by equation (27), and (24) is solved for u_c within the model-storm program by the Runge-Kutta method with the initial value of $u_c = u'$ at $z = z_B$.

τ_{SH} and τ_{AM}. τ_{SH} is simply computed by equation (1) using the mass transport $M_c(z)$ and temperature difference $T_c(z) - T'(z)$ obtained for the whole storm. τ_{AM}, on the other hand, is obtained by adding the hourly angular momentum transports which are computed individually from equation (2) using the hourly values of M_c and $u_c - u'$. τ_{SH} and τ_{AM} are calculated for z = 1, 2, ... 10 km.

J. Examples of calculations

The results obtained from the model-storm program for a particular storm are typified by the following examples.

On 24-25 March 1969, precipitation fell at the West Concord, Mass., rain-gauge site during the period 2200 to 1400 EST. The rainfall record for the hours 1000 to 1200 EST is shown in Figure 18; the precipitation considered cellular, meso-scale, and synoptic may be seen in the figure. The rainfall parameters for the whole

storm are listed in Table 9.

A number of photographs of the MIT radar Range Height Indicator are available for this storm; an example of these photographs is in Figure 19. From these, a cell top height of z_T = 7.0 km was found to be representative.

Temperature soundings made at Nantucket, Mass., before, during and after the passage of the storm over West Concord are plotted in Figure 20. Also shown there is the moist adiabat, identified by θ_e = 310K, used to estimate $T_c(z)$. Soundings for Albany, N.Y., and Portland, Me., are similar to those shown for Nantucket. Since these radiosonde data do not show any strong low level inversions which would indicate a cell base at a higher level, z_B is prescribed to be 1 km.

The westerly winds between 850 and 400 mb and the least-square fits to them are plotted in Figure 21 for soundings taken before, during, and after the storm at Albany, Nantucket, and Portland. The least-square shears for these stations are averaged at each sounding time; the following values were obtained:

Date	Time (EST)	Ave. shear (m sec^{-1} km^{-1})
24	1900	3.4
25	0700	2.2
25	1900	1.7

Hourly shears for West Concord are obtained by interpolating between these values.

For the input quantities thus obtained, the various outputs were calculated by the model-storm program for eight combinations of α and β, the parameters which determine the cellular condensation from measured rainfall amounts.

Table 9. Precipitation parameters for storm of 24-25 March 1969.

Hour (EST)	R_c (in)	R_m (in)	R_s (in)	Δt_c (sec)	Δt_m (sec)	Δt_s (sec)
22-23	.02	.08	.00	420	2490	690
23-00	.00	.10	.02	0	2010	1590
00-01	.00	.02	.04	0	510	3090
01-02	.01	.06	.01	210	1290	2100
02-03	.00	.00	.00	0	0	3600
03-04	.00	.00	.00	0	0	3600
04-05	.00	.00	.00	0	0	3600
05-06	.00	.00	.00	0	0	3600
06-07	.00	.06	.04	0	1230	2370
07-08	.00	.15	.04	0	2010	1590
08-09	.00	.11	.04	0	2010	1590
09-10	.07	.11	.04	810	1530	1260
10-11	.08	.03	.00	630	930	2040
11-12	.13	.09	.00	1770	1260	570
12-13	.01	.01	.02	210	390	3000
13-14	0	.02	.01	0	990	2610

The values of α and β for which computations are made are: α = 0, 0.33, 0.67, 1.00 and β = 1, 3. By the criteria established in section F, β = 3 is not considered realistic since this storm lasts longer than 4 hr. The values of W^* obtained for the remaining combinations of α with β = 1 are:

(α, β)	(0, 1)	(.33, 1)	(.67, 1)	(1.00, 1)
W^* (m sec^{-1})	63	124	187	249

None of these exceeds the vertical velocity of 5 m sec^{-1} given in Table 6 for cells 6 km in depth, and therefore all of these combinations of α and β are considered to give kinematically consistent estimates of M_c according to the reasoning given in section F. By the rules in that same section, (α, β) = (1.00, 1) is viewed as an upper limiting case since it gives the largest value of M_c, and (.67, 1) is considered the best estimate since it gives a cellular condensation of approximately 3 R_c by equation (13).

The curves for $M_c(z)$ computed with (α, β) = (0, 1), (.67, 1), and (1.00, 1) for the hour 1100-1200 EST are shown in Figure 22a. Figure 22c gives the function $T_c(z) - T'(z)$ obtained in the model-storm program by interpolating between the stored solutions to (18) and (22). Figure 22e contains $u_c(z) - u'(z)$ calculated from the shear, B = 1.7 m sec^{-1} km^{-1} obtained by interpolating between sounding times. Finally, Figures 22b and 22d show $\tau_{SH}(z)$ and $\tau_{AM}(z)$, respectively, for the three combinations of α and β.

The model calculations for another example are shown in Figure 23. This example is representative of summer thunderstorms at Boston. The transports

in this type of storm are clearly more vigorous than the storm illustrated by Figure 22 which is more typical of other seasons at this station.

The climatological study of cumulus transports which is discussed in the next chapter was based on a large number of model-storm calculations similar to those illustrated in Figures 22 and 23.

CHAPTER IV

CLIMATOLOGICAL STUDY OF CUMULUS TRANSPORTS

In this chapter, the model storm is applied in a climatological investigation of the vertical transports of sensible heat and angular momentum by cumulus cells. Calculations are made for a large number of storms at four stations which are expected, on the basis of air mass properties, to have degrees of cumulus activity characteristic of different climatic locations. From the quantitative evaluations for these representative stations, a global climatology of cumulus transports is constructed.

A. Data sample

1. Selection of stations

The geographical regions represented in this study were determined by climatological reasoning to be given below. The particular stations examined within each region are ones for which radar, tipping bucket rain gauge, and radiosonde records were available.

The amount of cumulus convection observed in a particular geographical area will depend largely on the frequency with which unstable air of tropical maritime (mT) origin is found there. The warmth and high relative humidity of this type of air mass, along with its convective instability, make it the most conducive to vigorous cumulus activity. The tropical oceans are the source regions of mT air. However, only in the western halves of the oceanic subtropical anticyclones does air of this origin usually become unstable over a deep layer. In the eastern portions of

these highs, subsidence produces stable mT air masses which are unfavorable for cumulus development. Consequently, it is the eastern parts of continents which are most notably characterized by influxes of unstable mT air. These inflows may occur as a persistent southerly onshore flow develops in the southeastern region of a continent on occasions when a subtropical anticyclone is particularly well-developed. Unstable mT air is also transported northward into the eastern parts of continents in advance of migratory cyclones. Along west coasts of continents, onshore flow from subtropical highs will be characterized by a large degree of stability, and cumulus activity will, therefore, be infrequent in this regime. Unstable mT air occasionally invades west-coastal regions in advance of migratory cyclones, but it does so only after travelling across the ocean from a source region on the southwest side of a subtropical high. It is likely that by the time it arrives much of its original convective instability has been released in cumulus activity along its path. Also, the cooler ocean surface along west coasts must stabilize the air to some extent.

The foregoing discussion suggests that cumulus convection should be observed in more abundance in the eastern parts of continents and less extensively along west coasts. Its influence decreases northward, i.e. with increasing distance from the source of mT air. It should be observed to a considerable degree in the western parts of subtropical oceans and should be subdued in the eastern portions. Nearer the equator, away from the major influence of the subtropical anticyclones, the tropical oceans should be characterized by quite general occurrence of cumulus activity.

The four stations which were selected for study are: Boston, Massachusetts; New Orleans, Louisiana; San Juan, Puerto Rico; and Tatoosh, Washington. Boston and New Orleans represent the northern and southern extremities of a continent's eastern portion which is characterized by frequent inflows of mT air. San Juan is in a source region of tropical maritime air; its location in the southwest sector of a subtropical anticyclone during summer and fall indicates that the air in this region during half of the year is characteristically unstable. Tatoosh is typical of a west-coastal region with less common incursions of unstable mT air. These stations thus represent a wide variation of climatic types. Practical limitations on the amount of data which could be examined prevented the representation of other regions in this study. Most climates which have significant amounts of precipitation, however, bear a resemblance to one or more of the regions represented by the stations in this study.

2. Description of data

The number of storms studied for each station and the total hours of precipitation that they comprised are given in Table 10. The term storm in this chapter again refers to a continuous period of precipitation at a station. The records for Boston include all of those collected for three years, 1962, 1963, and 1969, by the Weather Radar Research Project at the Massachusetts Institute of Technology. In addition, all of the MIT data for January and February of 1966 and 1967 were also examined for Boston since these two months were sampled least frequently in the other three years. Less data is always obtained during the winter since the rain gauge cannot be used to measure snowfall intensity. The records for the other

Table 10. Number of storms* and total number of hours with at least 0.01 inches of precipitation for each station in data sample.

	Number of storms	Number of hours
Boston	139	1066
New Orleans	30	166
San Juan	125	207
Tatoosh	62	453

*The term storm refers to a period of precipitation at a station.

stations were obtained from the National Weather Service and Environmental Data Service of the National Oceanic and Atmospheric Administration. All of the data for a single January, April, July and October were examined for each of the three Weather Service stations. The particular years from which these months were chosen were ones in which the month had a large number of hours during which rain fell.

To obtain estimates of the input quantities for the model-storm program according to section H of Chapter III three basic types of data are needed: tipping-bucket rain-gauge records, radar range-height information, and upper-air sounding data. The rain-gauge traces should be available continuously for the duration of each storm, while the radar data and soundings need to be provided at only a few times in each case.

Rain-gauge records. These are available on long rolls of paper on which a mark is made automatically each time a certain amount of rain accumulates and the rain-gauge bucket tips. The paper moves past the marking pen at a constant rate; therefore, the density of marks on the chart is a measure of the rainfall rate. There are several gauges at MIT; the most sensitive one tips for every .01 mm of rain. The National Weather Service gauges tip for every .25 mm of precipitation. The records of the higher-resolution gauge at MIT were accompanied by simultaneous records either from a gauge which tips for a larger amount of rain or from a Hudson-Jardi flowmeter. These additional records were useful when rainfall rates were excessive and the spacings between marks for the more sensitive gauge became indistinguishable. Most of the rain-gauge records used to represent Boston in this study were actually obtained at a field station in West Concord, Mass., which is 30 km from Boston.

Radar data. Only records of the Range-Height Indicator (RHI) were considered. For the MIT radars discussed in Appendix A, these data are in the form of photographs on 35 mm film. An example is shown in Figure 19. These RHI observations are obtained for selected azimuths at successively increased intensity levels--or gain settings in the case of the older radars. The National Weather Service data were obtained on form WBAN60 which is a written record of the appearance of the radar scopes at hourly intervals; no pictures of the RHI are available. Radar observations used to represent San Juan were actually taken at Ramey AFB, Puerto Rico.

Soundings. Rawinsonde observations are available for the National Weather Service stations at Tatoosh and San Juan but not for New Orleans or Boston. For dates prior to August, 1965, data from Burrwood, Louisiana, were used to represent the upper-air conditions over New Orleans. After August, 1965, Boothville, Louisiana was used. For Boston, information was taken from three stations: Portland, Maine; Albany, New York; and Nantucket, Massachusetts. Observations made every day at 0000 GMT and 1200 GMT at each of these stations were published in Northern Hemisphere Data Tabulations by the U.S. Weather Bureau (presently the National Weather Service) and are available on cards and magnetic tape from the National Climatic Center, Asheville, North Carolina.

B. Data Processing

This section outlines the specific methods of analysis used to obtain input quantities for the model storm from the data described in the preceding section.

1. Rain-gauge records

For the higher-resolution gauges at MIT, the number of tips recorded in each 30-second interval during the storm was tabulated. This number was converted to an average rainfall rate for the half-minute. When a maximum (or minimum) of rainfall rate occurred in a 30-second period, the distance between the tips spaced closest together (or farthest apart) during that period was also measured. The time between these tips when converted to rainfall rates gave the most accurate possible determination of extrema in the records. For the lower-resolution gauges the times between all of the tips were measured and tabulated since these gauges tip less often.

All of the information obtained manually and tabulated as tips per thirty seconds or as time between tips was punched on cards and a computer program was written to plot, analyze, and print out the rainfall records for each storm. An example of the plotted output from this program is in Figure 18. The average rainfall rate for each 30-second period is indicated by the top of the area covered by asterisks. A minimum of rainfall rate within a half-minute is indicated by an "O" and a maximum by an "X". Precipitation which is considered cellular according to the criterion in section H of Chapter III is denoted by "C" atop the asterisks. The minimum, average, and maximum rates for each 30 seconds are also printed out numerically. This program was also designed to calculate the total cellular precipitation R_c and the total time Δt_c that cells were over the rain gauge for each hour of a storm.

Estimates of the model input quantities R_s, Δt_s, R_m, and Δt_m were obtained in a less objective manner. According to the general guidelines in section H of Chapter III, it was decided on the basis of the appearance of the rain-gauge traces when mesoscale and synoptic areas were over the gauge. A maximum synoptic precipitation rate was thus arrived at for each hour of rainfall. R_s was assumed to be the total amount of rain which fell in 30-second intervals with average rates less than or equal to the maximum synoptic rates while Δt_s was the total time during which R_s fell. The mesoscale quantities, R_m and Δt_m, were the amounts of rain and time not included in R_c and R_s and in Δt_m and Δt_s, respectively.

The values of R_c, R_m, R_s, Δt_c, Δt_m, and Δt_s calculated for each hour of each storm were punched on cards in a format suitable for input to the model-storm program.

The above procedures were followed for Boston, New Orleans, and San Juan. For Tatoosh, however, the rainfall data were treated in a simplified manner in the interest of saving time. For this station, the cellular precipitation was determined from inspection of the rain gauge recorder charts by mentally applying the criterion for cellular rainfall. Precipitation not called cellular was classified as synoptic; thus, no attempt was made to identify the mesoscale precipitation. The quantities R_c, R_s, Δt_c, and Δt_s were recorded manually directly from the recorder charts and R_m and Δt_m were assumed to be zero. The detailed computerized analysis of the rainfall data was thus bypassed. Since R_m is zero, the parameter α is meaningless in equation (13) and estimates of the cellular condensation for Tatoosh were made for two cases only, β equal to 1 and 3. The former is the lower limit while the

value of 3 for β is considered the best estimate since it implies that only a third of the cellular condensate reaches the ground and therefore more realistically represents the inefficient nature of cumulus convection.

2. Radar data

The model-storm input quantities z_T and z_p were obtained by direct examination of photographs and written records of RHI displays exactly as described in section H of Chapter III. In storms for which radar records were missing at Boston, a seasonally averaged value of the cell-top height z_T was used and z_p was set equal to z_T. RHI data were available for all storms at New Orleans and San Juan; however, it was discovered during the analysis that no records of the RHI were kept at Tatoosh. Therefore, $z_T = z_p = 6$ km was used with $z_B = 1$ km for all storms at Tatoosh. These values are representative of the average conditions at Boston which, although of a different climate, is at approximately the same latitude as Tatoosh.

3. Soundings

The model-storm inputs obtained from sounding data are the representative equivalent potential temperature θ_e, the humidity parameters H_1, H_2, and H_3, the cell base z_B, and the westerly wind shear B. All of these except B were obtained by inspection of plotted soundings of temperature and humidity as described in section H of Chapter III.

Soundings published in Northern Hemisphere Data Tabulations were plotted by hand on pseudo-adiabatic diagrams. Those obtained on punched cards from the National Climatic Center were plotted by computer. The plotting program that was used was written by this author. In all, about 1000 soundings were plotted.

The shear B for each sounding was determined from the slope of the least-square curve computed for the winds between 850 and 400 mb. Examples of these least square curves are shown in Figure 21. For Boston, an average B was obtained for the three soundings at Albany, Portland, and Nantucket at each observational time. Only one sounding was involved at each time at the other stations. The B obtained for each standard observational time before, during and after a storm was fed into the model-storm program. Within that program an appropriate value of B was obtained by interpolation between sounding times for each hour of the storm.

C. Monthly transports for each station

1. Computation of monthly curves

For each storm in the data sample, the sensible heat and angular momentum transports $\tau_{SH}(z)$ and $\tau_{AM}(z)$ were calculated for various combinations of α and β, the parameters which determine the cellular condensation from measured precipitation amounts. The combinations of α and β which give a lower limit, best estimate, and upper limit for the cellular condensation were determined for each storm according to the kinematic and water budget considerations given in sections F1-3 of Chapter III. Three curves were thus considered for each storm; these are illustrated in Figures 22 and 23 where the solid curves were determined by the best estimate of the cellular condensation while the dashed ones were obtained from the lower and upper limits.

The transport curves were summed at each level for all of the storms in a particular month of the year for all of the years sampled. For example, the transports for all of the storms which occurred at a particular station in January,

regardless of the year, were added together to give a grand total transport for January. This was done separately for lower limits, best estimates, and upper limits. The grand total transport was then multiplied by the ratio of the climatologically averaged number of hours of precipitation to the number of hours of precipitation sampled for the station and month under investigation. An hour of precipitation is defined as an hour during which at least .01 in of precipitation was measured. The resulting curves represent the total cellular transport which would occur in a month with an average number of hours of measurable precipitation. These curves will be referred to as the monthly transports. The monthly transports for sensible heat and angular momentum at each station are shown in Figures 24 - 31. The solid curves are the best estimates while the dashed curves on either side are for the combinations of α and β which give lower and upper limits for the amount of cellular condensation. For Tatoosh only two curves are shown for each month. Since the rainfall data were processed in a simplified manner, only lower limits and best estimates for the cellular condensation were computed, from the cases $\beta = 1$ and $\beta = 3$ respectively, as described above.

The average number of hours of precipitation used in the calculation of the monthly transports was obtained for different months and stations from the Decennial Census of United States Climate - Summary of Hourly Observations, published by the U.S. Weather Bureau. Ten-year statistics on the hourly occurrence of precipitation were not available for Tatoosh; data for Salem, Oregon, were, therefore, substituted with the following modification. The number of hours of rainfall

in any given month at Salem was doubled to approximate the conditions at Tatoosh where the monthly rainfall amounts are approximately twice those at Salem.

The crossing of the monthly transport curves which is noted in some months at the uppermost levels in Figures 24 - 31 results from a peculiarity of the modelling. As noted in section C2 of Chapter III, the mass transport at the cell tops was required to connect with the pro-rated mesoscale mass transport curve above the cells. It is seen from equations (7), (13), and (16) that as α is increased, larger cellular mass transports are produced at most levels within the cells; however, since the mesoscale transports are simultaneously reduced the cumulus transports near the cell top are actually reduced as α is increased. The monthly transport curves in Figures 24 - 31 occasionally cross at the top level since the upper limit curves are usually determined from larger values of α which give smaller values of mesoscale lifting and thus smaller cumulus transports at cell tops. It is to be noted that this behavior of the transport curves, introduced by a feature of the modelling which may or may not be realistic, does not affect the results of the transport computations except at the cell tops where the transports are small in any case.

It is recalled that the monthly cumulus-scale transports which are computed are just a part of the total cumulus transport. Only precipitating cumuli are included in the calculations and the effect of downdrafts is not evaluated.

2. Standards of comparison

The relative significance of the cumulus-scale transports in the total atmospheric spectrum is judged by comparing the computed monthly transports with fluxes of heat and angular momentum by circulations of other scales. It would be

desirable to make comparisons with larger-scale transports computed directly from atmospheric data. Although estimates of the mean meridional transports have been made from atmospheric observations (e.g. Palmen and Newton, 1969), synoptic-scale fluxes cannot be adequately computed because of difficulties in estimating vertical velocities from the present station network, as pointed out by Oort and Rasmusson (1971). However, computations of vertical transports by synoptic-scale eddies in numerical models of the general circulation have been made by several investigators. A latitude-height distribution of the upward transport of heat by large-scale eddies in a nine-level model of the atmosphere is shown in Figure 32; these calculations were made by Manabe et al (1970). The vertical transport of angular momentum computed similarly, but with a somewhat less sophisticated model, by Smagorinsky et al (1965) is given in Figure 33. Calculations have also been made of the total required vertical eddy fluxes which are considered to be the residuals of all the observed components of the heat and angular momentum budgets. Results of this type for heat and angular momentum transports have been obtained by Palmen and Newton (1969) and are reproduced in Figures 34 and 35. It should be noted that their values are for winter conditions. Starr et al (1970) calculated the required vertical transport of angular momentum by eddies of all scales for annual conditions and their results are in Figure 36. Also shown in Figure 35 are the angular momentum fluxes by the mean meridional circulations at low and high latitudes as calculated by Palmen and Newton (1969).

The vertical transports computed by the various investigators and shown in Figures 32 - 36 are used as standards of comparison for the monthly

cumulus transports computed for the stations in this study. In each case, the cumulus-scale transports were compared with fluxes which appeared to be of primary importance at the latitudes of the individual stations. The fluxes obtained for comparison at different latitudes were read directly off of Figures 32 - 36 and are shown in Figures 24 - 31 with the monthly cumulus transports.

3. Results for Boston

The seasonal variation of the cumulus phenomenon at Boston is clearly shown by the monthly transport curves in Figures 24 and 25; it is particularly evident from a comparison of the monthly transports for January, April, July, and October. In summer, the convection is distributed through most of the troposphere with a level of maximum transport near 6 km. During the winter months, cumulus cells are observed only in the lower half of the troposphere with a maximum effect near a height of 4 km. In the spring and fall, the convective elements are generally intermediate between the summer and winter cells in their vertical development and general effectiveness in carrying out transports. The particularly high transports for March may not be representative since the sample size was relatively small for this month. The angular momentum transports for November and December are notably smaller in relation to transports for other months than are the sensible heat transports for November and December. This difference is a reflection of the fact that the westerly wind shear in the environment of the cumulus cells was often negative as well as positive during periods of heavy cumulus activity during these two months.

The seasonal variation in the vertical extent and overall magnitude of cumulus transports observed at Boston is what would be expected from climatological reasoning. In summer, this station is often found within essentially unmodified tropical maritime (mT) air with considerable potential instability favoring development of vigorous penetrative convection. During winter, however, mT air usually arrives at Boston after having undergone a certain amount of turbulent mixing in advance of an extra-tropical cyclone. The instability in this air is usually marginal and deep convection apparently is not favored.

The curve labelled MSE (Manabe-synoptic eddy) and shown with the January, April, July, and October monthly heat transports in Figure 24 is the annual average upward transport of heat by synoptic-scale eddies at latitude 40N. It was obtained by reading values directly off of Figure 32. The curve labelled PTH (Palmen-total eddy, high latitude) is the total upward transport of heat required of synoptic and smaller-scale eddies to balance the other components of the heat budget of the region poleward of 32N, as illustrated in Figure 34.

The importance of the cumulus-scale transports in the atmospheric heat budget may be assessed at the latitude of Boston by comparison with synoptic-scale transports. Since the mean meridional circulation transports heat downward at middle latitudes, the synoptic and smaller-scale eddies must accomplish the required upward transport. In January, at the 4 km level where the cumulus transport is a maximum, the best estimate is only 10% as large as Manabe's annual synoptic-scale flux. In July, at the 6 km level the best estimate of the cumulus transport is 70% as large as the synoptic-scale flux computed by Manabe et al. It therefore

appears that at Boston the cumulus transport of heat during summer is about as important as the annual synoptic-scale transport, but considerably less important in the winter.

The cumulus transports of angular momentum at Boston may be compared in a meaningful way with the transport accomplished by the mean meridional circulation in middle latitudes. It is evident from the results of Palmen and Newton (1969) in Figure 35 that the major part of the downward transport of angular momentum is accomplished by this circulation. Only a small fraction of the downward transport remains to be carried out by synoptic and smaller-scale eddies. The results of Starr et al (1970) in Figure 35 in fact suggest that in some locations at mid latitudes the total required eddy flux may not only be small, but upward as well. The variation among the various estimates of vertical fluxes of angular momentum by eddies and the generally small magnitude of these fluxes emphasize that the mean meridional flux must account for the largest share of the angular momentum transport at most latitudes and is, therefore, the most stringent standard by which to judge the cumulus-scale transports.

The curve labelled PMH (Palmen-meridional, high latitude) in Figure 25 was derived from the angular momentum budget in the higher-latitude portion of the atmosphere shown in Figure 35. Comparison of the monthly cumulus-scale transports of angular momentum at Boston with this curve shows that in January the best estimate for the cumulus transport at the 4 km level where it is a maximum is about 15% as large as the mean meridional flux in mid latitudes. In July, on the other hand, the cumulus transport curve and the Palmen curve become almost identical in

magnitude above a height of 6 km. It is concluded, then, that in summer at Boston the cumulus-scale transport of angular momentum is of the same sign and about as large as the mean meridional flux in the mid to upper troposphere. In winter, however, the cumulus transport of angular momentum is apparently a small effect compared with that of the mean meridional circulation.

4. Tatoosh

The simplifications which were made in the data processing for this station are evident in the monthly transport curves shown in Figures 26 and 27. As explained in section C1 of this chapter, only two curves are shown for each month where the right-hand curve in each case is considered the best estimate. Also, it is noted that all of the curves terminate at 6 km since no radar RHI data were available and the cell tops were therefore assumed to always be at this height. As a result no seasonal variation in the vertical development of cumulus cells can be observed in the results for this station.

The seasonal variation in the magnitude of the cumulus transports is, however, evident. The largest values occur in October while during July there is negligible cumulus activity. The latter fact is expected since during the summer Tatoosh is under the influence of the subsiding eastern edge of the Pacific subtropical anticyclone. The cumulus transports in January are almost as large as those in October. It is noted, however, that this results partially from the fact that precipitation of any type is more than twice as likely to occur in a typical January than in October. The transports in January thus result from less frequent and weaker cumulus activity spread over a longer total duration of rainfall. Although transports

were computed for only January, April, July, and October, rain-gauge data for Tatoosh were analyzed for the other eight months of the year as well. The results, listed in Table 11, show that the months for which transports were computed are indeed representative of their respective seasons and that the maximum cumulus activity probably occurs in October or November.

The monthly cumulus heat transports in Figure 26 are compared with the vertical distribution of the upward flux of heat by synoptic-scale eddies at latitude 50N calculated by Manabe et al (1970) and with the total required flux of heat by synoptic and smaller-scale eddies at mid latitudes computed by Palmen and Newton (1969). It is evident from Figure 26 that the cumulus heat transport in October when it is maximum is about 60% as large as the synoptic-scale flux computed by Manabe et al. The cumulus transports of angular momentum are again compared with the mid- to high-latitude mean meridional flux evaluated by Palmen and Newton (1969). At the 5 km level the cumulus transports in October are approximately as large as the mean meridional flux of angular momentum. Therefore, at Tatoosh in autumn, and perhaps winter as well, cumulus transports apparently become significant in comparison with larger-scale effects. In summer, however, the cumulus fluxes are completely negligible and in spring they are also quite small.

5. San Juan

The cumulus transports for this station in Figures 28 and 29 have a pronounced seasonal variation. During January the cells are confined to the lowest 5 km of the atmosphere with a maximum transport occurring between the 2 and 3 km levels. The vertical extent and intensity of the convection increase steadily through

Table 11. Total rainfall and the amounts considered cellular for 12 months at Tatoosh.

Month	Total Rainfall (in)	Cellular Rainfall (in)
Jan. 1964	12.79	.90
Feb. 1963	8.97	.51
Mar. 1963	6.29	.13
Apr. 1962	9.23	.39
May 1963	3.41	.13
June 1963	1.98	.03
July 1964	3.23	.02
Aug. 1962	4.75	.42
Sep. 1962	3.63	.64
Oct. 1963	13.26	2.49
Nov. 1962	4.95	1.76
Dec. 1963	15.22	.45

April and July. There is a maximum of activity in October when cumulus transports are observed through at least 10 km of the troposphere and the largest transports are found at a height of 7 km. This is the type of behavior which would be expected from the seasonal variation of the Atlantic subtropical anticyclone. During winter and spring, San Juan is in the south-central extremity of this high pressure system where the air is generally stable. In the summer and fall, San Juan is found in the characteristically unstable southeastern quadrant of the Atlantic high.

In Figure 28 the Manabe-synoptic eddy (MSE) curve for latitude 20N and the Palmen-total eddy, low latitude (PTL) curve are shown with the monthly cumulus transports of sensible heat. Comparison of the Manabe and Palmen curves suggests that synoptic-scale eddies do not account for much of the total required eddy flux of heat. In January and April the cumulus-scale transports are very similar to the synoptic-scale flux shown by the Manabe curve. This indicates that in winter and spring the cumulus transports of sensible heat at San Juan are of no more significance than the synoptic-scale flux of heat. However, in summer and fall the cumulus transports between heights of 4 and 8 km range from 40% to 100% as large as Palmen's total required eddy flux and are generally much larger than Manabe's annual synoptic-scale heat flux.

The monthly cumulus-scale transports of angular momentum in Figure 29 are compared with the Palmen-mean meridional, low latitude (PML) curve. While the cumulus transports of angular momentum are downward, the mean meridional flux is upward. The magnitudes of the downward cumulus transports are from 25% to 55% as large as the upward mean meridional flux below the 3 km level

in January and April, while the best estimates range between 25% and 100% as large throughout 10 km of the atmosphere during July and October. The vertical transport of angular momentum by cumulus-scale cells therefore appears to be a moderately important effect year round; however, its effect is felt through a much deeper layer of the troposphere during the summer and fall.

It was found by Starr et al (1970), Figure 36, that the total transport of angular momentum by eddies at the latitude of San Juan (18N) should be upward. Since the cumulus transports are downward, the net upward eddy transport at this latitude must be accomplished by synoptic-scale eddies. The results of Smagorinsky et al (1965), Figure 33, whose model did not contain cumulus-scale convection, do show an upward transport of angular momentum by synoptic-scale eddies. From a comparison of Figures 29 and 33, it appears that these upward fluxes by the larger-scale eddies near latitude 18N may be smaller in magnitude than the cumulus transports at San Juan.

6. New Orleans

The monthly cumulus-scale transports for this station are given in Figures 30 and 31. Their seasonal variation is again well-defined and consistent with climatological expectations. The close proximity of New Orleans to a source of unstable mT air favors considerable cumulus development in all seasons. Somewhat less convection occurs in winter when most of the precipitation is connected with cyclones that develop over the southern United States or over the Gulf of Mexico. However, the air undergoing lifting in advance of these systems is usually of tropical maritime origin and unstable; consequently, penetrative convection is frequently

found within them. The monthly transports for January in Figures 30 and 31 are significant up the 8 km level. During other seasons, essentially unmodified mT air with high degrees of instability prevails and vigorous cumulus activity frequently develops. In April, July, and October the effect of the convection is felt well above the 10 km level although the calculations were truncated at that height. The maximum activity is found in April and July.

In Figure 30 the monthly cumulus-scale heat transports are compared with the synoptic-scale eddy flux for latitude 30N computed by Manabe et al (1970). In January, the cumulus heat fluxes between 6 and 7 km are 35% to 50% as large as the synoptic-scale transports in Manabe's model. In October, above 6 km the cumulus heat transports almost coincide with Manabe's curve while in April and July the cumulus flux is about 5 times as large as the synoptic-scale transport above 6 km. The cumulus transport of sensible heat therefore appears to be quite significant at all seasons at New Orleans, and especially during spring and summer.

The total required eddy flux of heat computed by Palmen and Newton (1969) is also shown in Figure 30 for comparison with the monthly cumulus transports. Since New Orleans is located on the boundary which separates the low and high latitude regions of their idealized atmosphere (Figures 34 and 35), the curves for both regions are given in Figure 30.

The curves of Palmen and Newton (1969) for the mean meridional flux of angular momentum are shown in Figure 31 for both low and high latitude regions for comparison with the monthly cumulus transports. The behavior of the cumulus-scale transports of angular momentum is similar to that of the heat transports except

in one respect. The maximum angular momentum transports occur only in April, whereas the maximum heat transports were found with about equal intensity in both April and July. This difference arises because the cumulus convection in April had larger westerly wind shears associated with it. This might have been expected climatologically since the cumulus activity in the spring at New Orleans is frequently of the type referred to as "severe storms." These are mesoscale systems of cumulus convection characterized by extreme potential instability which is released by an organized larger-scale lifting mechanism. The synoptic conditions which are favorable for this type of convection are characterized by strong wind shear. Severe storms are usually located in the warm sector of a migratory cyclone. In summer, when storm tracks are at higher latitudes the cumulus convection at New Orleans is primarily of the so-called "air mass" type which is usually triggered by surface heating and which is not noted for being located in regions of strong vertical wind shear.

D. Climatology of cumulus transports

The foregoing comparisons of cumulus-scale transports with heat and angular momentum fluxes by larger-scale circulations indicate that the cumulus transports at certain vertical levels are significant in various seasons and geographical areas. The comparisons which were made are summarized in Table 12. From the table it is seen that during seasons when the cumulus transports were large at each station, comparative values of 60% to 500% are found. The seasonal lows range from zero to 40%.

Table 12. Summary of comparisons of monthly cumulus-scale transports with transports by circulations of other scales. Percentages refer to the size of computed cumulus-scale transports relative to estimated larger-scale fluxes at the indicated heights and months and at the latitudes of the particular stations.

Station	Type of Transport	Comparative values for seasonal extremes		Type of flux compared with and investigators from whom it was obtained	
		Low	High		
Boston	Heat	10% at 4 km (Jan)	70% at 6 km (July)	Synoptic-scale eddy at 40N	Manabe et al (1970)
	Momentum	15% at 4 km (Jan)	100% at 6 km+ (July)	Mean meridional, high latitude	Palmen and Newton (1969)
Tatoosh	Heat	negligible (July)	60% at 4 km (Oct)	Synoptic-scale eddy at 50N	Manabe et al (1970)
	Momentum	negligible (July)	120% at 5 km (Oct)	Mean meridional, high latitude	Palmen and Newton (1969)
San Juan	Heat	20% at 2 km (Jan)	100% at 7.5 km (Oct)	Total eddy (mean meridional not included)	Palmen and Newton (1969)
	Momentum	25% at 3 km (Jan)	100% at 9 km (Oct)	Mean meridional, low latitude	Palmen and Newton (1969)
New Orleans	Heat	40% at 6.5 km (Jan)	500% at 6 km+ (April & July)	Synoptic-scale eddy at 30N	Manabe et al (1970)
	Momentum	35% at 7 km (Jan)	250% at 9 km (April)	Mean meridional, low latitude	Palmen and Newton (1969)

From the calculations and comparisons which have been made, a quantitative climatology of cumulus transports can be constructed. As in the preceding discussions for individual stations, the significance of the vertical transports of sensible heat by cumulus cells is determined by comparison with the vertical flux of heat by synoptic-scale eddies, as computed by Manabe et al (1970) and shown in Figure 32, and with the total required vertical eddy flux of heat estimated by Palmen and Newton (1969) in Figure 35. The cumulus transports of angular momentum are measured against the mean meridional fluxes estimated by Palmen and Newton (1969) in Figures 34 and 35.

As expected, the extent to which cumulus convection transports sensible heat and angular momentum vertically in a particular geographical area is determined largely by the proximity of that region to a source of unstable tropical maritime (mTu) air. Source regions for this type of air mass are found in the southwestern sectors of the semi-permanent oceanic anticyclones. The cumulus-scale transports observed in such a source area are illustrated by the computations for July and October at San Juan which show cumulus transports of sensible heat of 40% to 100% as large as the required eddy flux and much larger than the synoptic-scale vertical eddy transport at this latitude at levels between 4 and 8 km. The angular momentum transports are downward with magnitudes 25% to 100% as large as the upward mean meridional flux at low latitudes.

In other sectors of the subtropical highs, subsidence aloft confines cumulus convection to the lowest few kilometers of the atmosphere or inhibits it altogether. During January, San Juan is on the south-central extremity of the Atlantic

anticyclone and cumulus transports as shown in Figures 28 and 29 are found only in the lowest 4 to 5 km of the atmosphere. The magnitudes of the transports at these low levels were moderate or small. Below 3 km the downward angular momentum transport at San Juan in January was 25% to 55% as large as the upward mean meridional flux at low latitudes, while the sensible heat transport by cumulus cells appeared to be an order of magnitude smaller than the total required eddy flux of heat. On the eastern edges of the oceanic highs, convection is even more suppressed. This fact is illustrated by the results for July at Tatoosh in Figures 26 and 27 where practically no precipitating cumuli at all were found.

Around the western and northern perimeters of a subtropical anticyclone, unstable mT air is transported from its source region in the southwest sector of the high northward and eastward, either within the southerly flow in the western part of an especially well-developed subtropical high or in advance of migratory cyclones. As the mTu air progresses poleward it is continually modified by mixing, and the farther it is removed from its source region the less pronounced are the cumulus transports, both in magnitude and vertical extent. This is seen by comparison of the monthly cumulus-scale heat transports at New Orleans, Boston, and Tatoosh which are found respectively at increasing distances from sources of mTu air. For this comparison, reference may again be made to the monthly heat transports given in Figures 24, 26, and 30, and to Table 12. At New Orleans in January, the cumulus-scale heat fluxes between 6 and 7 km are 35% to 50% as large as the annual synoptic-scale transports, while in April and July they are as much as five times the magnitude of the synoptic-scale flux and extend well above a height of

10 km. At Boston, the cumulus-scale sensible heat transport ranges from 10% as large as the annual synoptic-scale flux at 4 km in January to 70% at 6 km in July. Tatoosh is much farther than New Orleans or Boston from a source of mTu air and might, therefore, be expected to have much smaller cumulus transports. However, since rainfall is such a common occurrence at this station in fall and winter, even relatively infrequent cumulus activity gives substantial total monthly transports in these seasons. For example, in October, the monthly cumulus-scale transport of sensible heat at 4 km at Tatoosh is 60% as large as the annual synoptic-scale flux at 50N. During summer, mTu air seldom reaches Tatoosh and very little rainfall occurs. Thus, cumulus transports at this time of year are negligible at this station.

Cumulus convection is notably weaker and less deep when the meso-scale precipitation areas containing the cumulus cells are located within cyclones rather than being more isolated as in classic thunderstorm situations. This is reflected in the seasonal variation of cumulus transports at New Orleans and Boston where the transports are found within shallower layers and are less intense in winter when precipitation is principally of the cyclonic type than in other seasons. During the summer at Boston and during the spring, summer, and fall at New Orleans cumulus convection occurs within mTu air which has undergone less mixing en route from its source regions and the cumulus transports are larger and extend through a greater depth of the atmosphere than in winter. The seasonal differences in transports are seen in Figures 24-25 and 30-31.

Several climatic types are not treated in this study. Since only precipitating cumuli are included in the computations, climates with little rainfall are

ignored. Regions poleward of latitude 60 deg are not considered; here cumulus-scale transports should be small since air masses are not characteristically unstable. The equatorial regions also are not represented by the stations in this study because of practical limitations on the sample size. However, since there is much cumulus activity in the "intertropical convergence zone" transports of physical quantities by cumulus-scale convection near the equator must be significant and should be dealt with in future studies.

From the climatological sampling in this study, the following conclusions are drawn concerning the relative importance of cumulus-scale convection as a transport mechanism in the atmosphere. The transports of sensible heat and angular momentum by precipitating cumulus updrafts become comparable in magnitude with fluxes of these quantities by larger-scale circulations in certain climatologically predictable regions and seasons. The vertical extent and magnitude of the cumulus transports at a particular time of year in a given region are determined by the frequency with which the region is under the influence of unstable tropical maritime air and the extent to which that air has been modified when it reaches the region. A complete consideration of the atmospheric budgets of heat and angular momentum should therefore include the regional and seasonal effects of cumulus convection.

The consistency of the findings of this study with climatological expectations indicates that the modelling technique gives quite plausible results when applied to real atmospheric situations. The uncertainties evaluated in Chapter III remain in the model, however, and further refinement is therefore needed. This refinement will come as the dynamics of cumulus convection and its associated

condensation and precipitation processes are better understood and as measurements of model input quantities are improved.

E. Comment on the temporal concentration of cumulus transports

It is noted that the monthly cumulus-scale transports which have been computed are not accomplished evenly over an entire month but rather only within periods of precipitation. Further, it was observed as the rain-gauge data was processed that the majority of cumulus activity was concentrated within relatively few of the hours when precipitation occurred. This finding points out that during certain periods of time, the cumulus transports at a point are of highly significant magnitude when compared with larger-scale fluxes, but remain zero most of the time.

CHAPTER V

CONCLUSIONS AND SUGGESTIONS FOR FURTHER RESEARCH

This study has been concerned primarily with the development and application of a model for computing the vertical transports of such quantities as sensible heat and angular momentum by precipitating cumulus-scale updrafts. Since precipitation is one atmospheric variable which can be mapped three-dimensionally on the cumulus scale, detailed rainfall data provide the basic input for the model. The investigation has three basic aspects. First, an analysis of the structure of precipitation patterns is made from which it is determined whether rainfall of cumulus origin is organized within larger-scale patterns in such a way that it may be readily identified and measured. Second, equations are developed from which cumulus-scale transports of sensible heat and angular momentum may be calculated given certain observed parameters of any given rainfall situation. Finally, the model equations are tested with input data collected from several stations with widely varying climates, and a climatological study of the transports is made.

The primary results of this investigation are:

(1) Precipitation patterns in all types of storms are composed of certain basic structures, namely cumulus-scale cells, mesoscale areas, and synoptic areas, which have consistent characteristics and behavior thereby allowing any given storm to be described or modelled in terms of its predominant features.

Detailed descriptions of these basic features in rainfall patterns give useful guidelines for determining the basic components of rainfall, including the cumulus component, for any given storm. Parameters of rainfall patterns may be used as input for computations of cumulus transports.

(2) Model calculations of cumulus-scale transports of sensible heat and angular momentum give results which agree qualitatively with climatological expectations and also appear to be plausible by comparison with computations of larger-scale transports. It is concluded therefore that the model provides a feasible way for computing vertical transports accomplished by cumulus-scale convection. The uncertainties in both the heat and angular momentum transports are each estimated to be about a factor of four.

(3) Computed vertical transports of sensible heat and angular momentum are comparable in magnitude with important larger-scale fluxes of these quantities during at least one season of the year in four widely varying climates represented by Boston, Mass.; New Orleans, La.; San Juan, P.R.; and Tatoosh, Wash. In future computations of atmospheric budgets of heat and angular momentum, serious consideration should be given to the effects of cumulus-scale convection in certain seasons and geographical areas.

Further progress in the study of cumulus transports may be made in three areas:

(1) The relationship between cellular and mesoscale precipitation which is always present in the vicinity of cells should be investigated further. The

importance of such an investigation lies in the fact that the cumulus-scale transports are related to the amount of condensation occurring in cumulus updrafts. This condensation is in turn deduced from cellular and mesoscale precipitation amounts and a major uncertainty in the model calculations is associated with how much mesoscale precipitation is originally condensed in cumulus cells. The relationships between cells and the mesoscale areas in which they are found may be explored from kinematical and microphysical considerations of the lifting and condensation processes in the different regions or from the point of view of the dynamic processes, such as CISK, which may be involved in the development of the mesoscale systems.

(2) The modelling technique would be improved if the effects of cumulus downdrafts in transporting heat and horizontal momentum could be incorporated. Downdrafts are not presently included because so little is known about the mechanisms involved that it is difficult to handle them in a quantitative manner. Consequently, the transports which have been computed so far only represent those accomplished by the upward branch of the convection.

(3) The climatological study of cumulus-scale transports could be enhanced by investigating other regions than those which have been treated in this investigation, notably attention should be directed toward equatorial regions.

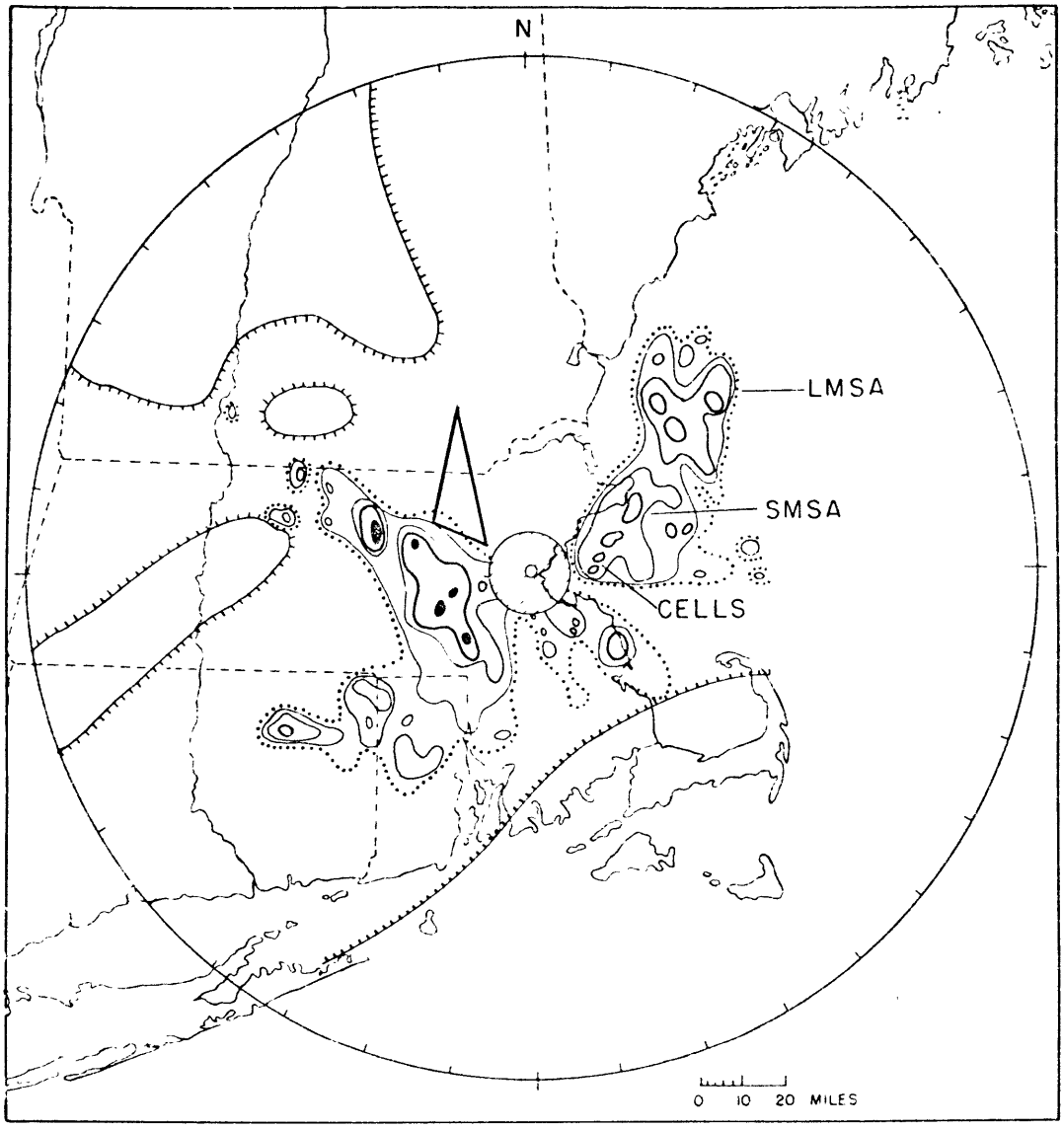


Figure 1. Precipitation pattern showing large mesoscale areas (LMSA), small mesoscale areas (SMSA), and cells. Data taken with AN/CPS-9 radar, 8 July 1963, 0635 EST. Contours indicate equivalent rainfall rates: 0 ( ), 1 ( ), 2,4,8, and 16 (solid) mm hr^{-1}. Triangle is observational area discussed in Appendix D.

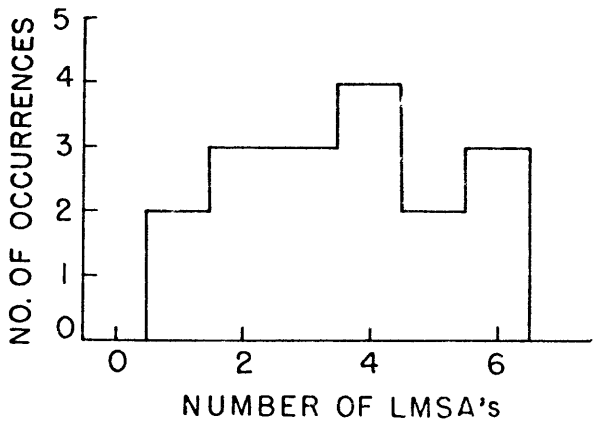


Figure 2. Distribution of number of large mesoscale areas (LMSA's) appearing simultaneously in area observed by the radar, a circle with 200 km radius.

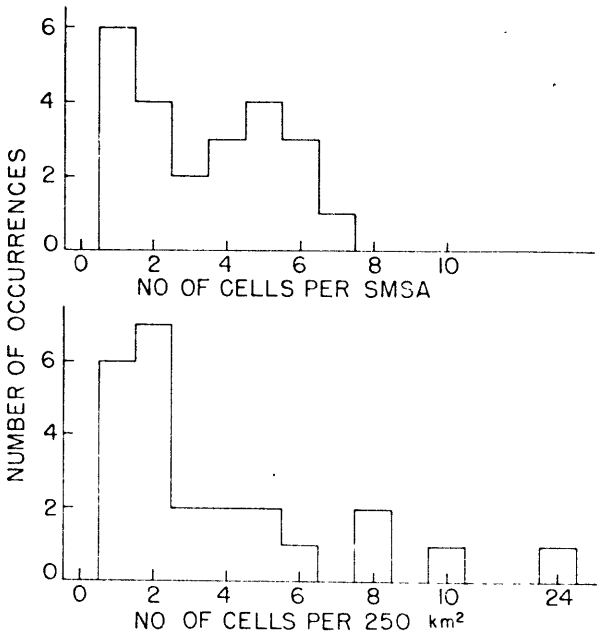


Figure 3. Distributions for average number at one time and density of cells within the small mesoscale areas.

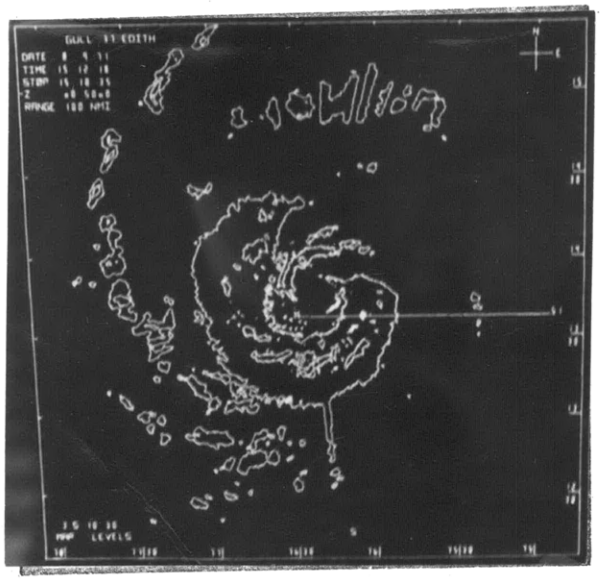


Figure 4. Plan position display of a hurricane as viewed with an airborne radar. Contours of two values of radar reflectivity are shown.

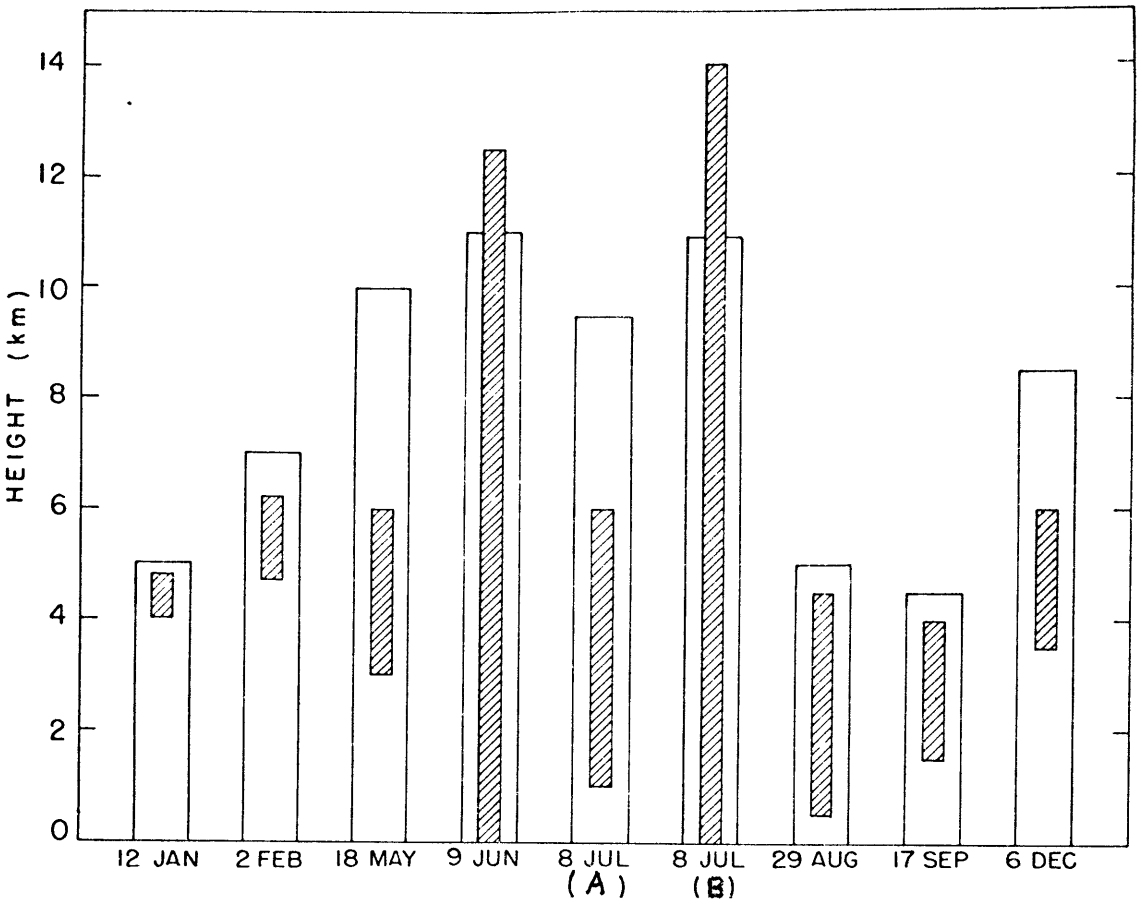


Figure 5. Average vertical extent of cells (shaded portion) and surrounding precipitation during different storms.

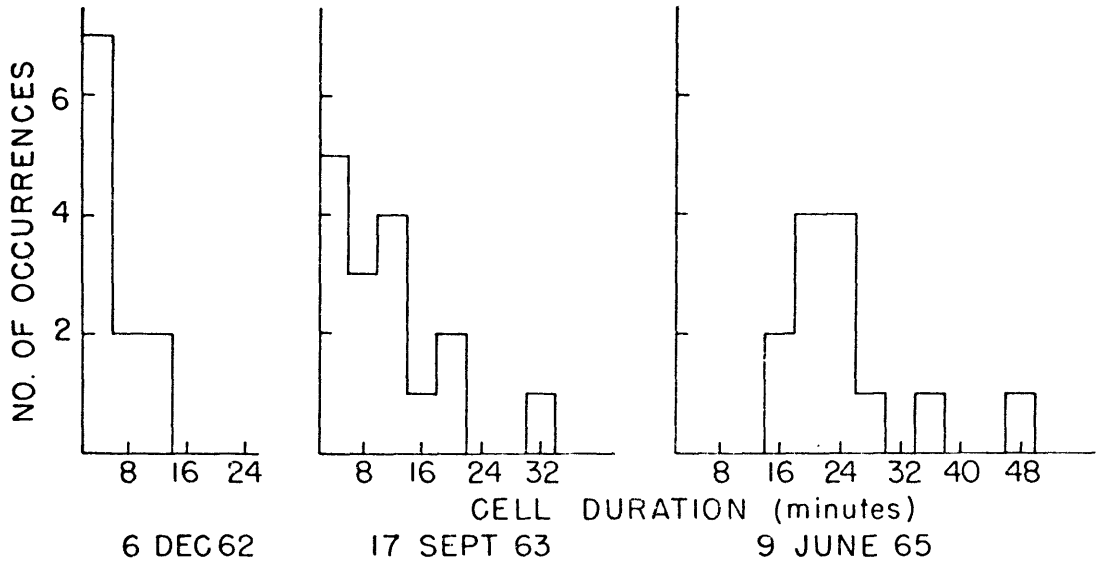


Figure 6. Examples of distributions of the durations of cells for individual storms.

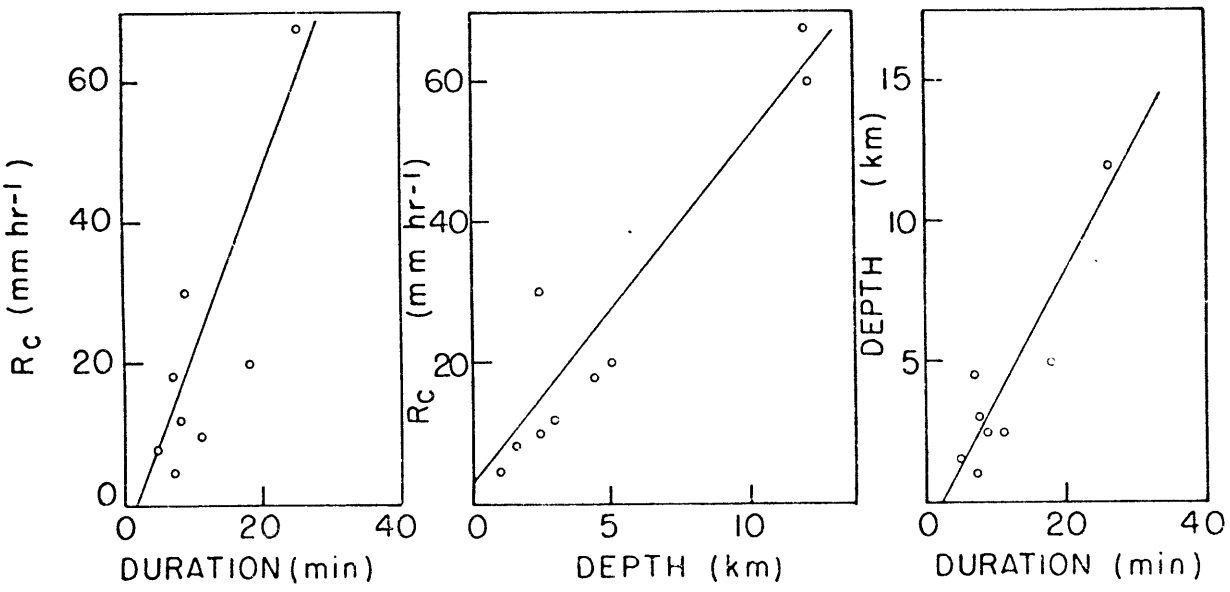


Figure 7. Relations between depth, duration and rainfall intensity, R_c, for cells. Each point represents average values for all cells in one storm.

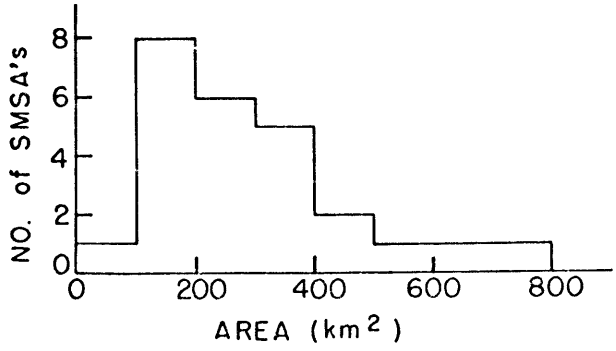


Figure 8. Distribution of areas of small mesoscale precipitation areas (SMSA's).

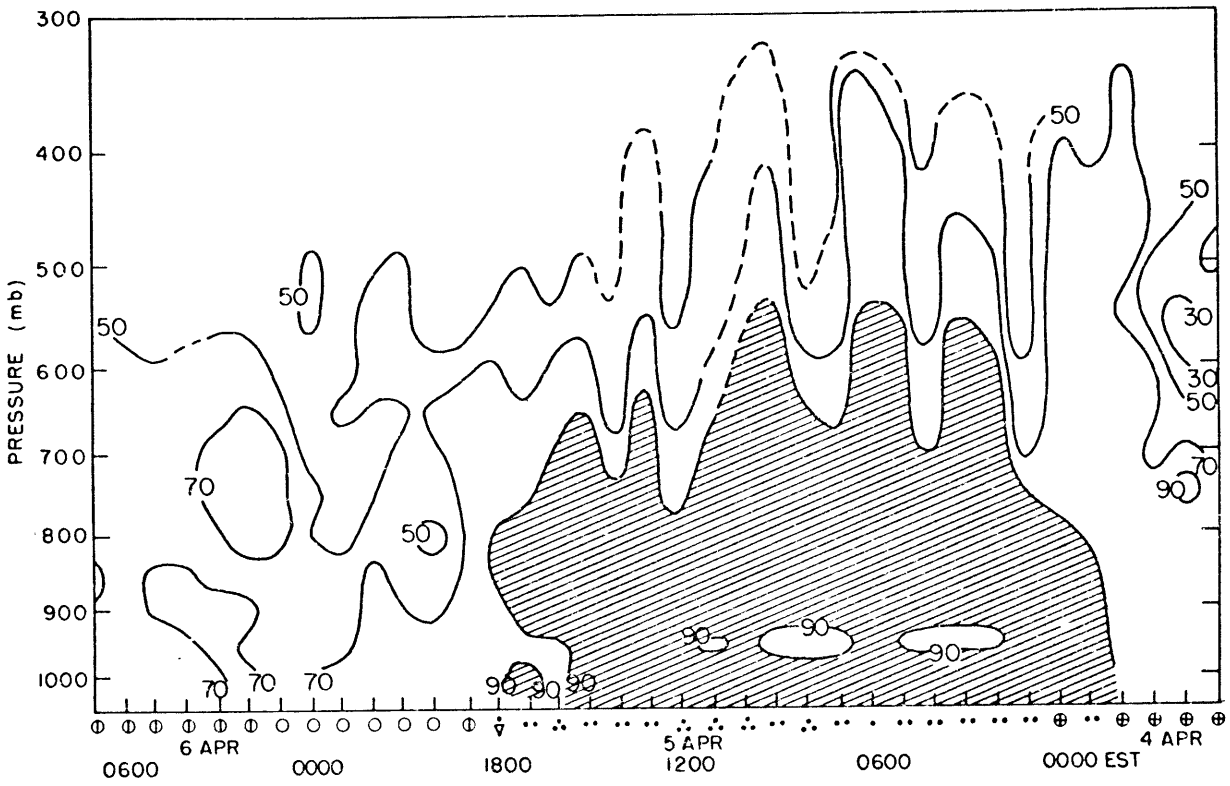


Figure 9. Relative humidity pattern shown by hourly soundings at Bedford, Mass., April, 1960. Values are in per cent.

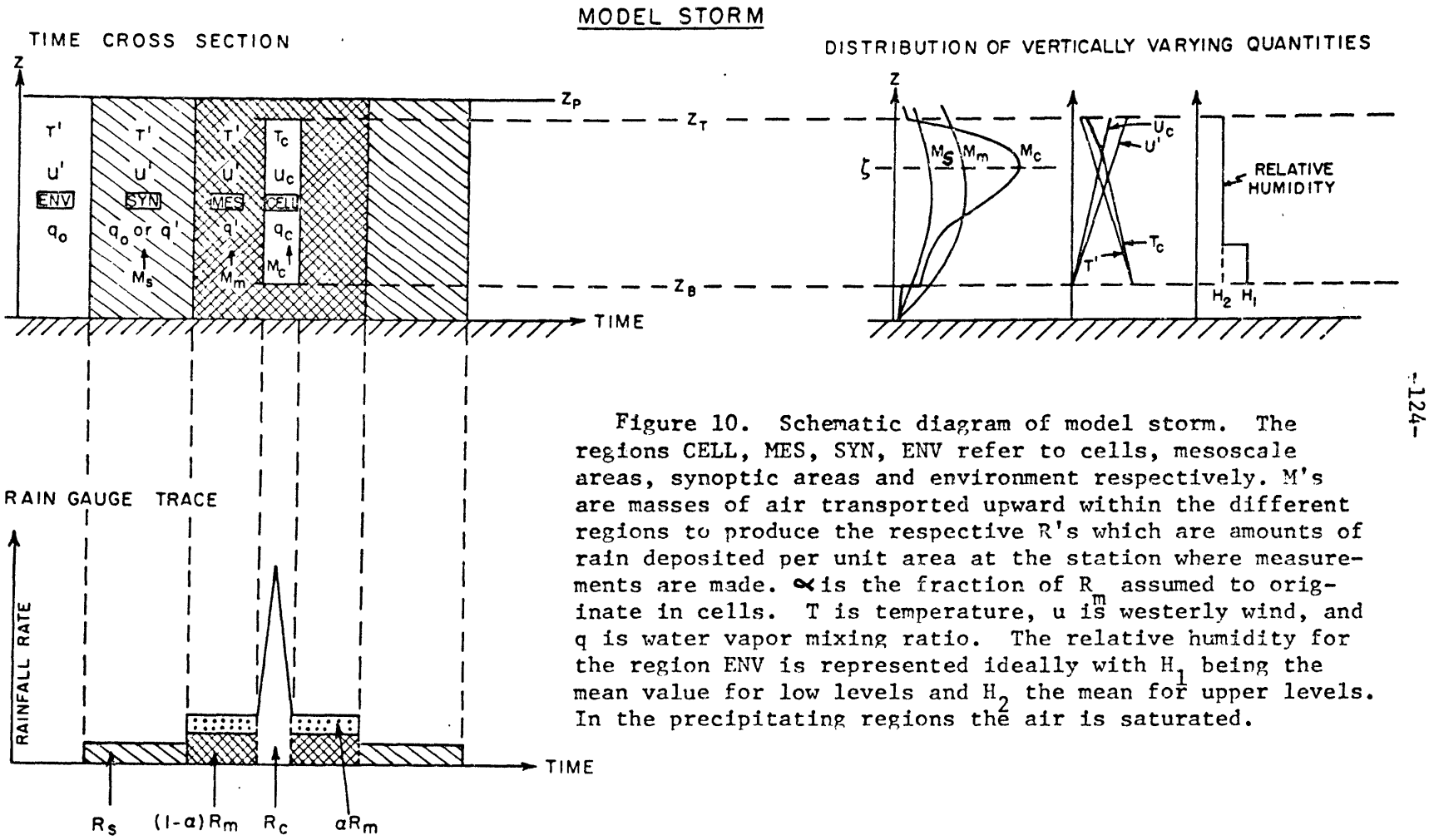


Figure 10. Schematic diagram of model storm. The regions CELL, MES, SYN, ENV refer to cells, mesoscale areas, synoptic areas and environment respectively. M's are masses of air transported upward within the different regions to produce the respective R's which are amounts of rain deposited per unit area at the station where measurements are made. α is the fraction of R_m assumed to originate in cells. T is temperature, u is westerly wind, and q is water vapor mixing ratio. The relative humidity for the region ENV is represented ideally with H_1 being the mean value for low levels and H_2 the mean for upper levels. In the precipitating regions the air is saturated.

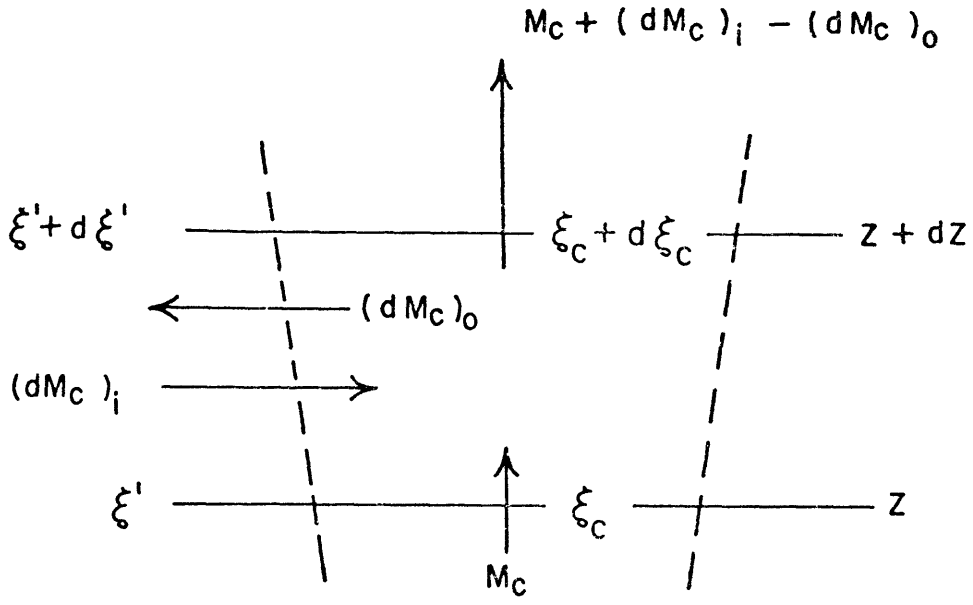


Figure 11. Sketch illustrating entrainment, detrainment and vertical transport of quantity ξ in cumulus cells.

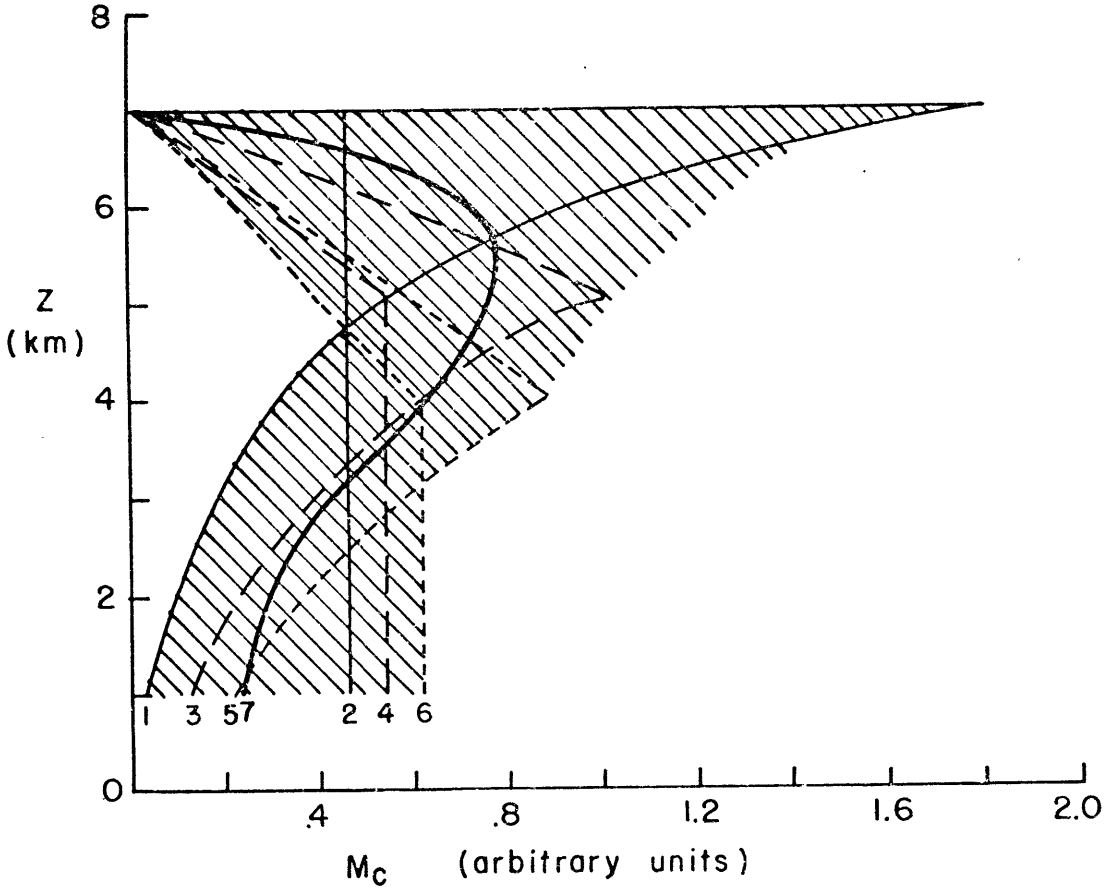


Figure 12. Computed vertical mass transports $M_c(z)$ for various assumptions about entrainment. Total condensate and the mixing ratio in the cells and the environment are the same for all curves. Labels on curves have the following meanings:

1 - Detrainment = 0, ξ = 7 km
2 - Detrainment = Entrainment, ξ = 7 km
3 - Detrainment = 0, ξ = 5 km
4 - Detrainment = Entrainment, ξ = 5 km
5 - Detrainment = 0, ξ = 4 km
6 - Detrainment = Entrainment, ξ = 4 km
7 - Curve used in computations

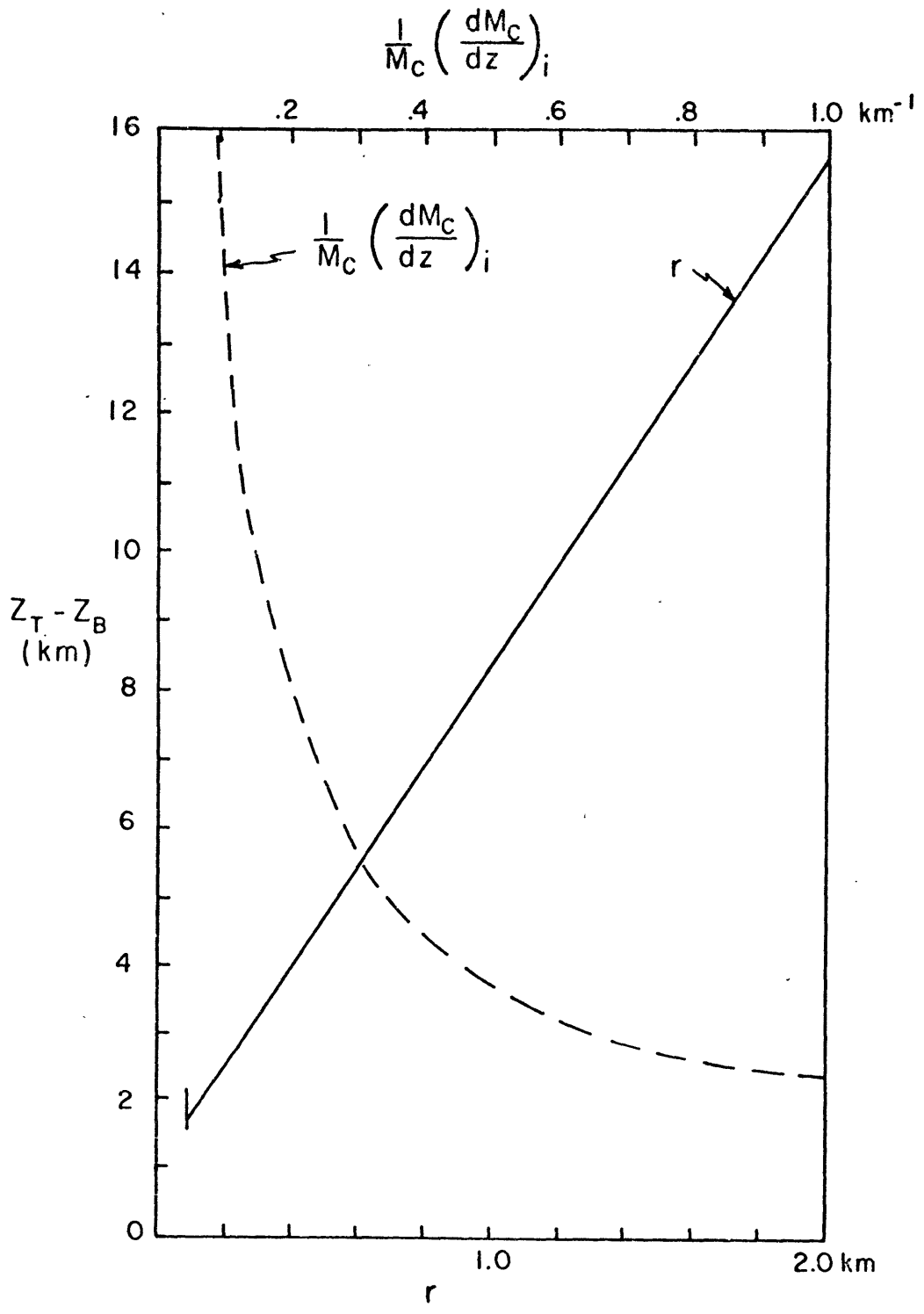


Figure 13. Model cell radius r and entrainment rate $M_c^{-1}(dM_c/dz)_i = 0.2/r$ as functions of cell depth, $z_T - z_B$.

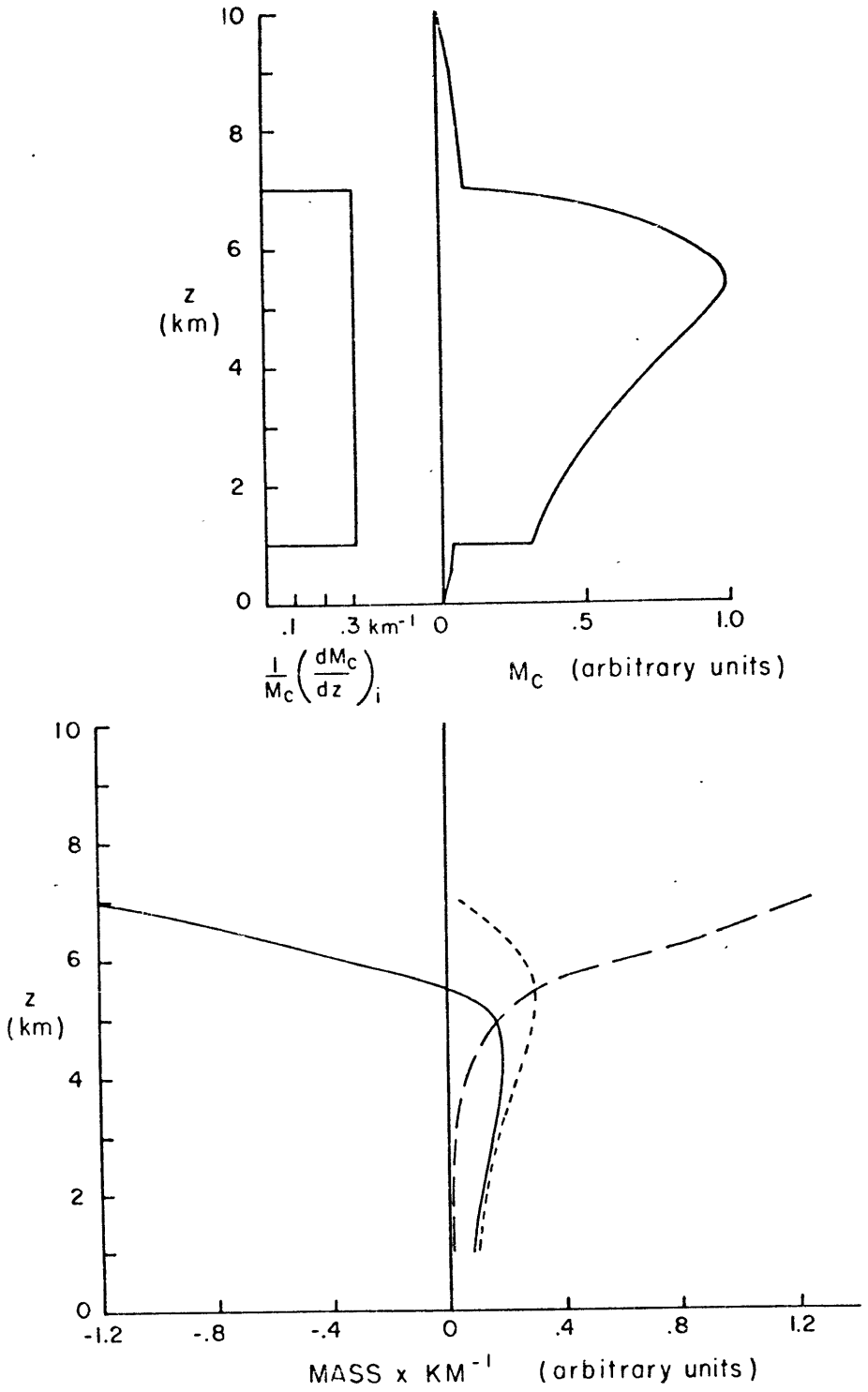


Figure 14. Profiles of model mass transport M_c and related quantities. M_c has the form of curve #7 in Figure 12. Constant value of "entrainment rate" $M_c^{-1}(dM_c/dz)_i$ is determined by the relations shown in Figure 13 for $z_T - z_B = 6$ km. Curves in lower graph are relations implicit in the simultaneous specification of $M_c^{-1}(dM_c/dz)_i$ and the shape of M_c. Curve indicated by --- is "entrainment" $(dM_c/dz)_i$, — — — is "detrainment" $(dM_c/dz)_o$, and ——— is dM_c/dz which is equal to the difference $(dM_c/dz)_i - (dM_c/dz)_o$.

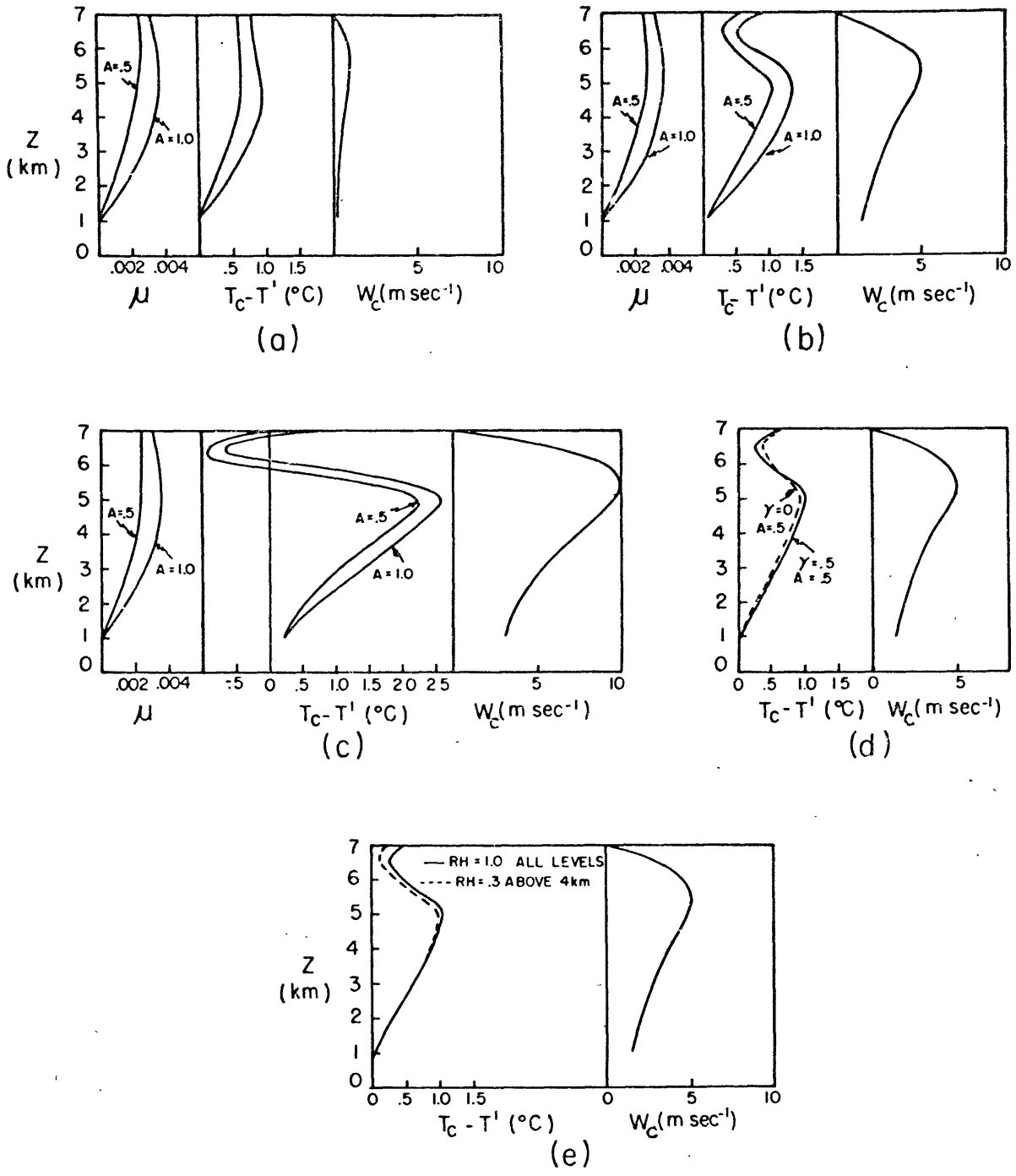


Figure 15. Calculations of $T_c - T'$, and μ for different sets of assumptions. In all cases, the temperature in the cellular updrafts was assumed to follow a moist adiabat with θ_e=321K. Except where indicated otherwise, the environment as well as the cell was assumed to be saturated. A=1.0 indicates that no precipitation was allowed; A=0.5 indicates half the water condensed in each vertical step was precipitated. γ is the virtual mass coefficient.

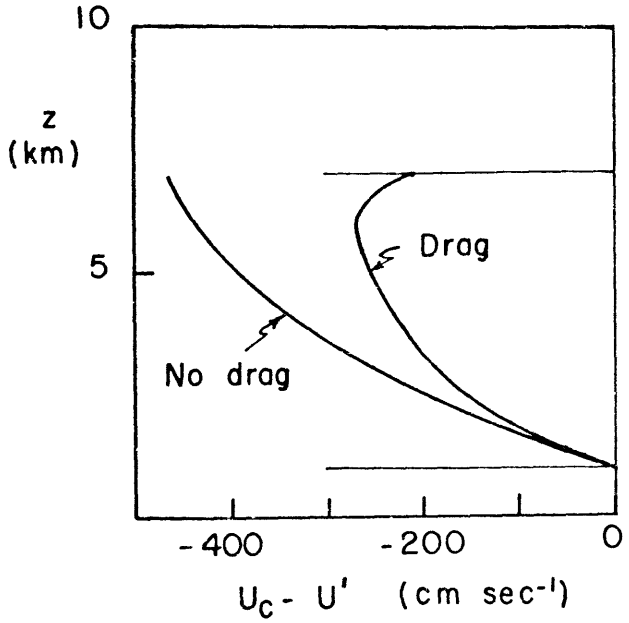


Figure 16. Computed values of difference in horizontal wind speed inside and outside of cells (u_c - u') for two extreme values of drag coefficient.

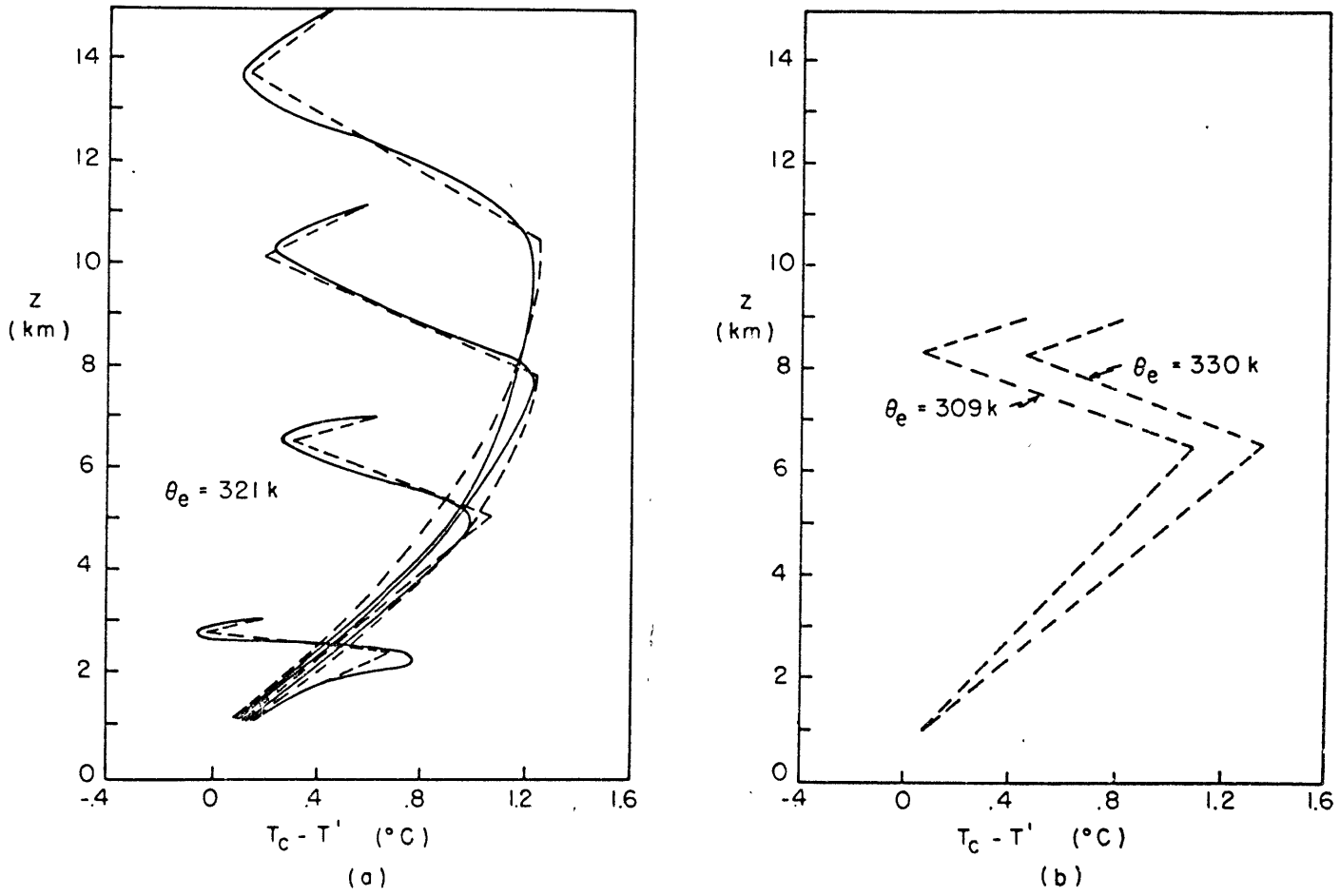


Figure 17. (a) Curves of cellular temperature excess for different cell depths; solid curves are calculated from equations (18) and (22); dashed curves are analytical approximations stored in model-storm program. (b) Stored solutions for two different values of θ_e which characterizes the lapse rate in the cells.

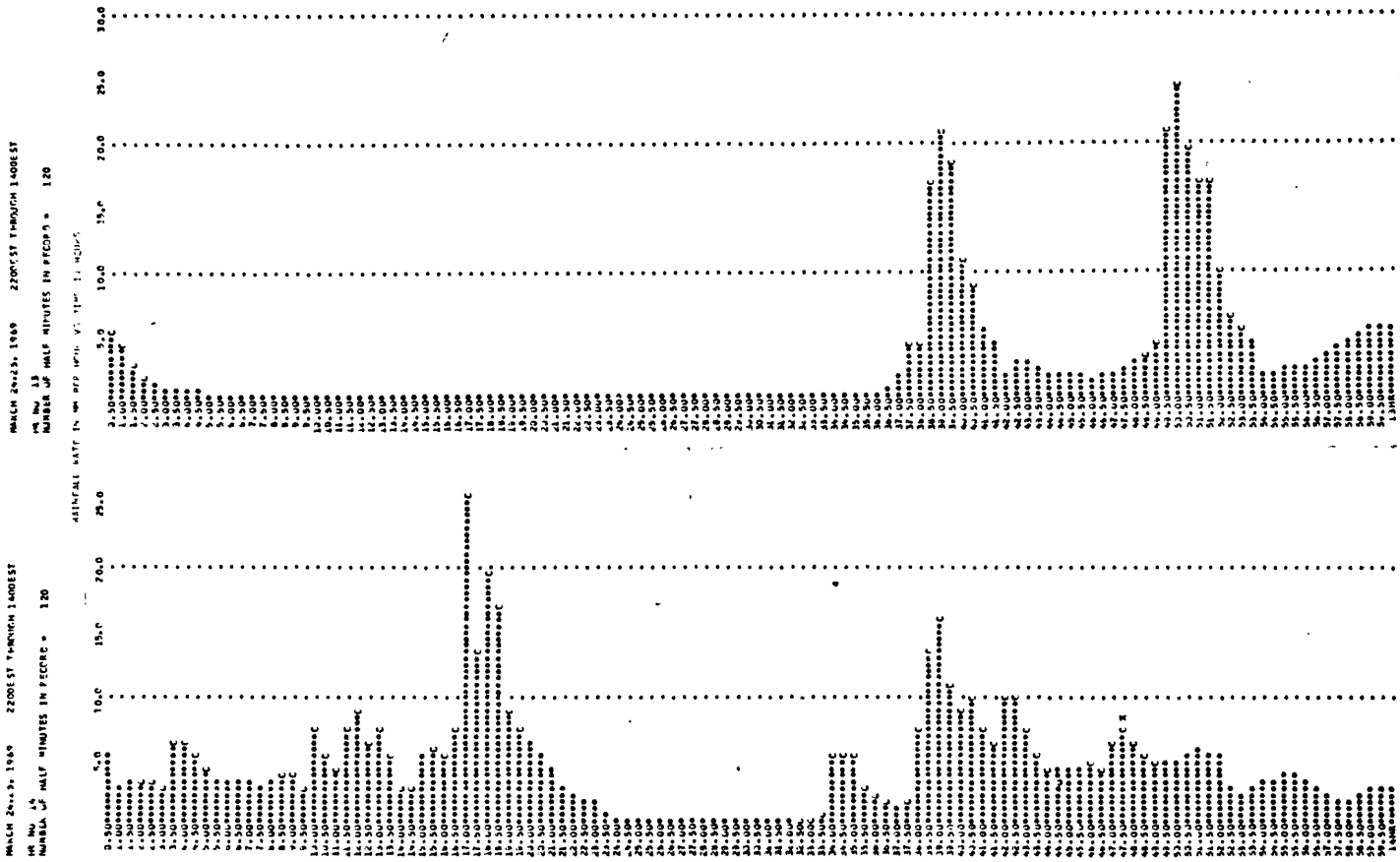


Figure 18. Thirty-second average rainfall rates printed out by computer for the hours 1000 to 1200 EST, 25 March 1969, West Concord, Mass. C atop asterisks indicates rainfall considered cellular. Rates less than 1.5 mm hr^{-1} are considered synoptic during the first hour while during the second hour rates less than 2.0 mm hr^{-1} are synoptic. Rainfall not classified as cellular or synoptic is called mesoscale. The notation X denotes the maximum rate in a 30-second interval while O denotes the minimum.

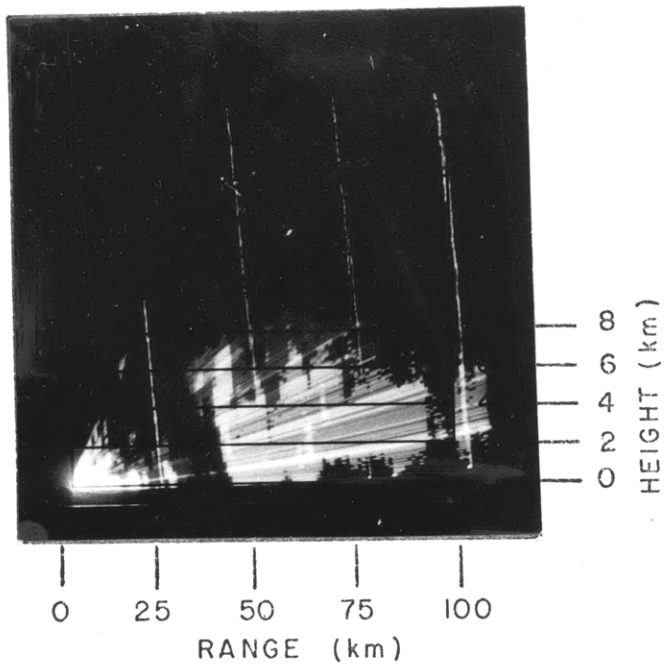


Figure 19. Photograph of MIT WR-66 radar RHI which shows three intensity levels by shades of gray. Data in picure was obtained on 25 March 1969, 1140 EST. Cell tops appear to be near 7 km.

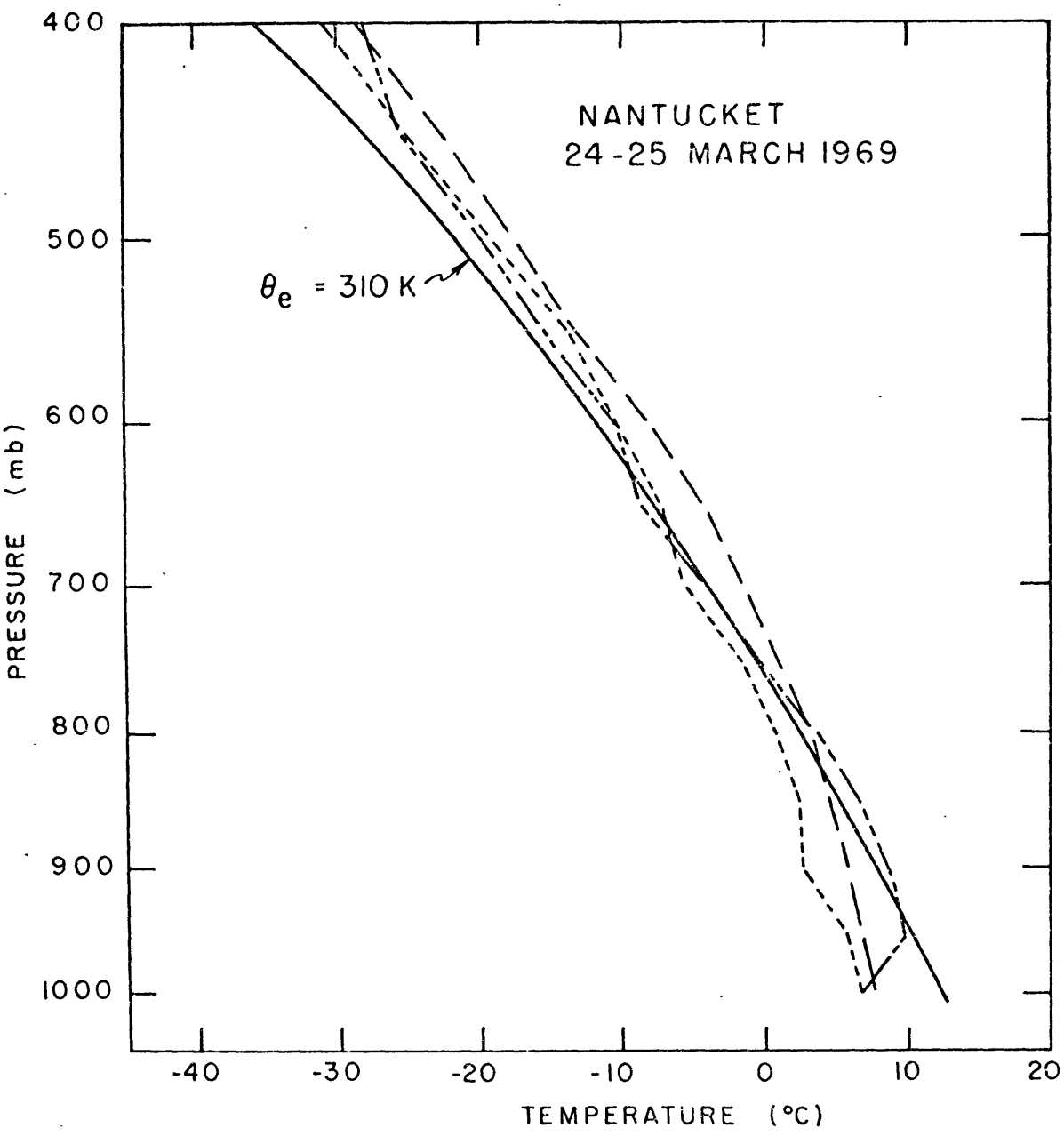


Figure 20. Temperature soundings for Nantucket for example case. The moist adiabat for Θ_e=310K was used to represent the temperature distribution in this storm. Soundings for Albany and Portland are similar.

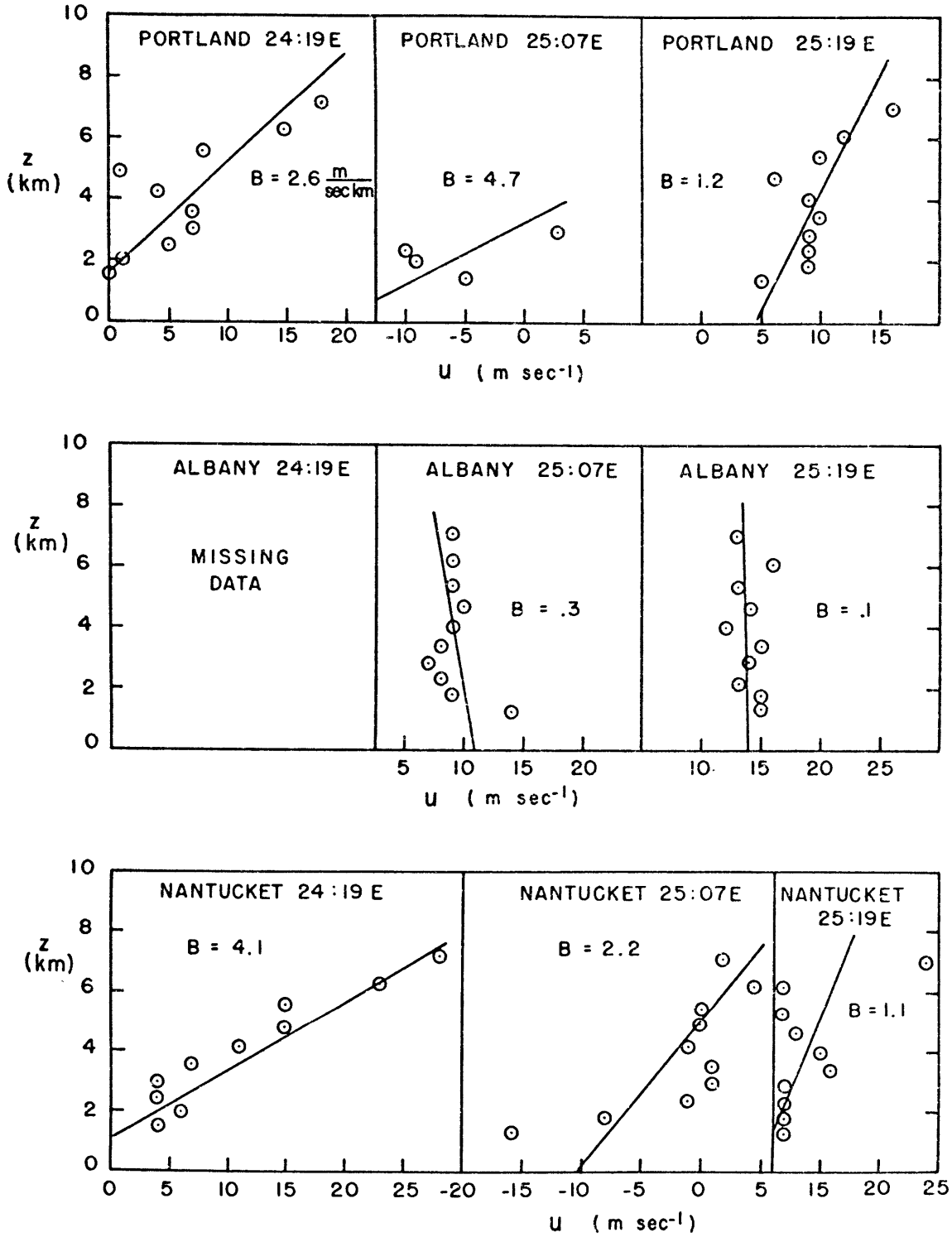


Figure 21. Westerly winds for 24-25 March, 1969. B is slope of line of least-square fit shown for each sounding.

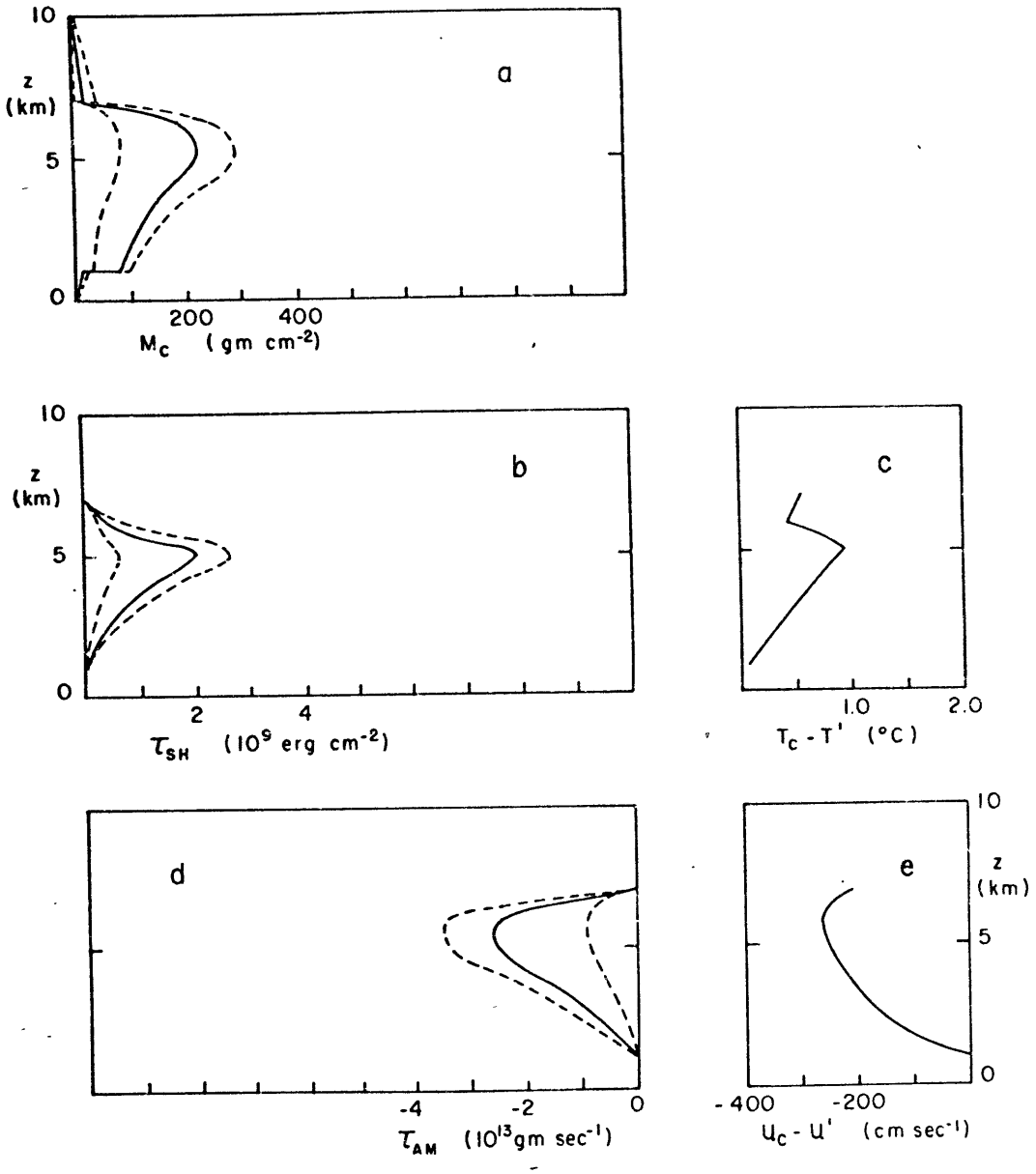


Figure 22. Model cumulus-scale vertical mass transport M_c, sensible heat transport τ_{SH}, angular momentum transport τ_{AM}, and associated model temperature difference, $T_c - T'$, and westerly wind speed difference, $u_c - u'$, between cells and their immediate environment for the hour 1100 to 1200 EST, 24-25 March 1969, at West Concord, Mass. Input quantities: z_B=1 km, z_T=7 km, θ_e=310K, R_c=.13 in, R_m=.05 in, Shear = 1.7 m sec^{-1} km^{-1}. Dashed transport curves on the left and right in a, b, and d are for lower and upper limits of cellular condensation determined by equation (13). Solid curves are best estimates within the range of possible values.

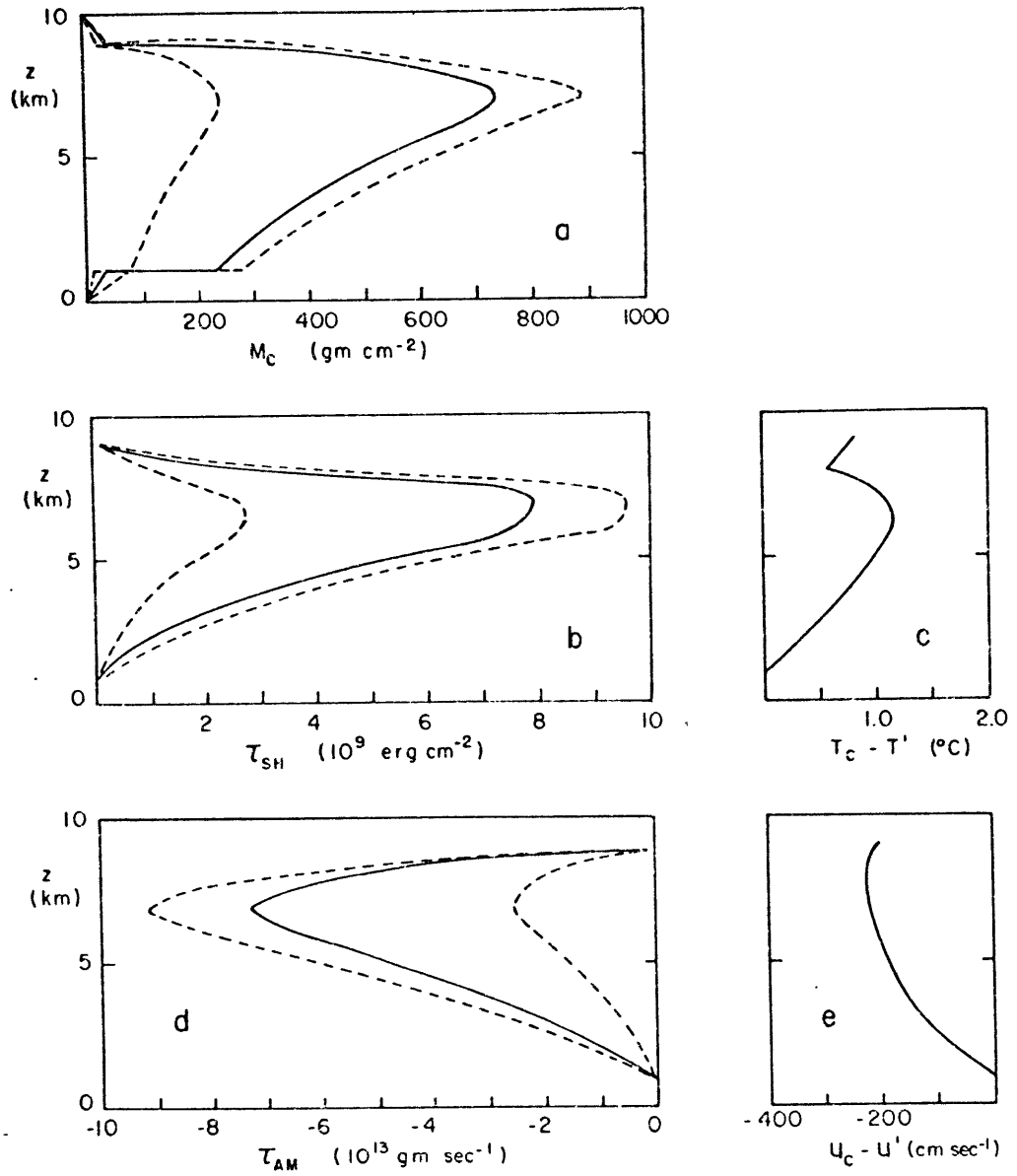


Figure 23. Model cumulus-scale vertical mass transport M_c, sensible heat transport. τ_{SH}, angular momentum transport τ_{AM}, and associated model temperature difference, $T_c - T'$, and westerly wind speed difference, $u_c - u'$, between cells and their immediate environment for the hour 1200-1300 EST, 9 July 1962, at West Concord, Mass. Input quantities: z_B=1 km, z_T = 9 km, θ_e=335K, R_c=.72 in, R_m=.09 in, Shear = 0.9 m sec^{-1} km^{-1}. Dashed transport curves on the left and right in a, b, and d are for lower and upper limits of cellular condensation determined by equation (13). Solid curves are best estimates within the range of possible values.

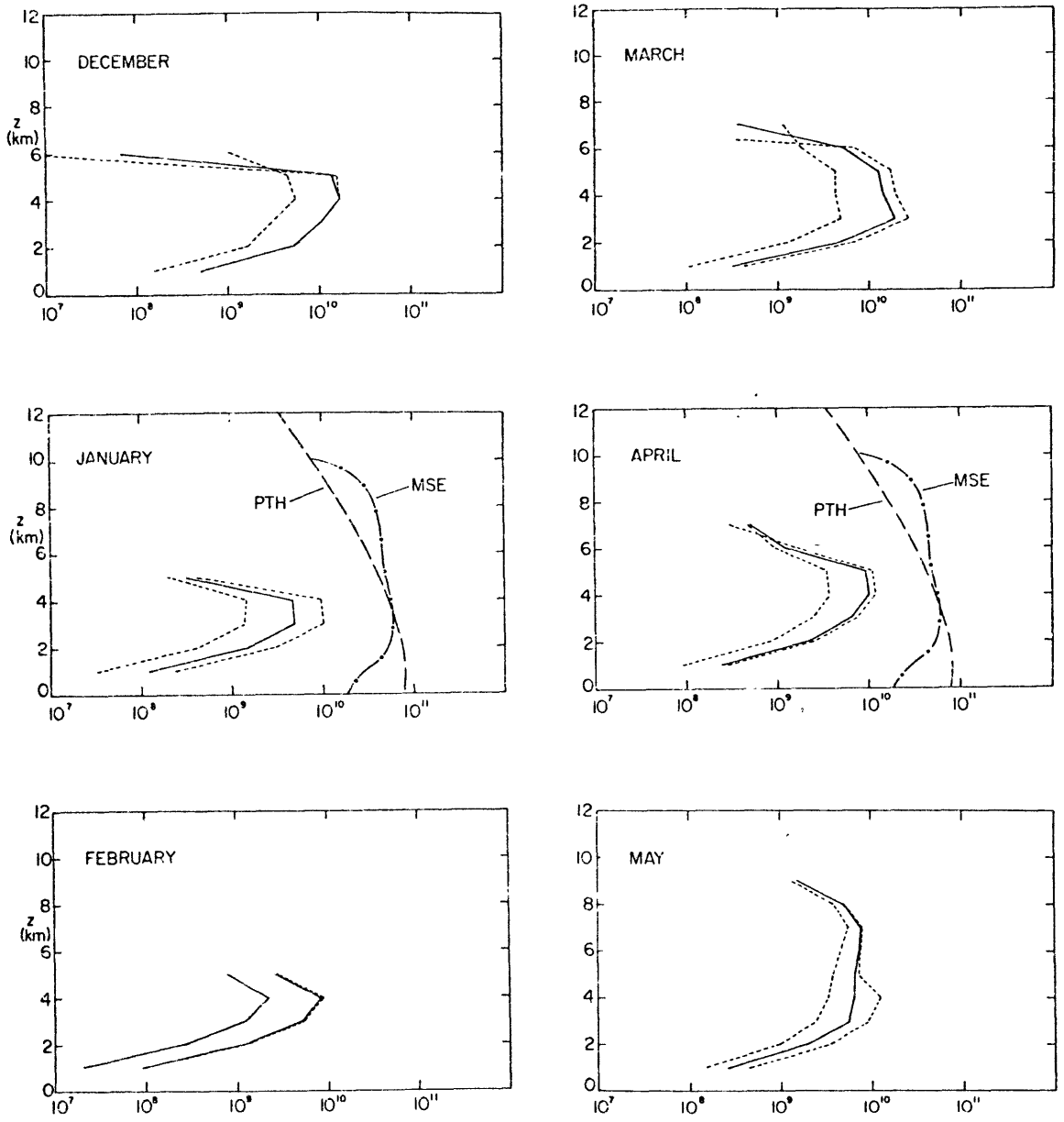


Figure 24. Monthly upward transport of sensible heat by cumulus-scale cells at Boston. Curves shown in short dashes are for lower and upper limiting values of cellular condensation determined from rainfall measurements. Solid curve is best estimate. Dot-dash curve (MSE) is from Manabe et al (1970) and represents the synoptic-scale eddy flux of heat at latitude 40N. Long-dash curve (PTH) is from Palmen and Newton (1969) and represents the total required upward flux of heat by eddies of all scales at high latitudes. Units: erg cm^{-2} mo^{-1}. Figure continued on page -139-.

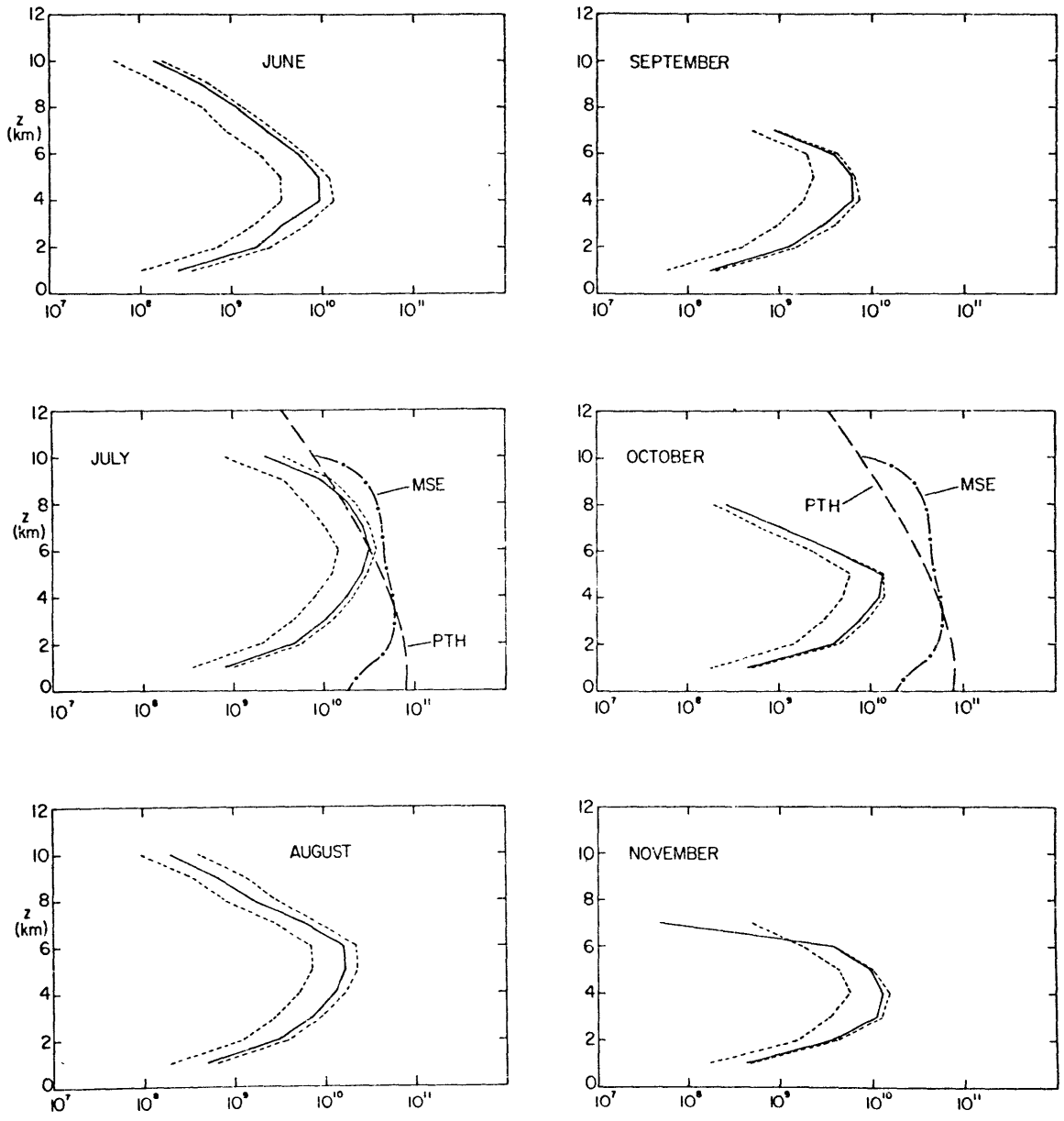


Figure 24. (Continued)

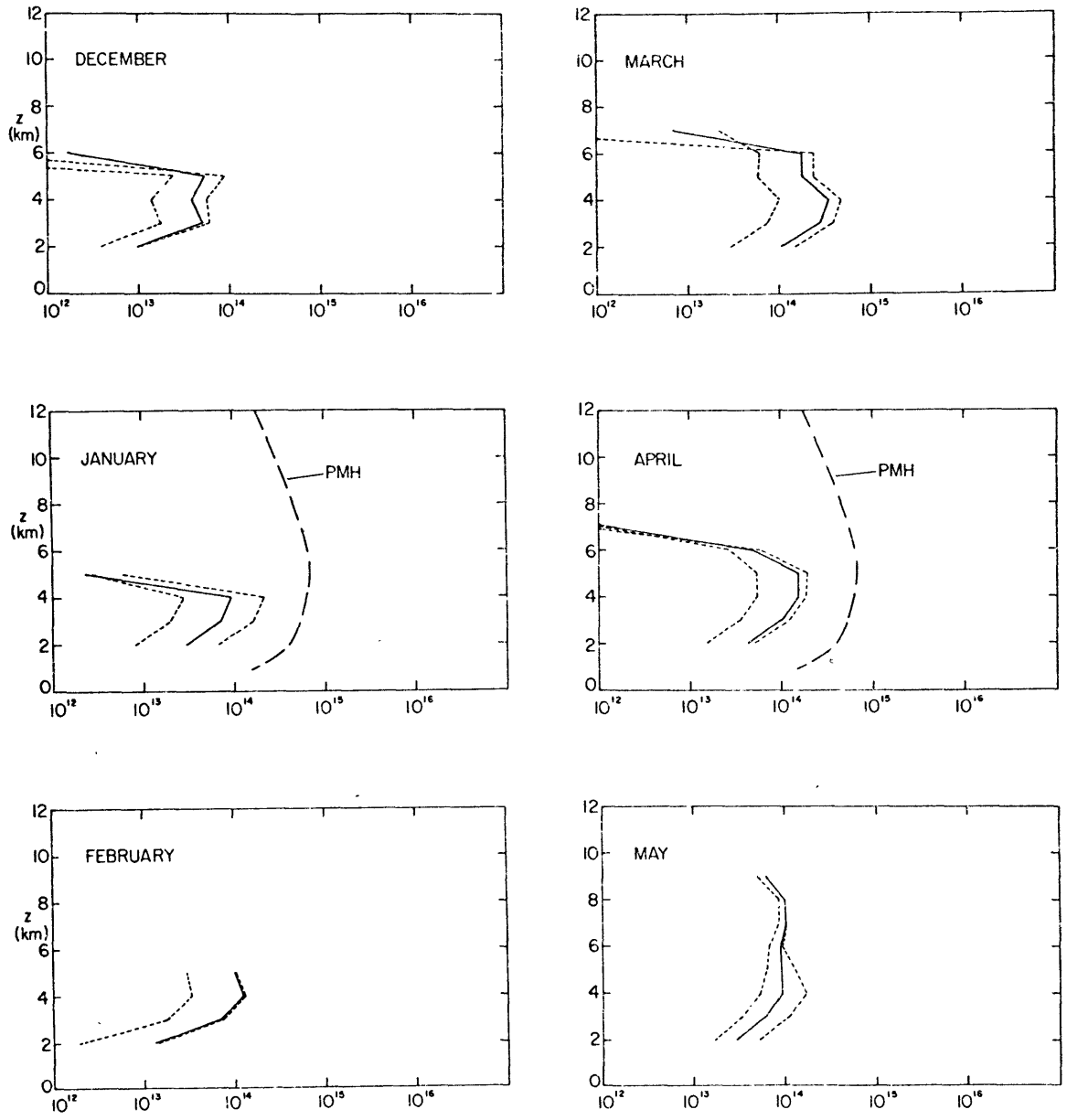


Figure 25. Monthly downward transport of angular momentum by cumulus-scale cells at Boston. Curves shown in short dashes are for lower and upper limiting values of cellular condensation determined from rainfall measurements. Solid curve is best estimate. Long-dash curve (PMH) is the average downward flux of angular momentum by the mean meridional circulation at high latitudes as computed by Palmen and Newton (1969). Units: gm sec^{-1} mo^{-1}. Figure continued on page -141-.

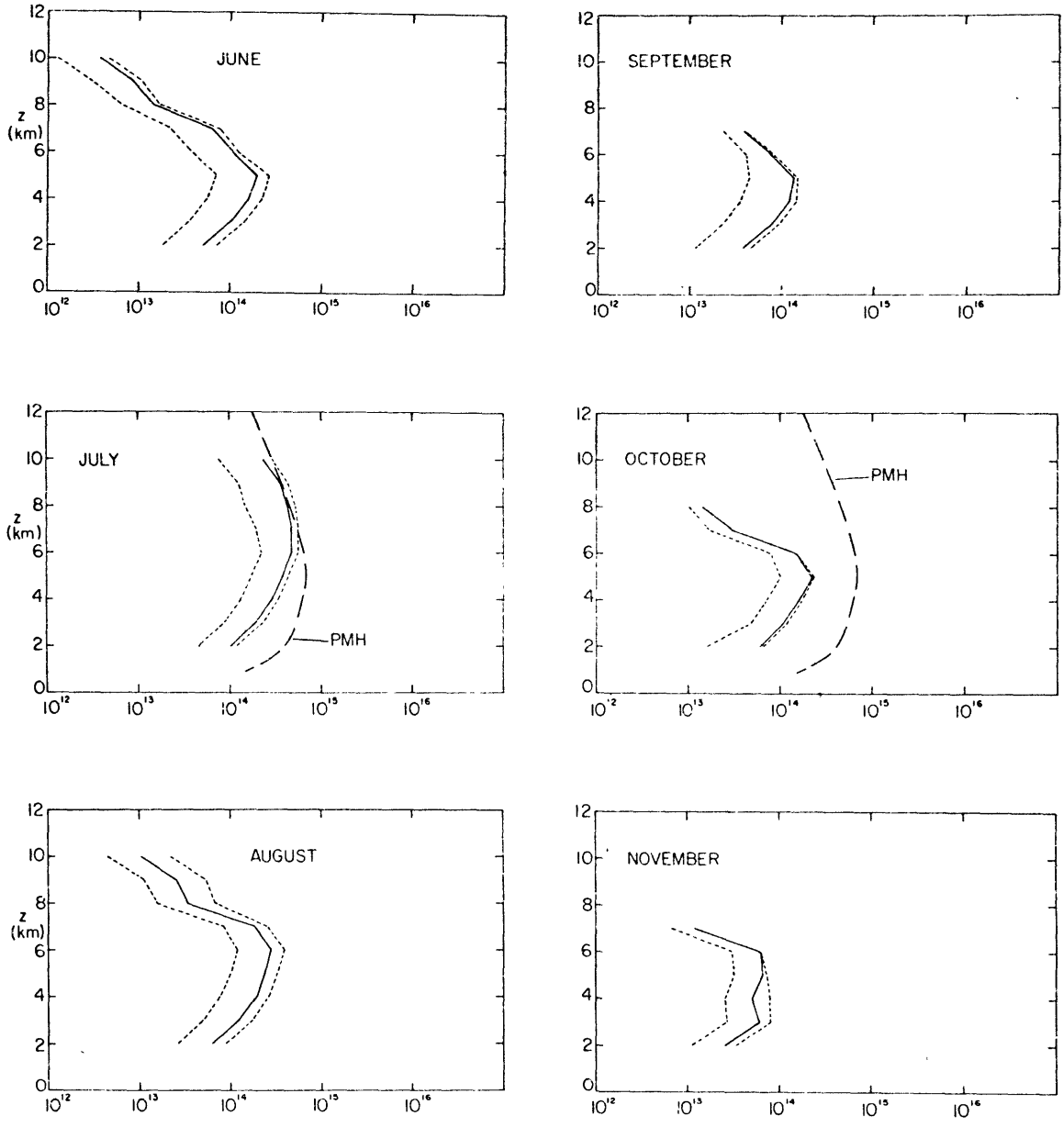


Figure 25. (Continued)

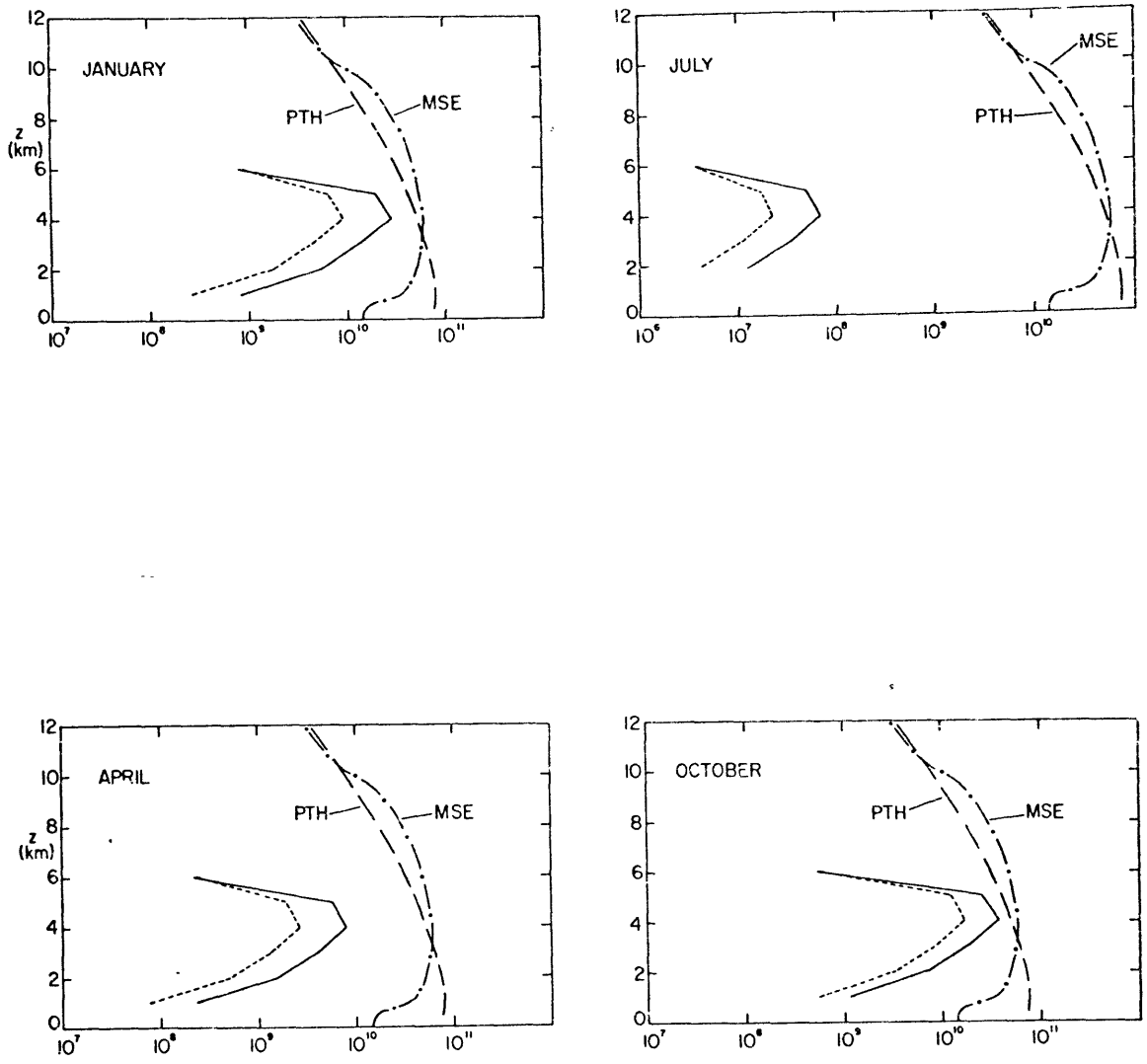


Figure 26. Monthly upward transport of sensible heat by cumulus-scale cells at Tatoosh. Curve shown in short dashes is for lower limiting values of cellular condensation determined from rainfall measurements. Solid curve is best estimate. Dot-dash curve (MSE) is from Manabe et al (1970) and represents the synoptic-scale eddy flux of heat at latitude 50N. Long-dash curve (PTH) is from Palmen and Newton (1969) and represents the total required upward flux of heat by eddies of all scales at high latitudes. Units: erg cm^{-2} mo^{-1}.

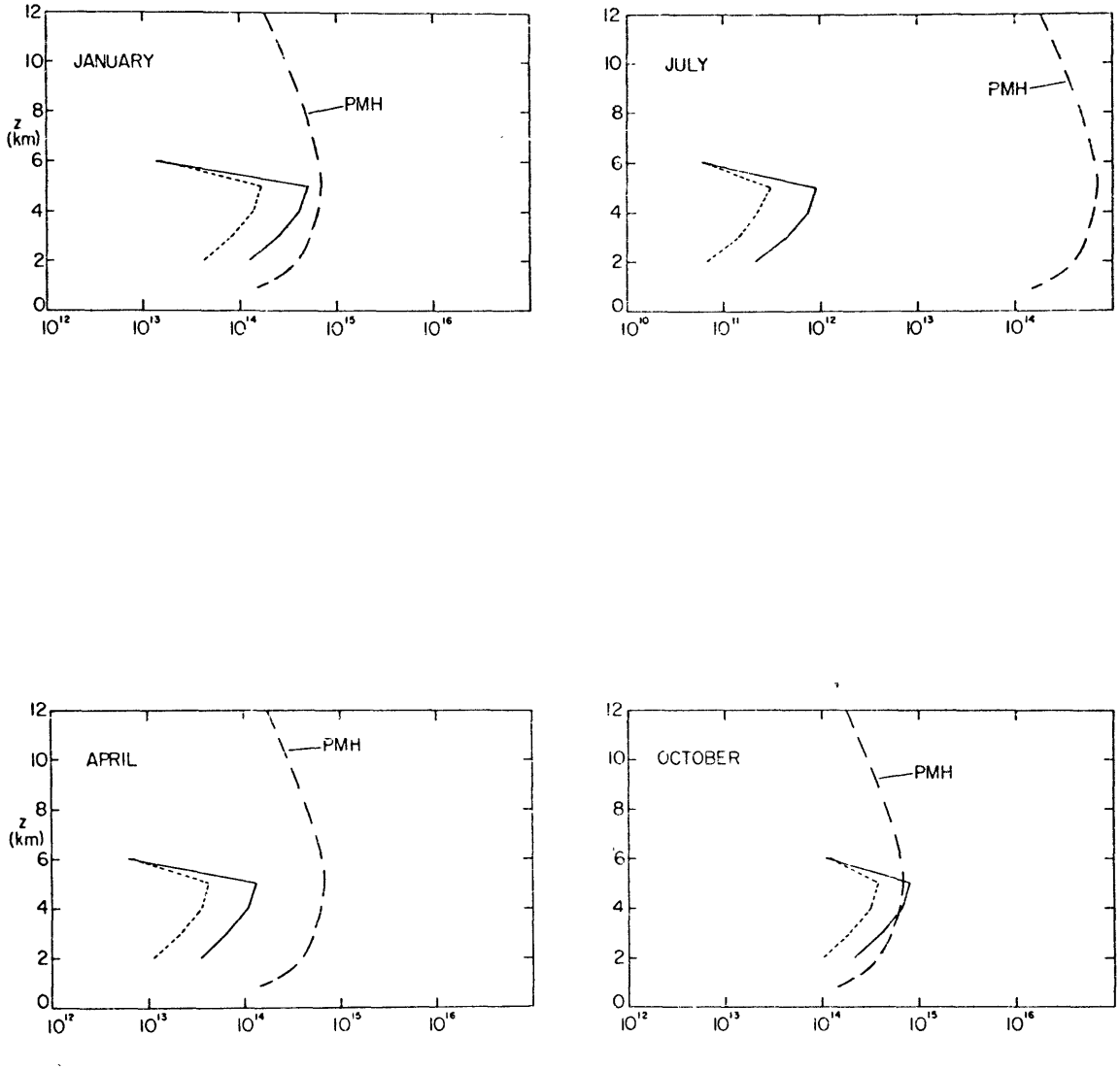


Figure 27. Monthly downward transports of angular momentum by cumulus-scale cells at Tatoosh. Curve shown in short dashes is for lower limiting values of cellular condensation determined from rainfall measurements. Solid curve is best estimate. Long-dash curve (PMH) is the average downward flux of angular momentum by the mean meridional circulation at high latitudes as computed by Palmen and Newton (1969). Units: gm sec^{-1} mo^{-1}.

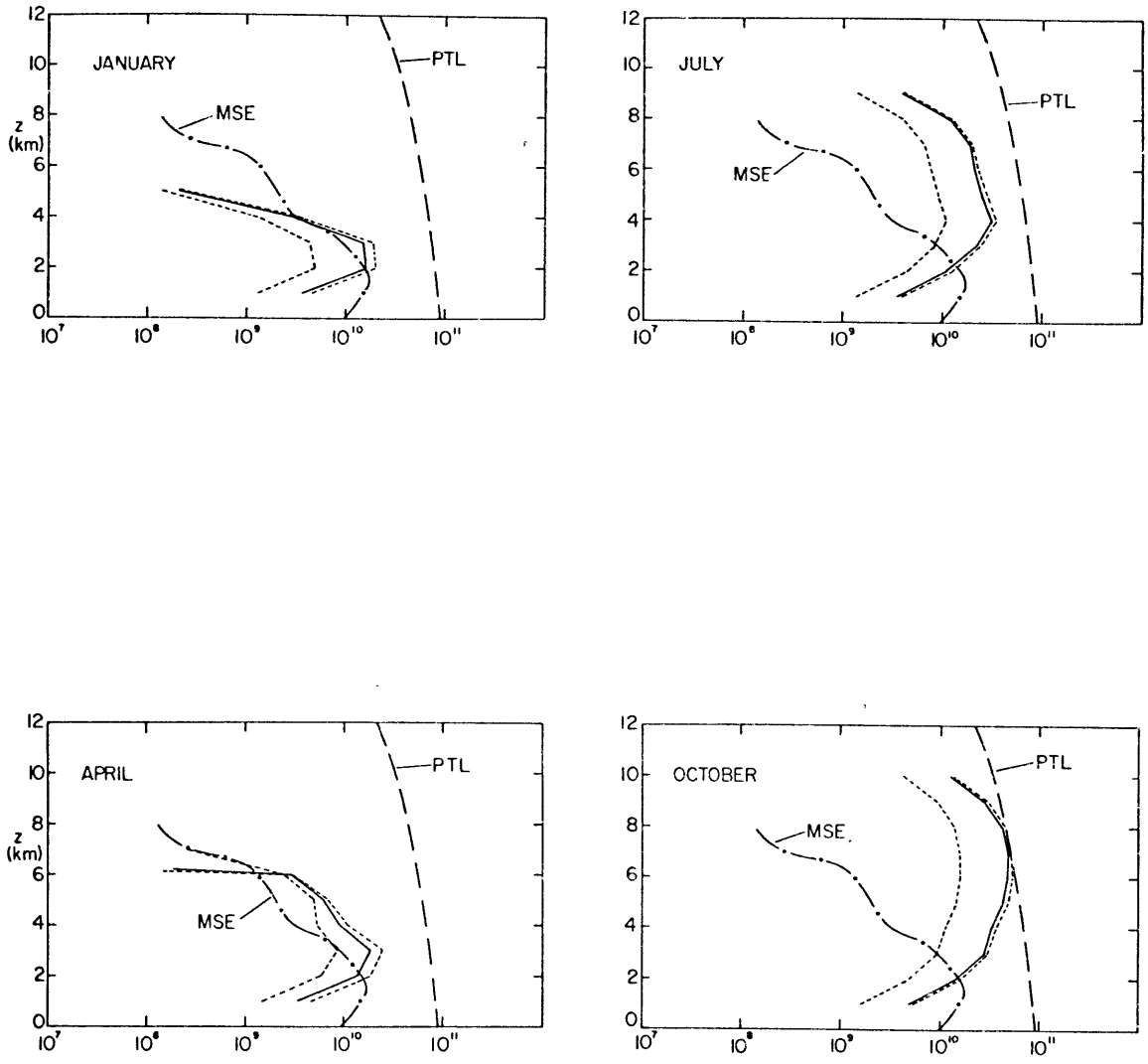


Figure 28. Monthly upward transport of sensible heat by cumulus-scale cells at San Juan. Curves shown in short dashes are for lower and upper limiting values of cellular condensation determined from rainfall measurements. Solid curve is best estimate. Dot-dash curve (MSE) is from Manabe et al (1970) and represents the synoptic-scale eddy flux of heat at latitude 20N. Long-dash curve (PTL) is from Palmen and Newton (1969) and represents the total required upward flux of heat by eddies of all scales at low latitudes. Units: erg cm^{-2} mo^{-1}.

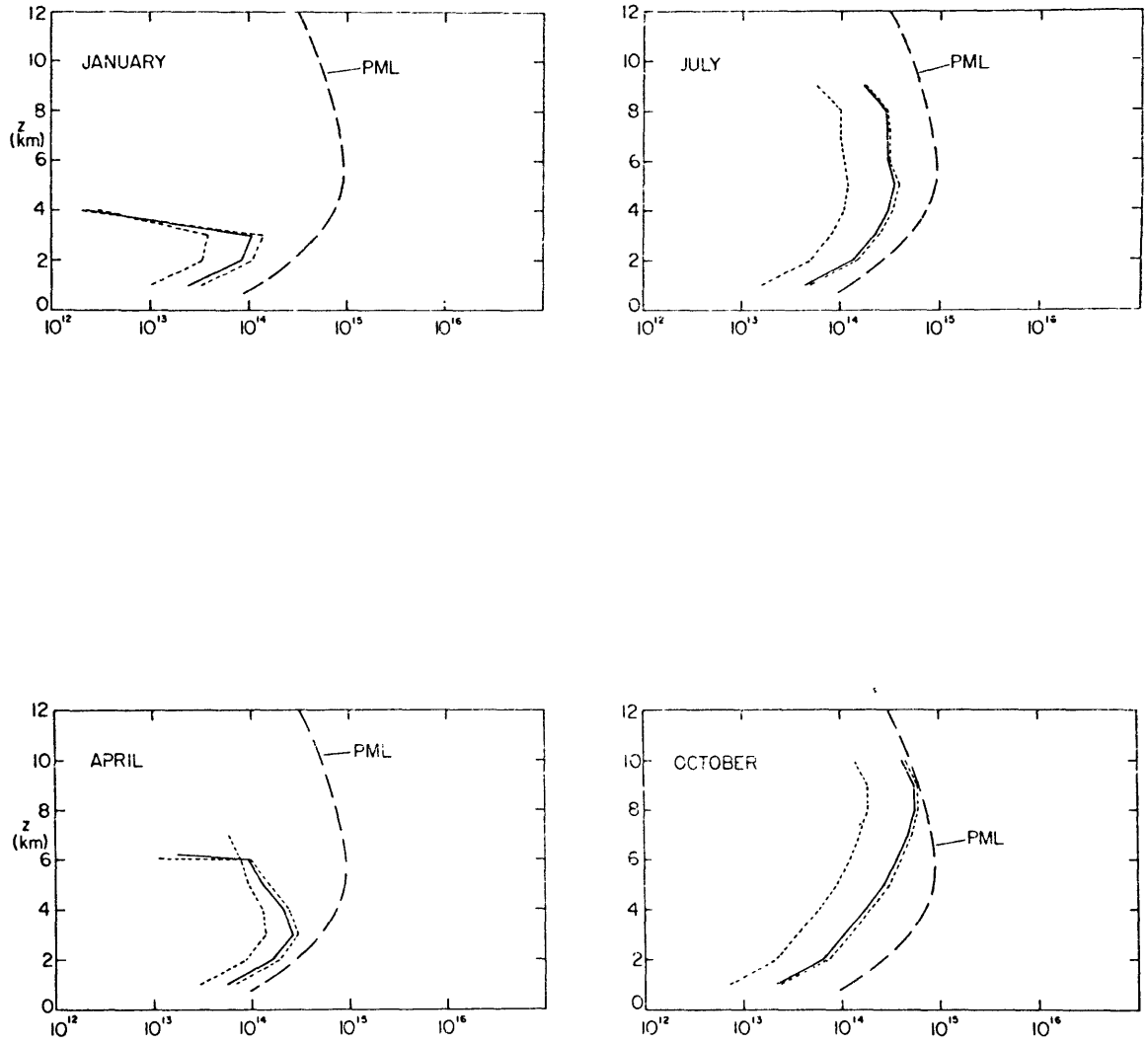


Figure 29. Monthly downward transport of angular momentum by cumulus-scale cells at San Juan. Curves shown in short dashes are for lower and upper limiting values of cellular condensation determined from rainfall measurements. Solid curve is best estimate. Long-dash curve (PML) is the average upward flux of angular momentum by the mean meridional circulation at low latitudes as computed by Palmen and Newton (1969). Units: gm sec^{-1} mo^{-1}.

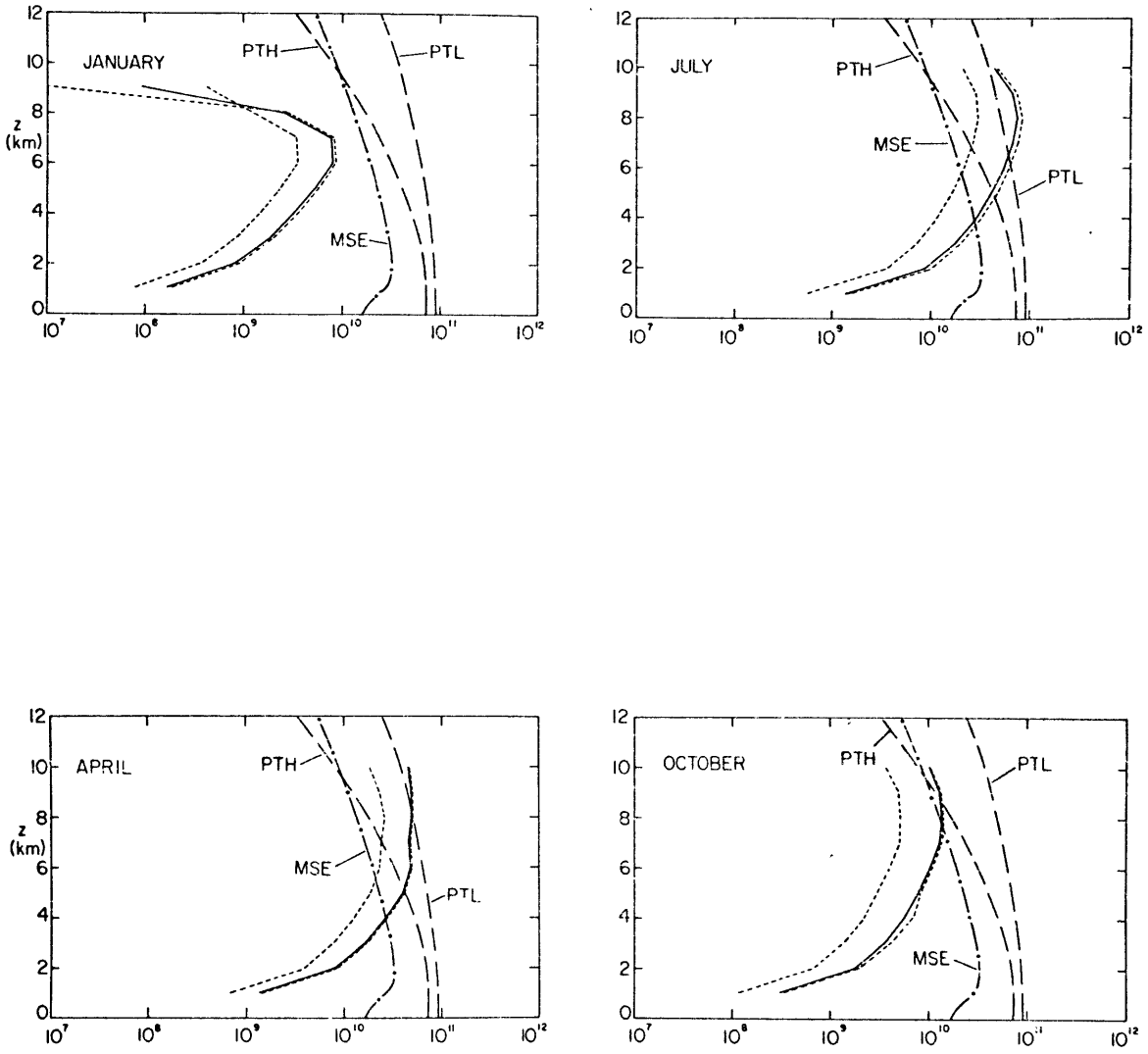


Figure 30. Monthly upward transports of sensible heat by cumulus-scale cells at New Orleans. Curves shown in short dashes are for lower and upper limiting values of cellular condensation determined from rainfall measurements. Solid curve is best estimate. Dot-dash curve (MSE) is from Manabe et al (1970) and represents the synoptic-scale eddy flux of heat at latitude 30N. Long-dash curves (PTL and PTH) are from Palmen and Newton (1969) and represent the total required fluxes of heat by eddies of all scales at low and high latitudes. Units: erg cm^{-2} mo^{-1}.

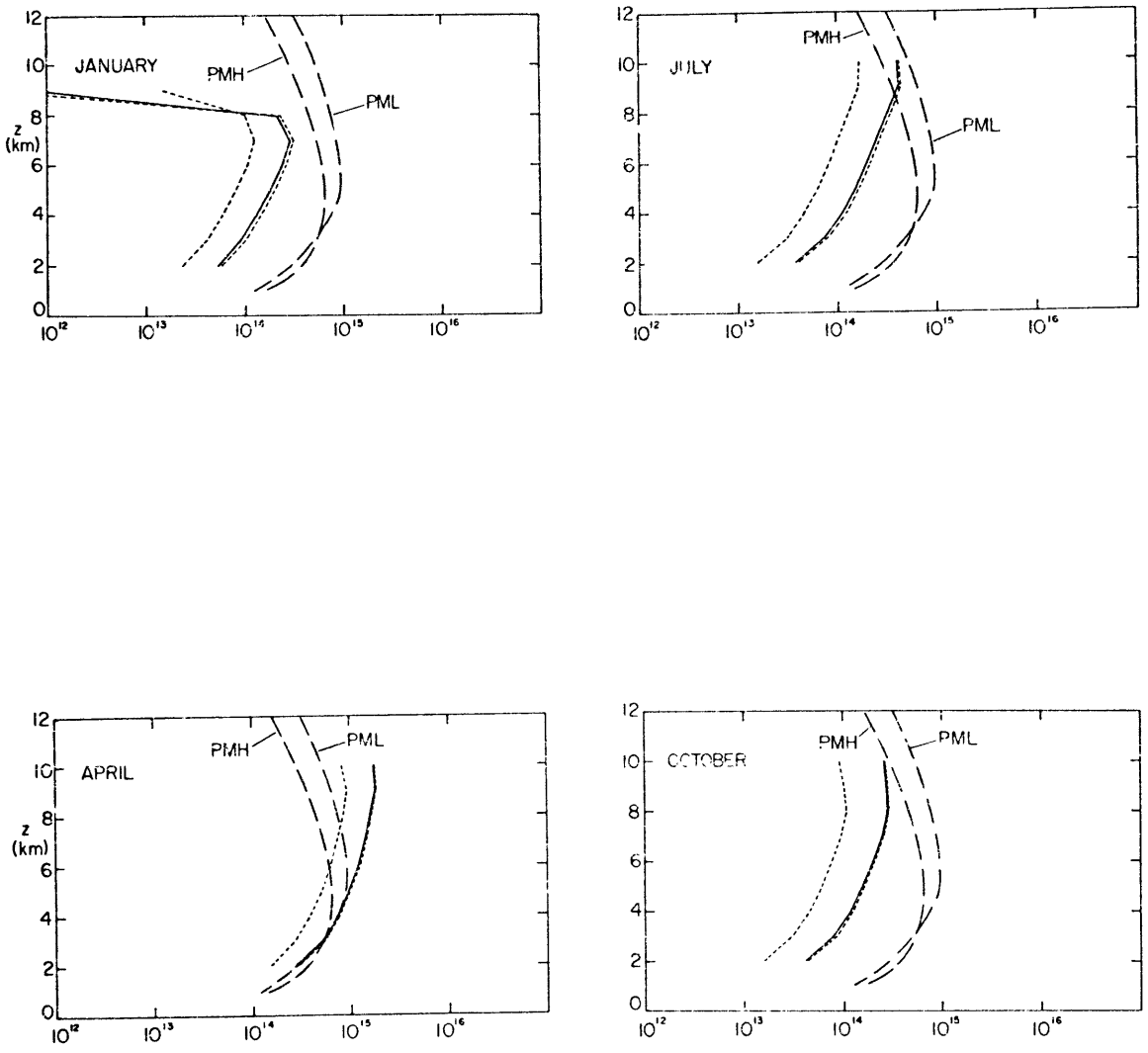


Figure 31. Monthly downward transport of angular momentum by cumulus-scale cells at New Orleans. Curves shown in short dashes are for lower and upper limiting values of cellular condensation determined from rainfall measurements. Solid curve is best estimate. Long-dash curves (PML and PMH) are the average downward fluxes of angular momentum by the mean meridional circulations at low and high latitudes as computed by Palmen and Newton (1969). Units: gm sec^{-1} mo^{-1}.

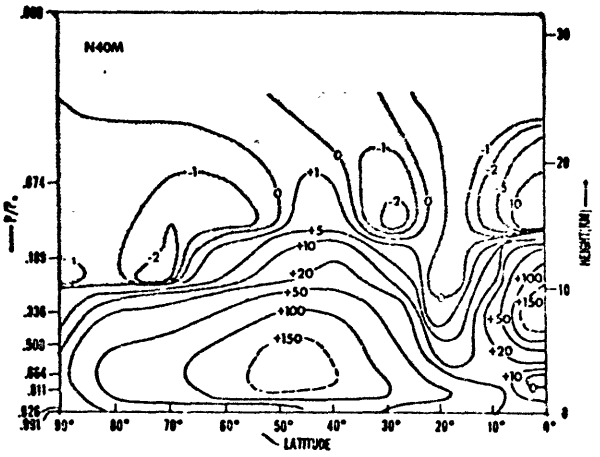


Figure 32. Latitude-height distribution of upward transport of heat by large-scale eddies in a model of the atmospheric general circulation, after Manabe et al (1970). Values in diagram have units of Joules cm^{-2} day^{-1} and may be converted to erg cm^{-2} mo^{-1} by multiplying them by 3×10^{8}.

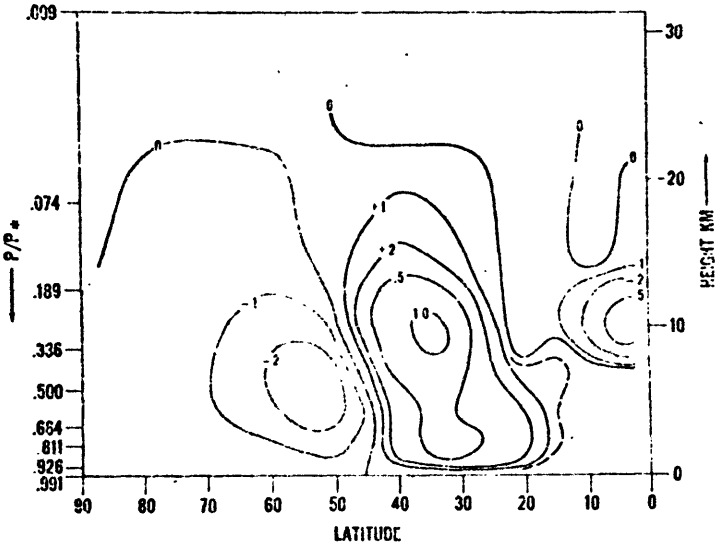


Figure 33. Latitude-height distribution of vertical transport of angular momentum by the large-scale eddies in an atmospheric general circulation model, after Smagorinsky et al (1965). Values in diagram have units of 10^{13} gm sec^{-1} day^{-1} and may be converted to gm sec^{-1} mo^{-1} by multiplying them by 3.0×10^{14}.

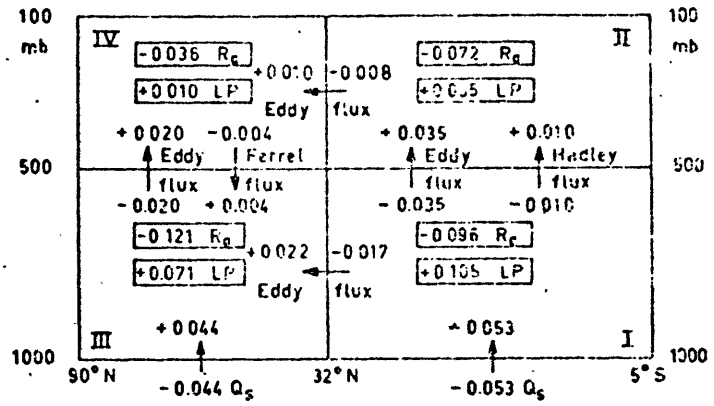


Figure 34. Winter heat budget for the belts 5°N to 32°N and 32°N to 90°N, and the vertical heat fluxes through the 500-mb surface and from the earth's surface. All quantities are expressed in Langleys per minute averaged over the areas concerned and may be converted to erg cm^{-2} mo^{-1} by multiplying by 1.8×10^{12}. After Palmen and Newton (1969).

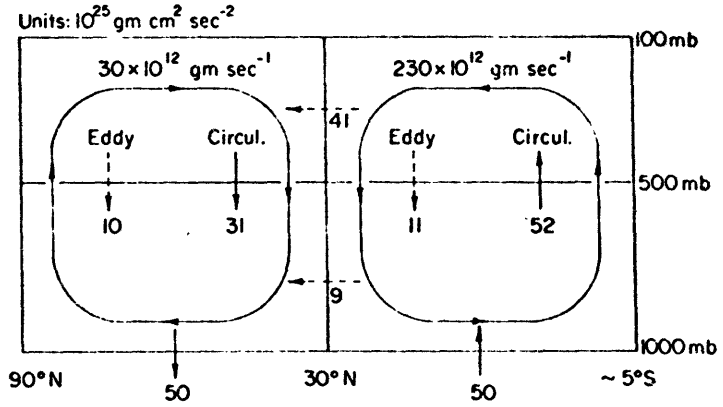


Figure 35. The winter total mass circulations and angular momentum budget north and south of latitude 30° in the northern hemisphere. Arrows denote angular momentum fluxes between atmosphere and earth, through the 500-mb surface, and across 30°N above and below 500 mb. Dashed arrows signify portions of fluxes due to eddies. Values in diagram have units of 10^{25} gm cm^2 sec^{-2} and may be converted to gm sec^{-1} mo^{-1} by multiplying them by 2.04×10^{13}, north of 30°N, and by 1.74×10^{13} south of 30°N. After Palmen and Newton (1969).

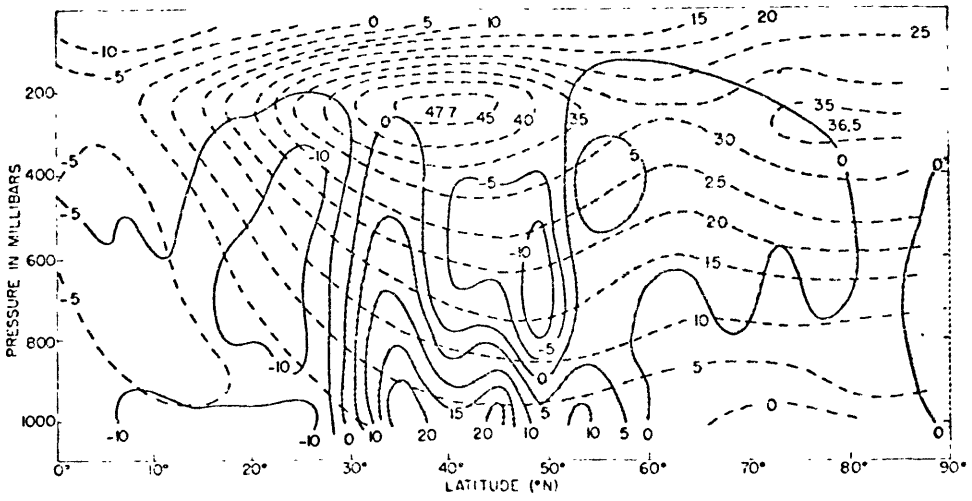


Figure 36. Vertical absolute angular momentum flow due to standing and transient eddies plus friction (full lines), drawn on a meridional cross section through the atmosphere. The units are 10^{19} dyne cm sec^{-2}. The dashed curves are the contours of the zonally averaged zonal angular velocity. The units are 10^{-7} sec^{-1}. The quantities shown are for the 60-month mean condition, and negative values indicate upward transports of angular momentum. After Starr et al (1970). Fluxes in diagram may be converted to units of gm sec^{-1} mo^{-1} by multiplying them by .57 x 10^{14} gm sec^{-1} mo^{-1}.

MIT Libraries
Document Services

Room 14-0551
77 Massachusetts Avenue
Cambridge, MA 02139
Ph: 617.253.5668 Fax: 617.253.1690
Email: docs@mit.edu
http://libraries.mit.edu/docs

DISCLAIMER OF QUALITY

Due to the condition of the original material, there are unavoidable flaws in this reproduction. We have made every effort possible to provide you with the best copy available. If you are dissatisfied with this product and find it unusable, please contact Document Services as soon as possible.

Thank you.

Pages are missing from the original document.

151

rates from the measured reflectivities. The 95% confidence limits for rainfall rates measured with the radars are approximately $\pm$ a factor of two. Comparison with rain gauge data has demonstrated that this is a realistic estimate.

At the field station there are two tipping-bucket gauges which have time resolutions of a few seconds in heavy rain and about a minute in light rain. The more sensitive one tips for every 0.01 mm of rain. These gauges are regularly checked against each other and a weighing gauge. Agreement is generally within five percent.

The data taken at M.I.T. are supplemented by conventional meteorological observations and by the hourly precipitation amounts for New England, published monthly by the National Weather Service. There are three radiosonde stations, 20 stations reporting hourly surface data, and 69 recording rain gauges within 200 km of the radar site.

Two studies were conducted by Austin and Houze (1972). In the first, eight storms were selected which had fairly large amounts of precipitation, good radar and rain-gauge coverage, and represented a variety of seasonal and synoptic situations. In no case was there specific knowledge of the precipitation pattern in a storm before it was chosen, nor was any storm rejected because of the patterns it was found to contain. These eight storms are listed below, the storm of 8 July 1963 being divided into two portions as indicated.

Date	Synoptic type
12 January 1963	Wave on stationary front
2 February 1963	Low moving from Great Lakes region

Date	Synoptic type
18 May 1963	Coastal low moving from southwest with overland low to west
9 June 1965	Air mass thunderstorms
8 July 1963 a	Occluded front moving eastward from Great Lakes, prefrontal precipitation
8 July 1963 b	Same storm, frontal passage with squall line
29 August 1962	Coastal low (ex-hurricane)
17 September 1963	Wave on stationary front
6 December 1962	Cyclone approaching from southwest

To facilitate systematic analysis, precipitation areas were categorized according to their horizontal extent. Areas of 10^4 km^2 or greater are referred to as synoptic areas since they are large enough to be delineated by the regular synoptic weather reports. They are not usually depicted to their full extent on the radars, and their locations and intensities were obtained primarily from maps of the hourly precipitation amounts. A small intense radar echo corresponding to an area on the order of 10 km^2 was assumed to represent a single cumulus convective element and is called a cell. A mesoscale precipitation area was specifically defined as being smaller than a synoptic area and larger than a cell, the limits being set, somewhat arbitrarily, at 50 km^2 and 10^4 km^2. Early in the analysis it became apparent that some of the precipitation patterns contained areas of two distinct sizes, both within the mesoscale range. These patterns showed several small mesoscale areas (SMSA's), from 50 to 1000 km^2 in size, located within large mesoscale areas (LMSA's) which

were in the range 10^3 to 10^4 km^2. Figure 1 shows an example of two large mesoscale areas, each containing several small mesoscale areas and a number of cells. Mesoscale areas and cells were identified from the intensity level sequences on the radar PPI. They were tracked for their entire lifetimes or as long as the data permitted. It should be noted that in general the patterns are complex and irregular in structure so that from the observations taken at a single time it is not always possible to identify positively separate mesoscale precipitation areas. This type of ambiguity is greatly reduced, however, when the areas are observed over a period of time. As they develop, move and dissipate, they can be recognized as individual entities. Subjectivity cannot be entirely eliminated from the analysis, but its influence on the results is not considered significant.

In the first study 8 LMSA's, 25 SMSA's and 125 cells were examined systematically. Areas, durations, motions and intensities of each were obtained from the radar PPI sequences. The intensities indicated by the radar were checked with those recorded by the gauges. Vertical extent of cells and of the surrounding precipitation were observed on the RHI.

Figure A-1, an example of the data from the sensitive gauge at the field station, shows the high degree of variability in rainfall rate as mesoscale areas and cells pass over the gauge.

In the second study undertaken by Austin and Houze (1972), a single instantaneous precipitation pattern as depicted by the radar was analyzed in each of seventeen cyclonic storms. This approach, which permitted examination of a greater number of large mesoscale areas, was aimed towards obtaining a more complete

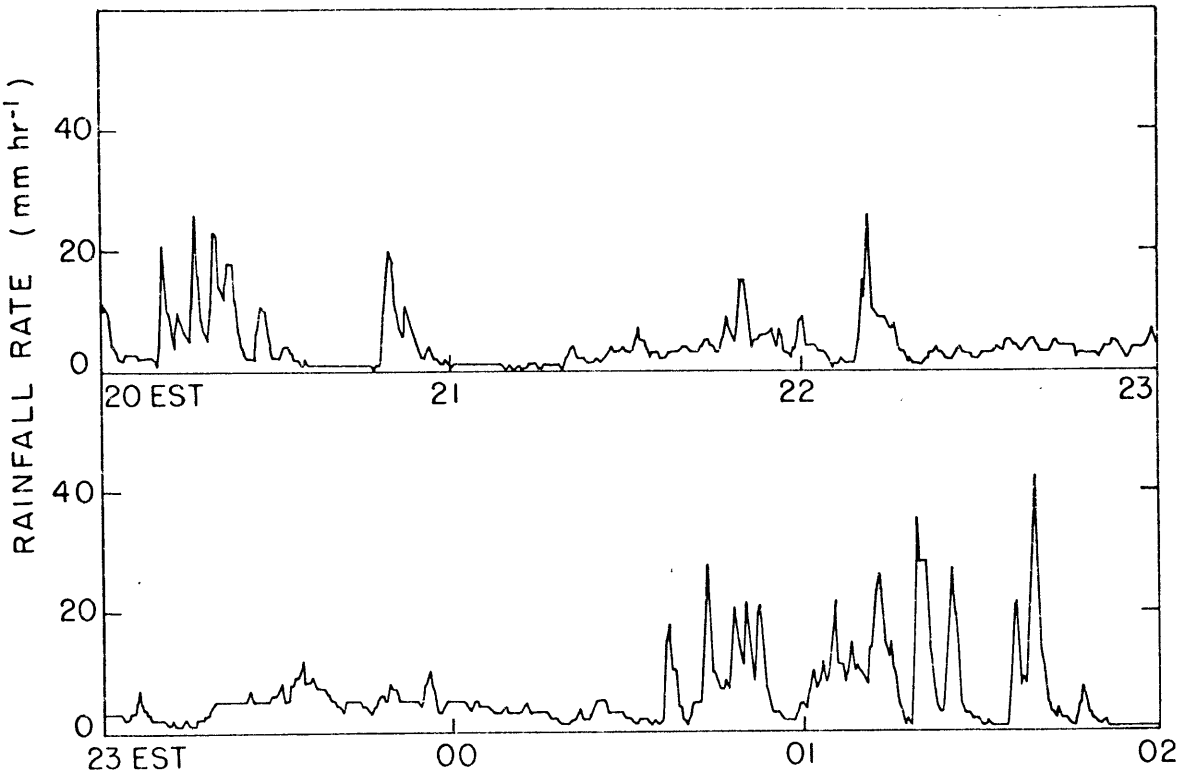


Figure A-1. Example of data from high-resolution tipping-bucket rain gauge, 29-30 November 1963.

description of the general configuration of LMSA's and of their distribution within the larger-scale pressure and wind fields. Storms selected for this study were fully developed cyclones and were ones for which the radar and rain-gauge records provided good coverage. Most of the data were taken with the WR-66 radar which shows the precipitation patterns clearly out to a range of 200 km. In the first study, range limitations in the radar data restricted rather severely the number of large mesoscale areas which could be analyzed in detail.

The shapes of precipitation areas were observed, and their orientations were compared with those of the surface isobars and with the surface wind directions during the hour sampled by radar.

APPENDIX B

SPECTRAL ANALYSIS OF RAIN-GAUGE RECORDS

This method for analyzing one-dimensional records of observed quantities is discussed by Blackman and Tukey (1958) and Munn (1970). What is obtained for each storm analyzed is a plot of the "spectrum" S, which is the normalized variance per unit frequency, versus the frequency. Spectra computed for this study are shown in Figure B-1. A flat or a monotonically decreasing spectral curve indicates that the process sampled contains only random fluctuations. A flat spectrum would indicate statistical independence of samples at successive time intervals, while a sharp upslope toward lower frequencies results from persistence or continued autocorrelation of the function over several intervals. Departures from a smooth spectrum, if they can be shown not to be merely sampling phenomena, indicate that the process analyzed contains relatively large amounts of variance in fluctuations with certain preferred periods. Tests of statistical significance of spectral peaks are described in the references cited above.

The spectra in Figure B-1 were computed for seven rainstorms of 10 hr or more in duration. The abscissa for these plots is labelled with a scale of inverse period P^{-1} rather than the frequency. The corresponding periods are also indicated on the upper scale. All of the computed spectra slope upward as the period increases (P^{-1} decreases) indicating a high degree of persistence or statistical dependence of 30-second observations, so that practically all of the total variance is contained by periods of 10 min or more. Each of the spectra has a number of

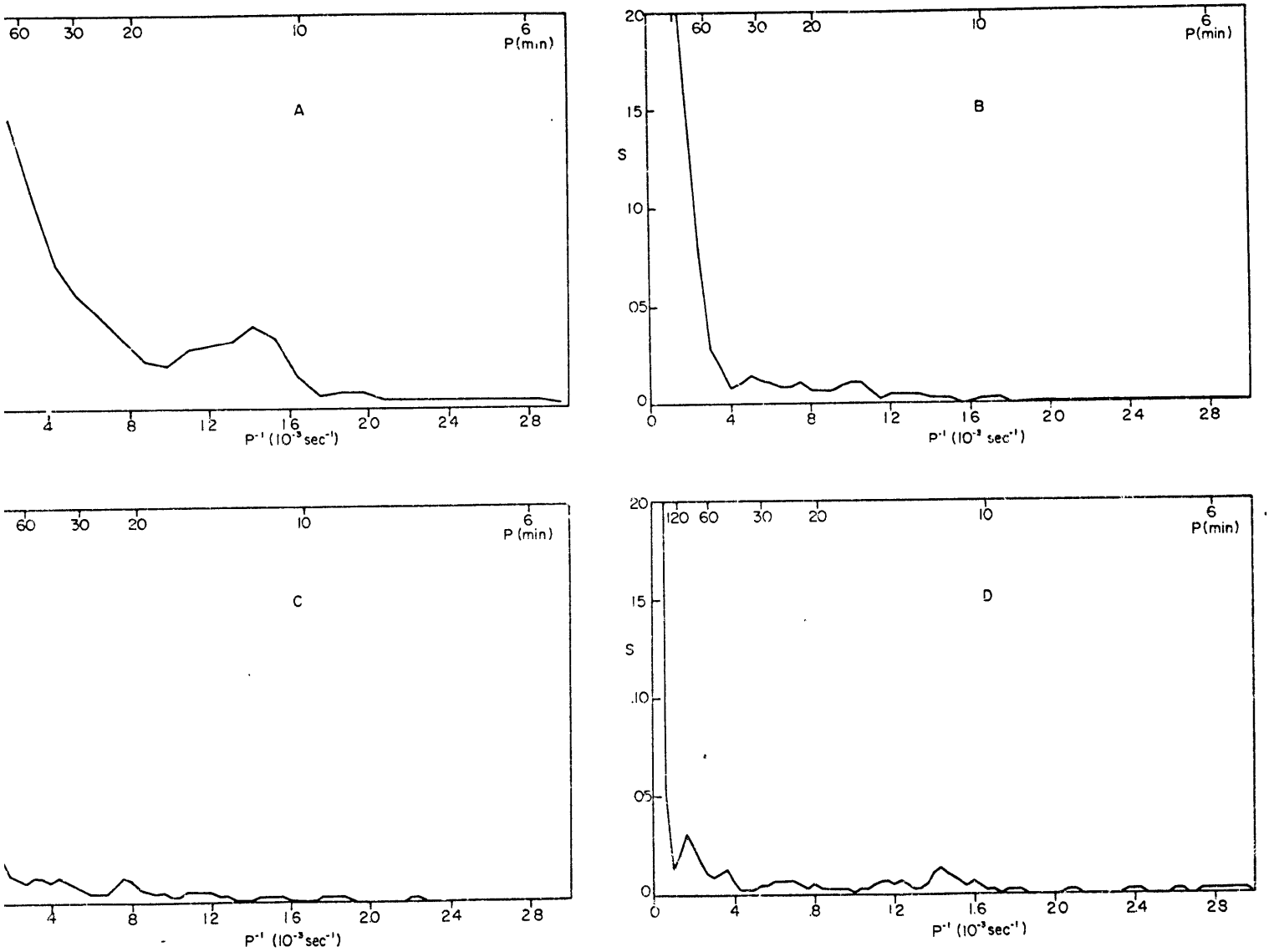
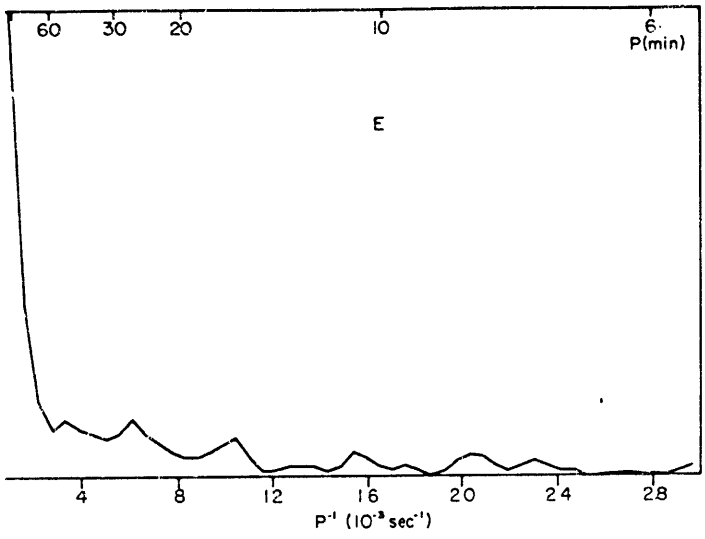
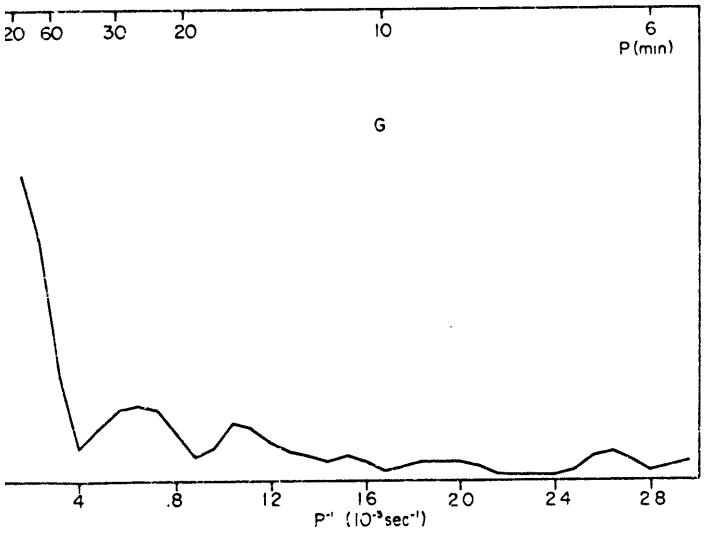


Figure B-1. Spectra of rainfall rate for seven periods of precipitation at Boston. S is the lance per unit frequency. Abscissae are labelled with period P and P^{-1} rather than actual quency. Total variance of a rainfall trace is normalized to the value 1.0 and is represented the total area under each curve. Figure continued on page -159-.





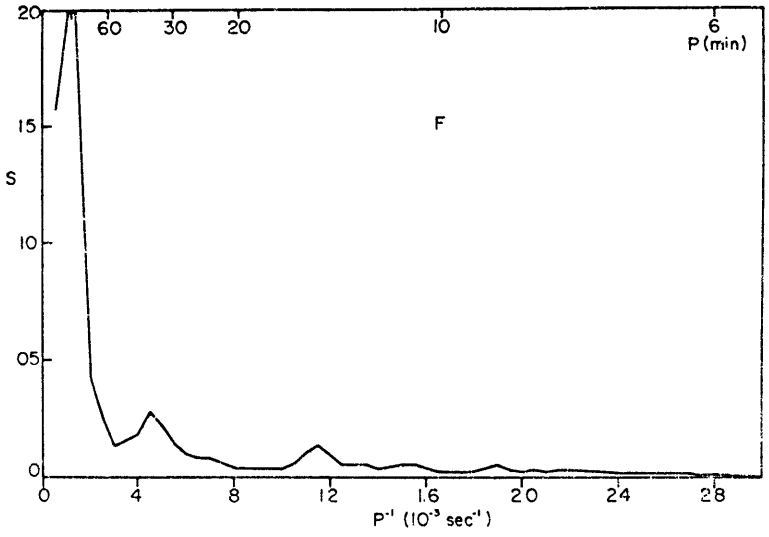


Figure B-1. Continued.

maxima in this range. By examining qualitatively the rainfall records themselves and radar data, most of these maxima could be associated with the passage of mesoscale areas or cells over the rain gauge. However, the only peak which showed much statistical significance is the one near $P^{-1} = 1.4 \times 10^{-3}$ sec^{-1} in Figure B-1 d. This peak reflects an extraordinarily high degree of cumulus activity in this storm.

It is thus apparent that variations in rainfall rate at a point due to the passage of successive mesoscale areas or cells over the rain gauge do not typically contain enough variance to be detected as statistically significant peaks in a spectrum. Practically all of the variance in any rainstorm is explained by persistence. Dyer (1970) found that snowstorms are also characterized by a high degree of persistence. The spectrum of the variance of precipitation rate, therefore, does not appear to be an adequate indicator of the scales present in rainstorms.

Since the spectral peaks did not occur strongly in individual storms, an investigation was made to determine if the average spectrum for the seven storms showed any more definite character. Since the aim was to investigate spatial characteristics, the period P in each storm was converted to a horizontal wavelength λ before the averaging. The appropriate conversion for each storm was based on the motions of mesoscale precipitation areas as shown by radar and on the observed winds in the mid-low troposphere. These speeds differed considerably from storm to storm and ranged from 10 to 40 m sec^{-1}. The average spectrum which was obtained is shown in Figure B-2. Rather weak maxima appear in the average spectrum near wavelengths of 10, 25, and 100 km. These maxima may

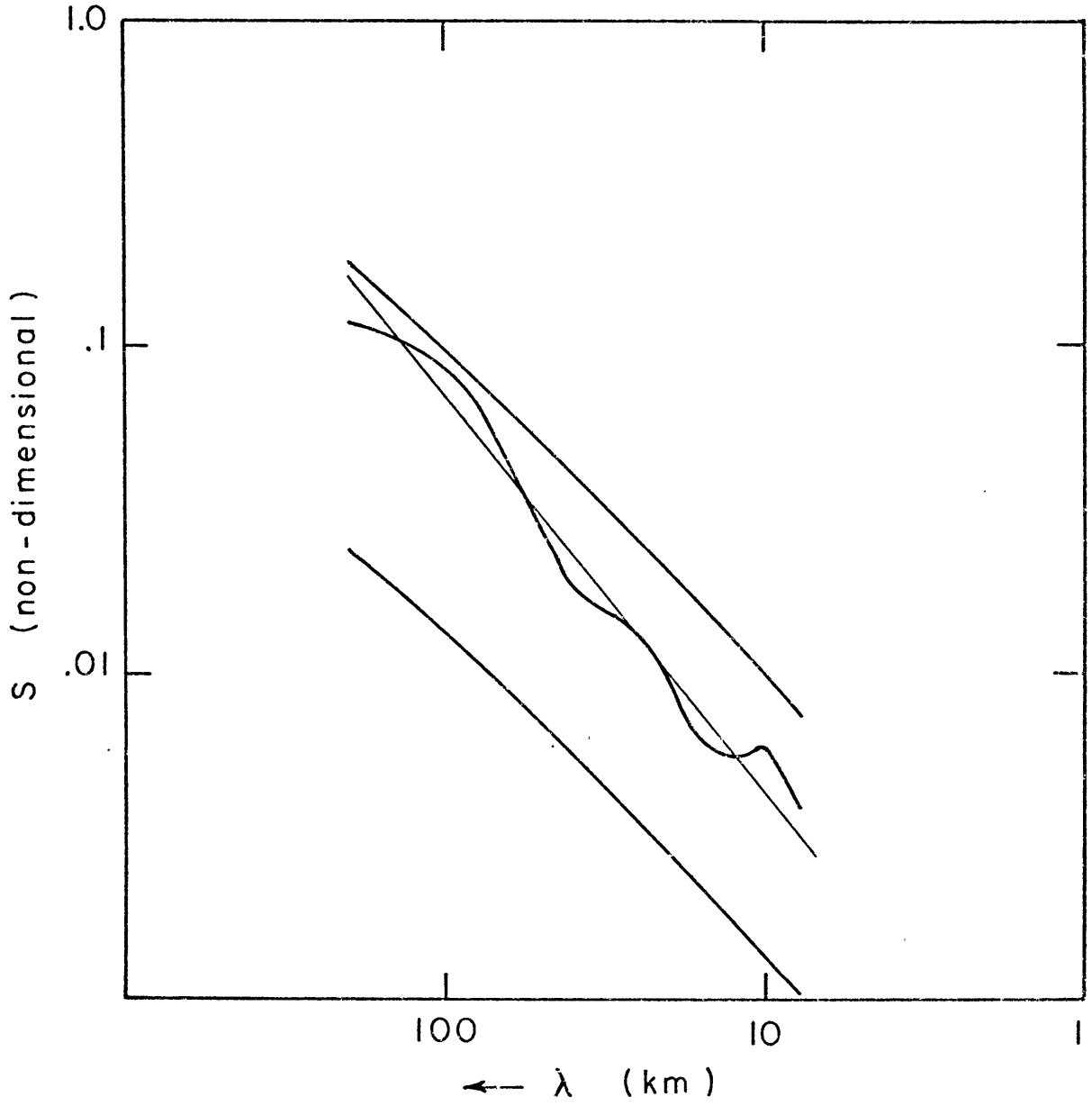


Figure B-2. Spectrum obtained by converting individual spectra to a scale of wavelength and averaging the spectra for seven storms. Outside lines are 90% confidence limits. Also shown is a best fit straight line which has a slope of -1.2.

reflect the occurrence of large mesoscale areas, small mesoscale areas, and cells, respectively; however, the 90% confidence limits show that the peaks do not have much statistical significance.

An additional difficulty in interpreting results such as shown in Figure B-2 is that the phenomena of interest, mesoscale areas and cells, have durations which are comparable with the time separating their passages over the rain gauge. The variation of rainfall rate with respect to the horizontal scale obtained by multiplying the time scale by the speed of the rainfall areas cannot be interpreted, therefore, as the spatial pattern at any one time. Another complication is that the horizontal patterns are highly anisotropic; this fact is evidenced by the frequent occurrence of banded structures in precipitation patterns as discussed in Appendix C. A one-dimensional presentation, therefore, does not fully describe the horizontal arrangement of mesoscale areas and cells.

It was originally thought that the spectrum of the variance of rainfall rate might be useful as an indicator of the spectrum of atmospheric turbulence in the cumulus and mesoscale ranges, as well as a method for simply analyzing the scales present in precipitation patterns. Spectra of atmospheric wind data are usually interpreted in terms of their slopes. The number most commonly used for comparison is that of Kolmogoroff (1941). According to his postulate, the eddy kinetic energy (variance of the wind speed) per unit wavelength would be expected to decrease proportional to $\lambda^{5/3}$. The functional dependence of the rainfall spectrum in Figure 7 is about $\lambda^{1.2}$ which is not greatly different from $\lambda^{5/3}$. However,

this comparison may not be especially meaningful. It is shown in section C of Chapter II that a number of explanations may be given for the occurrence of mesoscale variations of rainfall rate which do not involve enhanced lifting on the mesoscale. Since precipitation patterns may not be related in a point-by-point fashion to patterns of vertical velocity, the interpretation of spectra of rainfall rates as spectra of turbulence is questionable.

APPENDIX C

CHARACTERISTICS OF LARGE MESOSCALE AREAS

According to the definition of Austin and Houze (1972), a large mesoscale area (LMSA) is 10^3 to 10^4 km^2 in dimension. LMSA's are regions of precipitation which sometimes appear alone and on other occasions are manifested as areas of intensified rainfall rate within a larger, less intense synoptic precipitation area. Located within each LMSA are a number of small mesoscale areas (SMSA's) which are 50 to 1000 km^2 in dimension and which in turn contain several cumulus-scale cells. The data and methods of analysis used in the studies discussed here are described in Appendix A.

The observed relationship of LMSA's to the smaller-scale SMSA's and cells within them was investigated by tracking large mesoscale areas for their entire life histories. Of eight LMSA's studied in this manner, six were irregular in shape and were altering continuously during their lifetimes; their observed motions appeared to be about the same as those of the SMSA's and cells within them. Two of the LMSA's were definitely band-shaped; the frontal band on 8 July 1963 and an LMSA in the storm of 29 August 1962 which had been a hurricane. Within the band-shaped large mesoscale areas, the SMSA's and cells moved faster than the LMSA's and had large components of motion along the bands. Other detailed characteristics of LMSA's are given in Chapter II and in Houze's (1969) thesis.

The general configuration of large mesoscale areas within larger-scale cyclones was also investigated by Austin and Houze (1972). Instantaneous precipitation patterns in seventeen fully-developed cyclones prior to any occlusion were examined. The rainfall pattern and the surface isobars and wind vectors in Figure C-1 illustrate well the results which were obtained. In all of the cases elongated rain areas or band-shaped structures were observed. Many of these bands were similar in size to the large mesoscale areas examined in the first study, but some were considerably larger, ranging up to 2×10^4 km^2 in extent. It is not obvious, unless their life histories are studied, whether areas such as those marked A and B in Figure C-1 should be considered one LMSA or two. It is probable, therefore, that some of the bands observed in the second study consisted of two or more irregularly shaped LMSA's which formed an elongated rain area. In any case, the tendency to form elongated areas is very clear as demonstrated by the measured ratios of width to length in Figure C-2. It is noted that in the cyclonic storm analyzed by Browning and Harrold (1969) the rain patterns also exhibited banded structures. Also, Ligda et al (1961) observed banded structures in a number of occluded cyclones over the U.S.

The orientation of the bands was roughly parallel to the surface isobars. This is particularly noticeable in Figure C-1 where the cyclone center was within the region viewed by the radar and the structure bears some resemblance to the spiral bands of a hurricane such as the one illustrated in Figure 4. The distributions of orientation relative to surface isobars and surface wind direction is shown

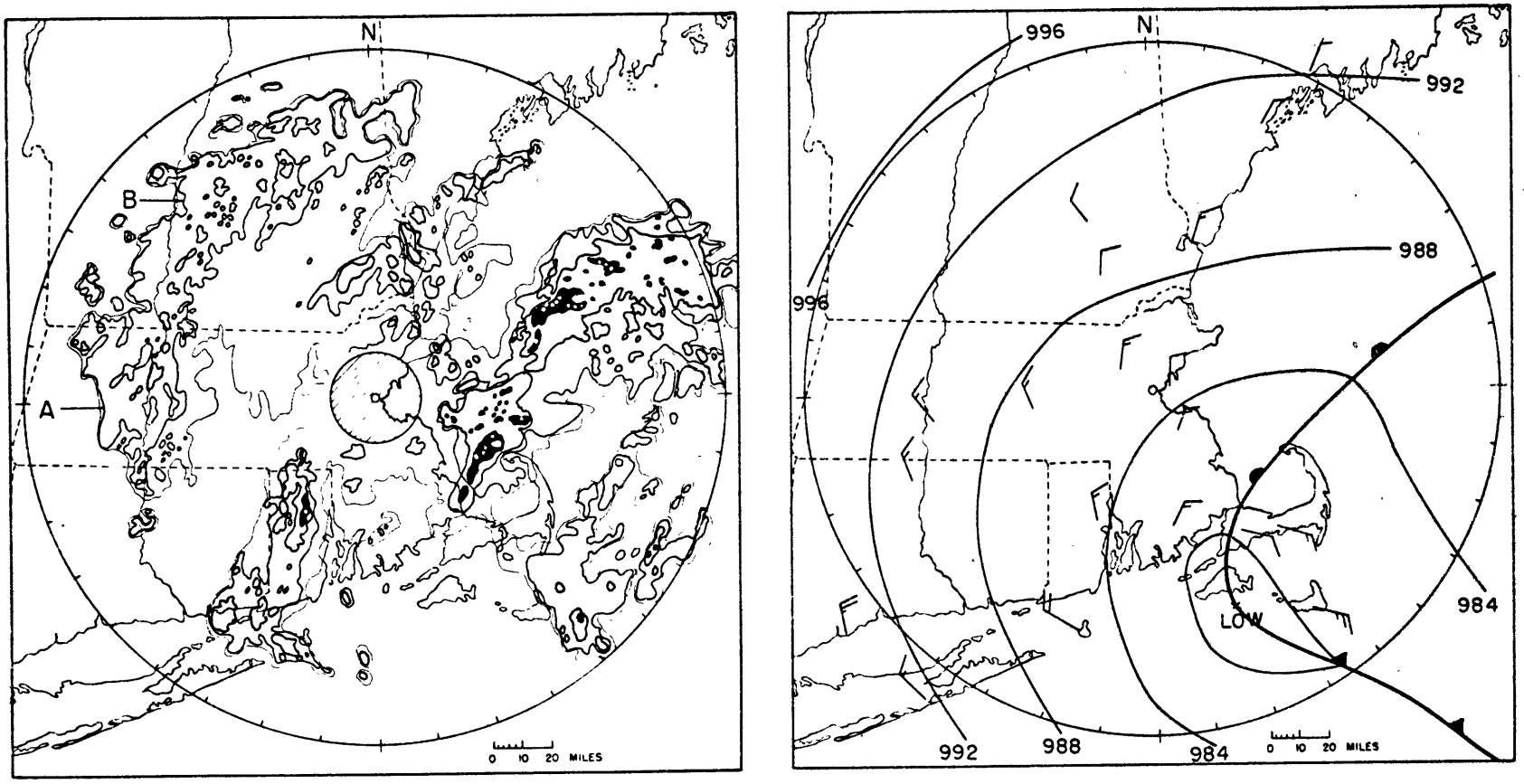


Figure C-1. Precipitation pattern, as depicted by Wr-66 radar, and surface winds and isobars for 5 November 1969, 1300 EST. Contours represent the following values of equivalent rainfall rate: 2,4,8,16 (solid black), and 32 (white spots) mm hr^{-1}.

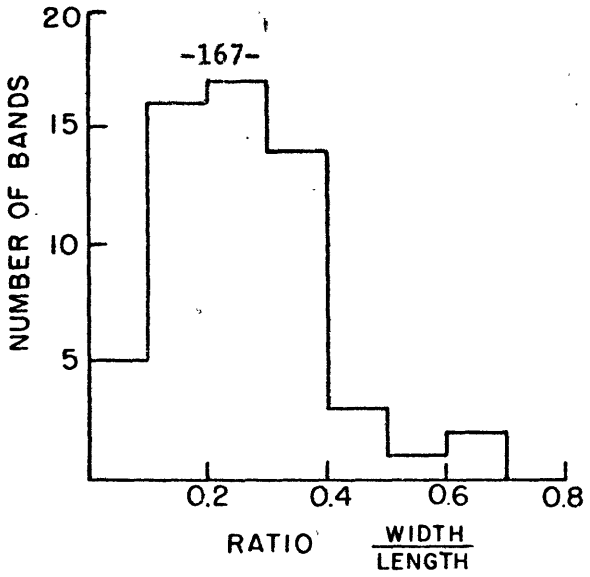


Figure C-2. Distribution of elongation of banded structures formed by large mesoscale areas.

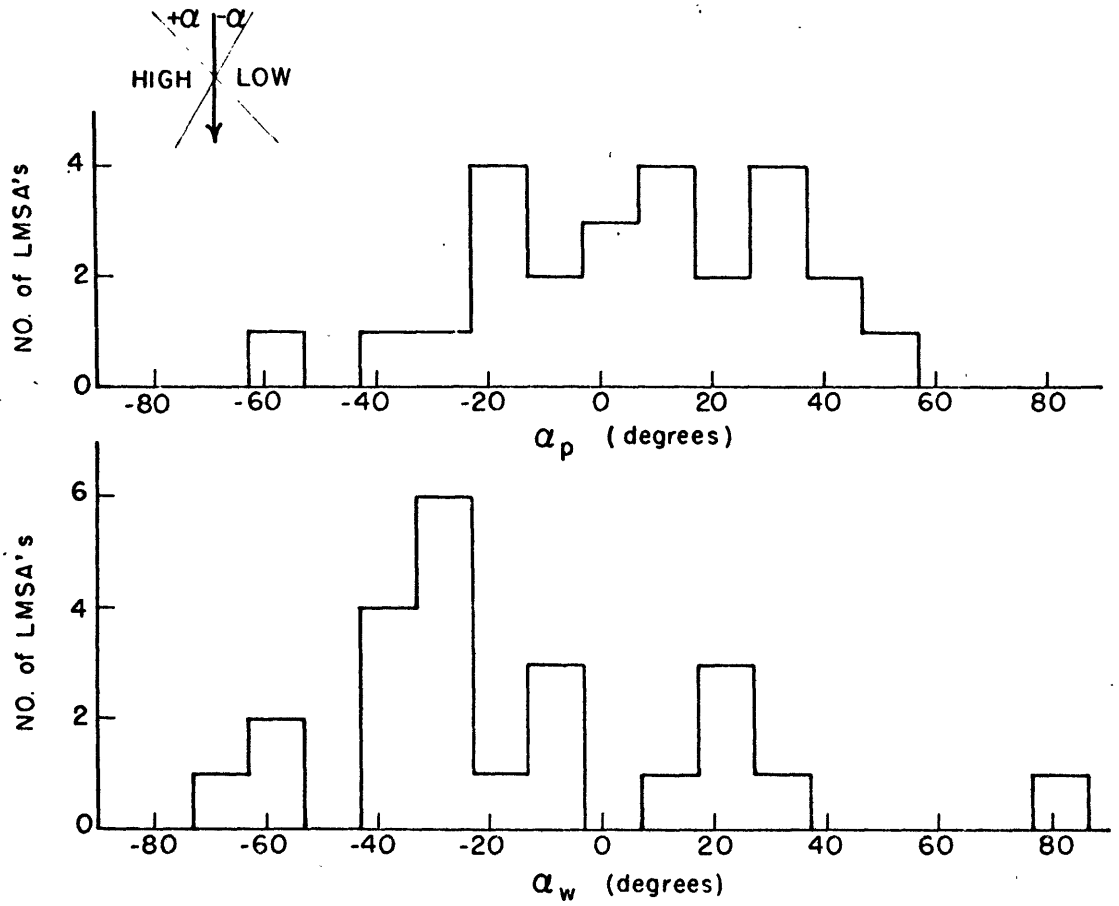


Figure C-3. Orientation of elongated rain areas relative to surface isobars, $_p$, and to surface wind direction, $_w$.

in Figure C-3; it can be seen that the angle between the band orientation and that of the isobars rarely exceeded 30^{o}.

Both of these studies indicate rather clearly the existence of large mesoscale areas which contain small mesoscale areas and cells. But the evidence with respect to their areas, shapes, motions, and configuration within larger-scale patterns is somewhat inconclusive. More comprehensive analysis is needed before the large mesoscale areas are fully described.

APPENDIX D

INVESTIGATION OF SURFACE VORTICITY AND DIVERGENCE IN THE VICINITY OF MESOSCALE PRECIPITATION AREAS

This study explores the possibility that "conditional instability of the second kind" (CISK) which apparently is important in the development of tropical cyclones (Charney and Eliassen, 1964) might also play a role in the development of the mesoscale areas which are observed within cyclonic precipitation areas at mid-latitudes. Similarity of precipitation patterns in tropical and extratropical cyclones may be noted by comparing Figures 4 and C-1. Resemblance of patterns in low- and high-latitude storms suggest that similar processes may be operating in the two situations. An important aspect of the CISK mechanism is that it is characterized by frictionally-induced convergence at low levels in regions of cyclonic vorticity. Therefore, the time variations of divergence and vorticity at the surface were analyzed for one storm.

Continuous surface wind records for 8 July 1963 were obtained for Bedford, Mass., Fort Devens, Mass., and Manchester, N.H., which form a triangle 605 km^2 in area, about the size of a small mesoscale area (SMSA), but much smaller than a large mesoscale area (LMSA) as they have been defined here. From winds averaged over 5 min, the divergence and vorticity were computed at intervals of 5 min for 24 hr according to the method of Bellamy (1949). Most of the record obtained is in Figure D-1.

During the first part of the day, before 1500 EST, the precipitation pattern in New England, rather typically, consisted of a synoptic precipitation area

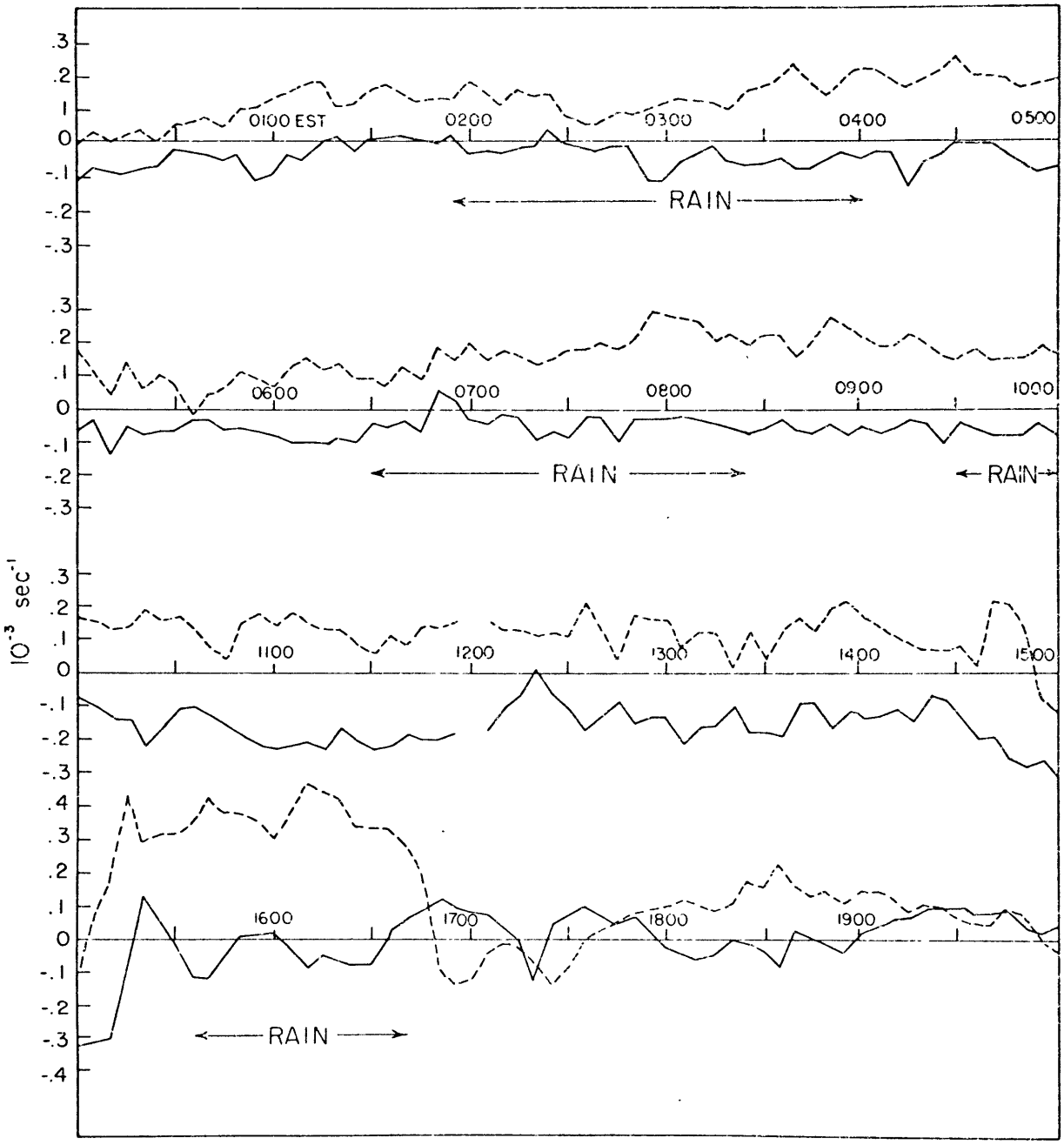


Figure D-1. Vorticity (– – – –) and divergence (———) computed by the triangulation method from surface winds at three stations enclosing an area of 605 km^2. Times labelled RAIN are periods when mesoscale precipitation areas were passing over the area.

containing several LMSA's. Each LMSA in turn contained several SMSA's, while within each SMSA there were a number of rather weak cumulus cells of 10-20 mm hr^{-1} in rainfall rate. This pattern of synoptic area, LMSA's, SMSA's, and cells at 0635 EST is shown in Figure 1 with the triangle for which the divergence and vorticity were computed.

The LMSA just south of the triangle passed over the triangle between 0645 and about 0800 EST. Mesoscale areas also passed over the triangle between 0200 and 0400 EST and between 0930 and 1030 EST. At these times, neither the divergence nor the vorticity shows any fluctuations clearly associated with the passages of the mesoscale precipitation areas. During the entire period before 1500 EST, however, it is noted that the vorticity is generally positive with an average of about $+ 1.2 \times 10^{-4}$ sec^{-1} and the divergence is generally negative with an average of $- 0.8 \times 10^{-4}$ sec^{-1}.

After 1500 EST, the synoptic precipitation area shown in Figure 1 moved away to the northeast and a band of frontal thundershowers approached from the northwest and passed over the triangle between 1530 and 1650 EST. This band, classified as a LMSA, was composed of a region of lighter precipitation approximately 20 km wide with several SMSA's aligned along it. In each of the SMSA's, several intense cumulus cells, generally 25 to 135 mm hr^{-1} in rainfall rate, were found. Immediately preceding the passage of this system over the triangle, a period of large negative divergence with individual values reaching $- 3.2 \times 10^{-4}$ sec^{-1} was observed. This is seen in Figure D-1 between 1420 EST and 1520 EST. During the

actual passage of the frontal band over the triangle between 1530 EST and 1650 EST, the divergence was small and erratic but the vorticity was large and positive, the largest individual value being 4.7×10^{-4} sec^{-1}.

Thus in this case study, the mesoscale areas observed with weak cumulus activity within a synoptic precipitation area were not associated with comparable mesoscale variations of surface divergence or vorticity. Such variations in the wind data may simply be too weak to separate from noise, so it cannot be concluded that CISK does not operate on this scale. A study based on a larger sample of data might illucidate some consistent relation between the surface wind field and the mesoscale precipitation patterns not evident from this one case.

Although boundary layer divergence and vorticity fluctuations were associated with the more intensely cellular frontal band, with the maximum convergence preceding and the maximum vorticity coincidental with its passage, it is not clear whether these fluctuations are necessarily related to the CISK mechanism. Before serious speculation, it should be determined if frontal bands or squall lines consistently have these variations in their surface divergence and vorticity fields.

A study based on a larger sample of data was not considered feasible as part of this thesis because of the time that would be involved in processing the available wind data. However, such a study is recommended.

APPENDIX E

FLOWCHART OF MODEL COMPUTATIONS FOR A STORM

Notation. (In order of appearance in flowchart)

$(R_c)_\eta$ = cellular precipitation for hour η .

$(R_m)_\eta$ = mesoscale precipitation for hour η .

$(R_s)_\eta$ = synoptic precipitation for hour η .

$(\Delta t_c)_\eta$ = time cells were over gauge during hour η .

$(\Delta t_m)_\eta$ = time mesoscale areas were over gauge during hour η .

$(\Delta t_s)_\eta$ = time synoptic area was over gauge during hour η .

N_η = number of hours in storm.

θ_e = representative equivalent potential temperature during storm.

H_1 = mean relative humidity outside storm in lower levels.

H_2 = mean relative humidity outside storm in upper levels.

z_o = height of level separating layers characterized by H_1 and H_2.

z_B = height of cell base.

z_T = height of cell top.

z_P = depth of layer of lighter rain surrounding cells.

$(B)_\sigma$ = westerly wind shear at sounding time σ .

N_σ = number of sounding times for which $(B)_\sigma$ obtained.

R_c = total cellular precipitation for storm.

R_m = total mesoscale precipitation for storm.

R_s = total synoptic precipitation for storm.

Δt_c = total time that cells were over gauge during storm.

Δt_m = total time that mesoscale areas were over gauge during storm.

Δt_s = total time that synoptic areas were over gauge during storm.

r = radius of cellular updraft.

$(B)_\eta$ = westerly shear for hour η .

$F[x]$ = function of x.

E = "entrainment rate" = $M_c^{-1} (dM_c/dz)_i$.

ζ = height of maximum mass transport.

z = height.

f_c = function specifying vertical shape of cellular mass transport profile and cellular vertical velocity profile below ζ . For example, the cellular mass transport profile is expressed $M_c = M_c(\zeta) f(z)$, $z \leq \zeta$.

g_c = function specifying shape of vertical shape of cellular mass transport profile and cellular vertical velocity profile above ζ . For example, the cellular mass transport is expressed $M_c = M_c(\zeta) g_c(z) + (1 - g_c(z)) M_c(z_T)$, $z > \zeta$.

w_c = cellular vertical velocity prescribed for temperature calculations.

T_c = temperature in cellular updrafts.

q_c = water vapor mixing ratio in cellular updrafts.

T' = temperature in environment of cells.

q' = water vapor mixing ratio in environment of cells.

μ = hydrometeor mixing ratio.

C_D = drag coefficient.

(u') = westerly wind in environment of cells at hour .

$(u_c)_\eta$ = westerly wind in cells at hour η .

α = fraction of mesoscale precipitation formed in cells.

β = ratio of total cellular condensation to precipitation formed in cells.

R_A = precipitation condensed above cells.

R_B = precipitation condensed below cells.

C = total cellular condensation for storm.

M_c = mass of air transported upward (per unit area) to produce cellular condensation C.

M_m = mass of air transported upward to produce mesoscale precipitation (per unit area) not condensed in cells.

M_s = mass of air transported upward to produce synoptic precipitation (per unit area).

W* = cellular vertical velocity inferred from computed cellular mass transport.

$\overline{W}$ = average vertical velocity for storm inferred from computed cellular, mesoscale, and synoptic mass transports.

τ_{SH} = sensible heat transport by cellular updrafts.

τ_{AM} = angular momentum transport by cellular updrafts.

Flowchart (See references to text for explanations of various steps. Bracket, { , indicates simultaneous solution of interdependent equations.)

INPUT QUANTITIES:

$(R_c)_n$, $(R_m)_n$, $(R_s)_n$, $(\Delta t_c)_n$, $(\Delta t_m)_n$, $(\Delta t_s)_n$, N_n

$\theta_e, H_1, H_2, z_0, z_B, z_T, z_P, (B)_\sigma$ for $\sigma = 1, 2, \ldots, N_\sigma$

Chap III, sections A, H, I

$$R_c = \sum_{n=1}^{N_n} (R_c)_n, \quad R_m = \sum_{n=1}^{N_n} (R_m)_n, \quad R_s = \sum_{n=1}^{N_n} (R_s)_n,$$

$$\Delta t_c = \sum_{n=1}^{N_n} (\Delta t_c)_n, \quad \Delta t_m = \sum_{n=1}^{N_n} (\Delta t_m)_n, \quad \Delta t_s = \sum_{n=1}^{N_n} (\Delta t_s)_n$$

$(B)_n$ determined by interpolating between $(B)_\sigma$'s

Pages 78-79

SPECIFICATION OF ENTRAINMENT AND VERTICAL PROFILES:

$n = F[z_B, z_T]$, Eq (12), Fig 13

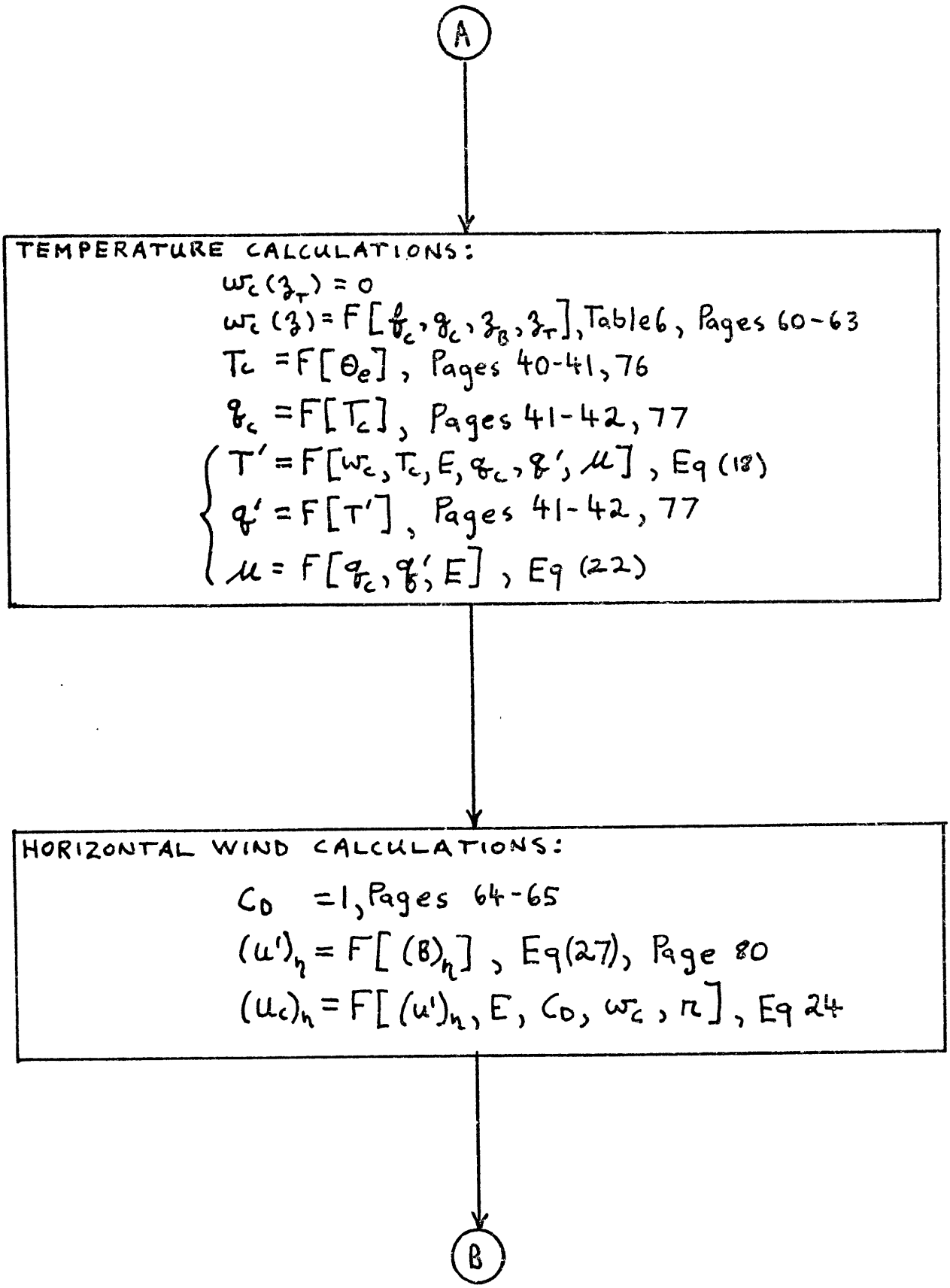
$E = F[n]$, Eq (5), Fig 13

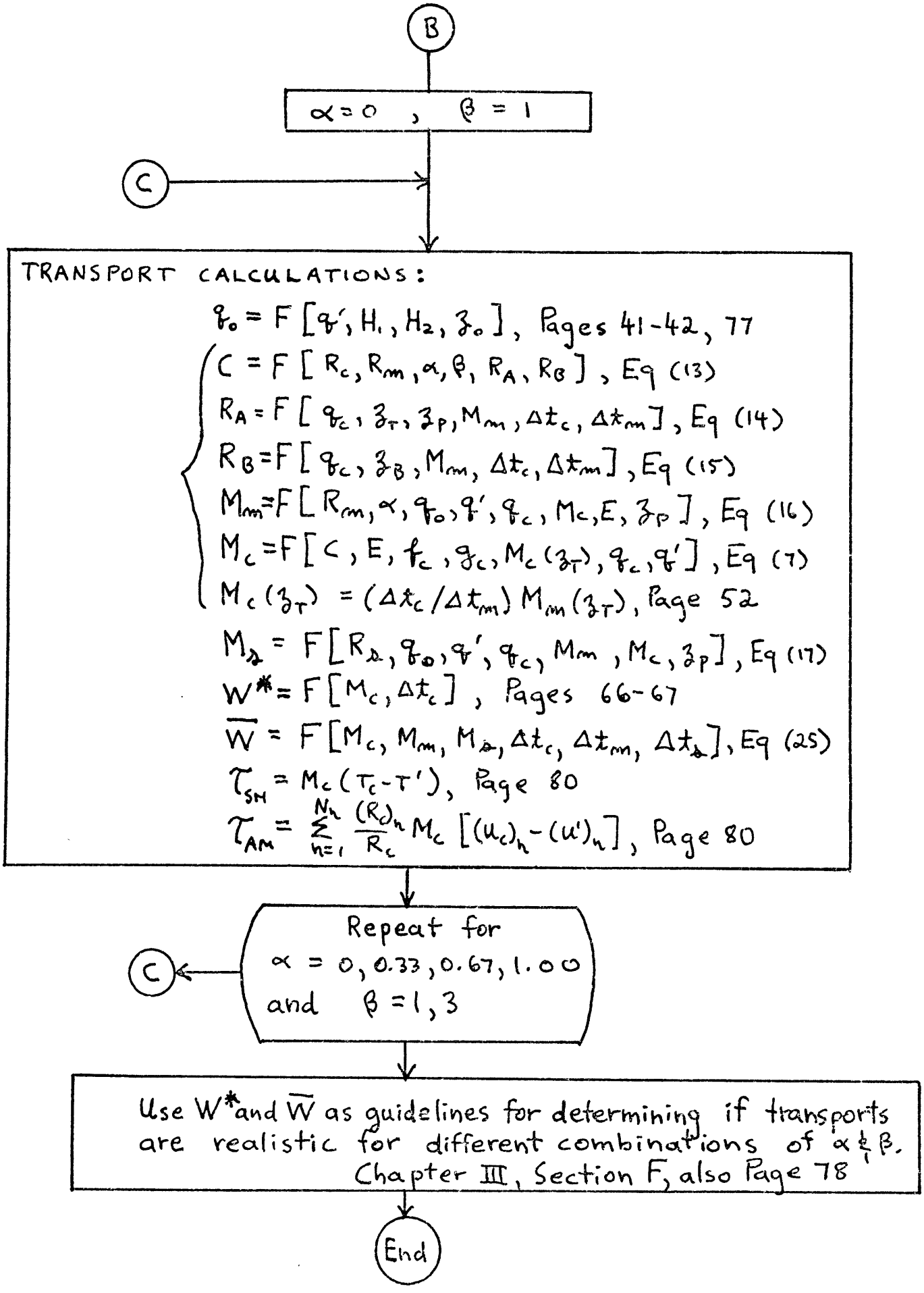
$\zeta = F[z_B, z_T]$, Eq (11)

$f_c = F[z, \zeta, n]$, Eq (10), Page 52

$g_c = 1 - [(z - \zeta)/(\zeta - z_T)]^2$, Page 52

(A)


A
TEMPERATURE CALCULATIONS:
$w_c(z_T) = 0$
$w_c(z) = F[f_c, q_c, z_B, z_T]$, Table 6, Pages 60-63
$T_c = F[\theta_e]$, Pages 40-41, 76
$q_c = F[T_c]$, Pages 41-42, 77
$T' = F[w_c, T_c, E, q_c, q', \mu]$, Eq (18)
$q' = F[T']$, Pages 41-42, 77
$\mu = F[q_c, q', E]$, Eq (22)
HORIZONTAL WIND CALCULATIONS:
$C_D = 1$, Pages 64-65
$(u')_n = F[(B)_n]$, Eq (27), Page 80
$(u_c)_n = F[(u')_n, E, C_D, w_c, \pi]$, Eq 24
B


B
$\alpha = 0$, $\beta = 1$
C
TRANSPORT CALCULATIONS:
$q_o = F[q', H_1, H_2, z_o]$, Pages 41-42, 77
$C = F[R_c, R_m, \alpha, \beta, R_A, R_B]$, Eq (13)
$R_A = F[q_c, z_T, z_P, M_m, \Delta t_c, \Delta t_m]$, Eq (14)
$R_B = F[q_c, z_B, M_m, \Delta t_c, \Delta t_m]$, Eq (15)
$M_m = F[R_m, \alpha, q_o, q', q_c, M_c, E, z_P]$, Eq (16)
$M_c = F[C, E, f_c, g_c, M_c(z_T), q_c, q']$, Eq (7)
$M_c(z_T) = (\Delta t_c / \Delta t_m) M_m(z_T)$, Page 52
$M_\Delta = F[R_\Delta, q_o, q', q_c, M_m, M_c, z_P]$, Eq (17)
$W^* = F[M_c, \Delta t_c]$, Pages 66-67
$\overline{W} = F[M_c, M_m, M_\Delta, \Delta t_c, \Delta t_m, \Delta t_\Delta]$, Eq (25)
$\tau_{SH} = M_c(T_c - T')$, Page 80
$\tau_{AM} = \sum_{n=1}^{N_n} \frac{(R_c)_n}{R_c} M_c [(u_c)_n - (u')_n]$, Page 80
Repeat for
$\alpha = 0, 0.33, 0.67, 1.00$
and $\beta = 1, 3$
C
Use W^* and $\overline{W}$ as guidelines for determining if transports are realistic for different combinations of α & β.
Chapter III, Section F, also Page 78
End

BIOGRAPHICAL NOTE

The author of this thesis, Robert Alvin Houze, Jr., was born on August 3, 1945, in Shamrock, Texas. On June 10, 1967, he married Yolonda Burkhalter, and their daughter Rebecca Diane Houze was born on May 29, 1970.

The author attended the A & M Consolidated Schools in College Station, Texas, from September, 1951, until graduation from high school in May, 1963. He was elected to the National Honor Society.

From June, 1963, until May, 1967, he was a student at Texas A & M University, also in College Station, Texas. He graduated with honors and was awarded the degree of Bachelor of Science in Meteorology. While at Texas A & M he was elected to the following scholastic societies: Phi Eta Sigma, Chi Epsilon Pi, and Phi Kappa Phi.

During the summers of 1964, 1965, and 1966, the author worked as a Student Trainee for the United States Weather Bureau at airport stations in Houston, Amarillo, and San Antonio, Texas. During the summer of 1967 he was employed as a meteorologist by the National Environmental Satellite Center, Applications Group, Suitland, Maryland.

In September, 1967, the author became a graduate student at the Massachusetts Institute of Technology where he has been in residence until the present time. After his first term at MIT, he was elected to the scientific scholastic honor society Sigma Xi. In January, 1969, he was awarded the degree of Master of Science.

During his stay at MIT, the author was supported financially for two years through a National Science Foundation Traineeship, for one and a half years as a Research Assistant for the MIT Weather Radar Research Project, and for one year as an MIT Teaching Assistant.

Published papers by the author of this thesis include:

Austin, P.M. and R.A. Houze, Jr., 1970: Analysis of mesoscale precipitation areas. Proc. of 14th Conf. on Radar Meteor., Amer. Meteor. Soc., Boston, 329-334.

Austin, P.M. and R.A. Houze, Jr., 1972: Analysis of the structure of precipitation patterns in New England, submitted to J. Appl. Meteor.

REFERENCES

Austin, P.M., 1968: Analysis of small-scale convection in New England. Proc. of 13th Conf. on Radar Meteor., Amer. Meteor. Soc., Boston, 210-215.

Austin, P.M. and R.A. Houze, Jr., 1972: Analysis of the structure of precipitation patterns in New England, submitted to J. Appl. Meteor.

Barnes, S.L., 1970: Some aspects of a severe, right-moving thunderstorm deduced from mesonetwork rawinsonde observations. J. Atmos. Sci., 27, 634-648.

Bates, F.C. and C.W. Newton, 1965: The forms of updrafts and downdrafts in cumulonimbus in a sheared environment. Text of talk, National meeting of the American Meteorological Society on Cloud Physics and Severe Local Storms, Oct. 18-22, 1965, Reno, Nevada.

Bellamy, J.C., 1949: Objective calculations of divergence, vertical velocity, and vorticity. Bull. Amer. Meteor. Soc., 30, 45-49.

Bjerknes, J., 1938: Saturated adiabatic ascent of air through dry-adiabatically descending environment. Quart. J. Roy. Meteor. Soc., 64, 325-330.

Blackman, R.B. and J.W. Tukey, 1958: The Measurement of Power Spectra. Dover Publications, Inc., New York, 190 pp.

Braham, R.R., Jr., 1952: The water and energy budgets of the thunderstorm and their relationship to thunderstorm development. J. Meteor., 9, 227-242.

Browning, K.A. and T.W. Harrold, 1969: Air motion and precipitation growth in a wave depression. Quart. J. Roy. Meteor. Soc., 95, 288-309.

Byers, H.R. and R.R. Braham, Jr., 1949: The Thunderstorm. Washington: U.S. Weather Bureau.

Charney, J.G. and A. Eliassen, 1964: On the growth of the hurricane depression. J. Atmos. Sci., 21, 68-75.

Court, A. and H.A. Salmela, 1961: Hourly Radiosondes for a Week. GRD Res. Notes, No. 60, AFCRL, Bedford, Mass., 350 pp.

Cunningham, R.M., M. Glass and T.N. Carlson, 1964: Properties of active cumulus clouds determined from coordinated ground photography and aircraft penetrations. Paper presented at National Conference on Physics and dynamics of clouds, 24-26 March 1964, Chicago; abstract in Bull. Amer. Meteor. Soc., 45, 59.

Dyer, R.M., 1970: Persistence in snowfall intensities measured at the ground. J. Appl. Meteor., 9, 29-34.

Elliott, R.D. and E.L. Hovind, 1964: On convection bands within Pacific coast storms and their relation to storm structure. J. Appl. Meteor., 3, 143-154.

Elliott, R.D. and E.L. Hovind, 1965: Heat, water, and vorticity balance in frontal zones. J. Appl. Meteor., 4, 196-211.

Fujita, T. and H. Grandoso, 1968: Split of a thunderstorm into anticyclonic and cyclonic storms and their motions as determined from numerical model experiments. J. Atmos. Sci., 25, 416-439.

Hitschfeld, W., 1960: The motion and erosion of convective storms in severe vertical wind shear. J. Meteor., 17, 270-282.

Houghton, H.G., 1968: On precipitation mechanisms and their artificial modification. J. Appl. Meteor., 7, 851-859.

Houze, R.A., 1969: Characteristics of mesoscale precipitation areas. SM Thesis, Dept. of Met., MIT, Cambridge, Mass., 77 pp.

Kolmogoroff, A., 1941: The local structure of turbulence in incompressible fluids for very large reynolds numbers. C.R. Acad. Sci. U.R.S.S., 30, 301-305.

Levine, J., 1959: Spherical vortex theory of bubble-like motion in cumulus clouds. J. Meteor., 16, 653-662.

Levine, J., 1965: The dynamics of cumulus convection in the trades. Ph.D. Thesis, Dept. of Met., MIT, Cambridge, Mass., 131 pp.

Ligda, M.G.H., S.M. Serebreny and R.E. Nagle, 1961: Weather Radar systems research, research toward effective use of weather radar data in weather analysis and forecasting. Final report, AFCRL-TR-61-200, Contract AF 19 (604)-3067, Stanford Research Institute, Menlo Park, California.

Malkus, J.S., 1952: The slopes of cumulus clouds in relation to external wind shear. Quart. J. Roy. Meteor. Soc., 78, 530-542.

Malkus, J.S., 1960: Recent developments in studies of penetrative convection and an application to hurricane cumulonimbus towers, in Cumulus Dynamics. Permagon Press, New York, 1960, 65-84.

Manabe, S., J. Smagorinsky, J.L. Holloway, Jr. and H.M. Stone, 1970: Simulated climatology of a general circulation model with a hydrologic cycle III. Effects of increased horizontal computational resolution. Mon. Wea. Rev., 98, 175-213.

Mason, B.J., 1970: Future developments in meteorology: an outlook to the year 2000. Quart. J. Roy. Meteor. Soc., 96, 349-368.

Matsumoto, S., K. Ninomiya and T. Akiyama, 1967: A synoptic and dynamic study on the three-dimensional structure of mesoscale disturbances observed in the vicinity of a cold vortex center. J. Met. Soc. Japan, 45, 64-81.

Melvin, G.L., 1968: The development of thunderstorm complexes and their associated vertical transports. SM Thesis, Dept. of Met., MIT, Cambridge, Mass., 65 pp.

Morton, B.R., G.I. Taylor and J.S. Turner, 1956: Turbulent gravitational convection from maintained and instantaneous sources. Proc. Roy. Meteor. Soc., A, 234, 1-23.

Munn, R., 1970: Biometeorological Methods. Academic Press, New York, 336 pp.

Oort, A.H. and E.M. Rasmusson, 1971: Atmospheric Circulation Statistics. Compilation made at Geophysical Fluid Dynamics Laboratory, NOAA, Princeton University, Princeton, New Jersey, to be published.

Oort, A.H. and A. Taylor, 1969: On the kinetic energy spectrum near the ground. Mon. Wea. Rev., 97, 625-636.

Palmen, E. and C.W. Newton, 1969: Atmospheric Circulation Systems. Academic Press, New York, 603 pp.

Plank, V.G., 1969: The size distribution of cumulus clouds in representative Florida populations. J. Appl. Meteor., 8, 46-67.

Scorer, R.S., 1957: Experiments on the convection of isolated masses of buoyant fluid. J. Fluid Mech., 2, 583-594.

Scorer, R.S. and F.H. Ludlam, 1953: Bubble theory of penetrative convection. Quart. J. Roy. Meteor. Soc., 79, 317-341.

Shmeter, S.M., 1966: Interaction between cumulonimbus clouds and the wind field. Izvestia, Atmospheric and Oceanic Physics, 2, 1025-1032 (pp. 618-621 in English translation published by the American Geophysical Union).

Simpson, J., R.H. Simpson, D.A. Andrews and M.A. Eaton, 1965: Experimental cumulus dynamics. Rev. Geophys., 3, 387-431.

Simpson, J. and V. Wiggert, 1969: Model of precipitating cumulus towers. Mon. Wea. Rev., 97, 471-489.

Simpson, J. and V. Wiggert, 1971: 1968 Florida cumulus seeding experiment: numerical model and results. Mon. Wea. Rev., 99, 87-118.

Smagorinsky, J., S. Manabe and J.L. Holloway, Jr., 1965: Numerical results from a nine-level general circulation model of the atmosphere. Mon. Wea. Rev., 93, 727-768.

Squires, P. and J.S. Turner, 1962: An entraining jet model for cumulonimbus updraughts. Tellus, 14, 422-434.

Starr, V.P., J.P. Peixoto and J.E. Sims, 1970: A method for the study of the zonal kinetic energy balance in the atmosphere. Pure and Applied Geophysics, 80, 346-358.

Turner, J.S., 1962: The 'starting plume' in neutral surroundings. J. Fluid. Mech., 13, 356-368.

Turner, J.S., 1963: The motion of buoyant elements in turbulent surroundings. J. Fluid Mech., 16, 1-16.

Van der Hoven, I., 1957: Power spectrum of horizontal wind speed in the frequency range from 0.0007 to 900 cycles per hour. J. Meteor., 14, 160-164.

Warner, J., 1970: On steady-state one dimensional models of cumulus convection. J. Atmos. Sci., 27, 1035-1040.

Weinstein, A.I., 1970: A numerical model of cumulus dynamics and microphysics. J. Atmos. Sci., 27, 246-295.